Geo-information Science and Remote Sensing

Thesis Report GIRS-2020-21

Influence of local data and local calibration on SoilGrids predictions

Merel Jager

May 2020

WAGENINGEN
UNIVERSITY & RESEARCH

Influence of local data and local modelling on SoilGrids predictions

Merel Jager

Registration number 950710387120

Supervisors:

S. de Bruin (Laboratory of Geo-Information Science and Remote Sensing)

G.B.M. Heuvelink (Soil Geography and Landscape / ISRIC – World Soil Information)

B. Kempen (ISRIC – World Soil Information)

A thesis submitted in partial fulfilment of the degree of Master of Science

at Wageningen University and Research Centre,

The Netherlands.

Date: 05/2020

Wageningen, The Netherlands

Thesis code number:	GRS-80436
Thesis Report:	GIRS-2020 -21

Wageningen University and Research Centre
Laboratory of Geo-Information Science and Remote Sensing

Abstract

Soils are the major component of the terrestrial ecosystem and the largest organic carbon pool on earth and therefore soils have to be managed properly. To facilitate proper management , digital soil maps of good quality are needed. This study aims to help ISRIC understand the impact of local data and local modelling to improve their digital soil maps.

This study aims to compare globally and locally calibrated SoilGrids (SG) models and assess the influence of adding local data to a globally calibrated SoilGrids model. This was assessed in three steps, using Soil Organic Carbon (SOC) and soil pH as soil properties to predict. The first step was calibrating an SG model using soil observations from a study area in India (Andhra Pradesh) and selecting local covariates. Predictions with this *local* SG model were compared to those of an SG model calibrated with soil observations from the entire globe and globally selected covariates, using a test dataset containing soil observations within Andhra Pradesh. The top ten most informative predictors differed 75% to 80% between the models. The predictions of local SG model were much closer to the observed values than those obtained by the global model with an RMSE of 0.286 for the local SOC model, 1.720 for the global SOC model, 0.467 for the local pH model, and 0.837 for the global pH model.

The second step compared the global SG model with an SG model calibrated using all global soil observations and all local observations. The covariates used for both models were identical, and predictions were made for three areas, i.e., Andhra Pradesh - India, Nampula – Mozambique (similar to Andhra Pradesh in feature space) and the Netherlands (very dissimilar to Andhra Pradesh in feature space). It was anticipated that for Nampula differences between the two models would be relatively large whereas for the Netherlands they would be small. Results showed that this was not the case. The areas dissimilar to Andhra Pradesh in feature space showed more deviation in the difference maps of the SG global and SG local predictions than the areas close in feature space. A reason for this deviation can be the difference in variable importance between both models, where predictions for the Netherlands ware more influenced by in variable importance of the SG model calibrated using all global soil observations and all local observations, than Nampula was. To find out what the exact influence of covariate importance is, future research is needed. The out-of-bag (OOB) (see appendix I, OOB) model statistics of both models, showed that adding local soil observations to an SG model resulted in a better RMSE, ME and R^2 for predictions around the entire globe. To find out if the model predictions accuracy also improved for Nampula and the Netherlands, future research is needed.

The third and final step of this research was to gain insight into the influence of the size of the dataset added to a globally calibrated SG model. This was done by adding the local data in seven successive steps to the global soil observations and subsequent calibration of the global SG model, each time using the same covariates. The models were used to make soil pH predictions for Andhra Pradesh and showed that adding more local soil observations to the model increased prediction accuracy to a power-law (the more training data, the more accurate the model) and then reached a plateau from whereon the accuracy of the predictions is just slightly changing, as expected.

This study shows that adding local data observations to the SoilGrids DSM changes the variable importance of the model. This resulted in different model results in areas close in feature space, but also areas distant in feature space. The OOB model statistics showed that adding local data to a global model positively influenced the model accuracy for predictions all over the globe. However, to make even more accurate predictions with a SoilGrids model, a combination between locally selected covariates and global soil observations can be used to make predictions for a local area.

Title page figure source: (Machmuller et al., 2015)

Acknowledgements

I would like to express my sincere gratitude to my supervisors Gerard Heuvelink and Sytze de Bruin for providing guidance throughout this research and for having the patience and time to read this document multiple times to provide feedback. In addition, a thank you to Bas Kempen who provided extra knowledge and information when needed and for helping me through the (dumb) mistakes I sometimes made when programming in R.

I also would like to thank all the people and supervisors of thesis ring 2 for their feedback and ideas regarding this thesis.

Last but not least, I would like to thank my family and friends for their constant source of inspiration and encouragements to keep going and finish this thesis in time.

Table of contents

Glossary:

Calibrating a model *Model calibration Is the process of adjustment of the model parameters. This includes that the model learns patterns, structures and parameters directly from the training data, and all settings that cannot be learned directly from the data are set manually. After a model is calibrated, it can be used to make predictions (Molnar, 2019). A synonym for calibration can also be; training a model.*

Covariates *A covariate is a variable that is correlated with the soil property of interest. According to this definition, any variable that is measurable, considered to have a statistical relationship with the dependent variable and that is available at all observation and prediction points would qualify as a potential covariate. (Fan, 2019).*

Depth interval layers *The six layers used by Soil Grids to represent soil properties at different depth intervals (0-5 cm, 5-15cm, 15-30cm, 30-60 cm, 60-100cm and 100-200 cm depth interval layers) (Hengl et al., 2017).*

Global model *A model is a global model when: the input soil profiles contain data of the entire globe, the covariate stack covers the entire globe and the model is calibrated using both global soil profiles and covariates.*

Horizons *A soil horizon is a layer in the earth with unique soil properties relative to parent and child layers (Zhang & Hartemink, 2019).*

Local model *A model is a local model when: the input soil profiles contain data of a country or region the covariate stack covers that same country or region and the model is calibrated using both country or region soil profiles and covariate stack.*

Machine Learning *(supervised) Machine learning are algorithms which can be trained to recognise patterns based on past event or experience with respect to some class of tasks. ML Algorithms are able to predict future events for any new input after sufficient training* (Frankenfield, 2018).

Prediction depth *This depth is the centre point of the depth interval layer you want to predict for (e.g. a prediction depth of 10 cm is used to predict for the 5-15 cm depth layer).*

Sample depth *The actual depth at which a soil observation sample was taken. This is the depth used as a covariate during model calibration. It stands apart from the depth interval layers and it should not be confused with prediction depth.*

Soil observations: *Soil observations are soil samples taken in the field and analysed in a lab to give a measure of the soil p. For this research, soil observations for Soil pH and Soil Organic Carbon are used.*

Soil properties *All soils contain mineral particles, organic matter, water and air. The combinations of these determine the soil's properties – its texture, structure, porosity, chemistry and colour. Soil properties can therefore be e.g. soil organic carbon, soil pH, proportion of clay particles, total nitrogen or the proportion of sand particles.*

List of figures

List of tables

1. Introduction

Many global problems such as climate change, freshwater scarcity, loss of agricultural land through erosion, biodiversity decline and feeding 10 billion people by 2050 present immense challenges to humanity (Bouma, Montanarella, & Evanylo, 2019). Soil has a vital part to play in all these challenges (Sanchez et al., 2009). Soil degradation has, for example, detrimental consequences for the already limited land and water resources available for agricultural productivity (Koch et al., 2013). To be able to protect our carbon-rich and biodiverse rainforests, wetlands, and grasslands from changing into croplands and still be able to feed 10 billion people in the near future, we will have to increase current crop yields on existing farmland through sustainable intensification. In many areas, it is possible to sustainably intensify crop production through proper soil management and the use of fertilisers (Kopittke, Menzies, Wang, McKenna, & Lombi, 2019). Soil information is important to determine the amount of fertilisers needed to increase in yield. Another reason why soil is essential is that soil constitutes the earth's largest terrestrial carbon (C) pool (Jobbágy & Jackson, 2000). Our challenge is to keep C in the soil through proper soil management and preferably increase soil C as a climate change mitigation measure. When soil is not rightly maintained (e.g. deforestation), it will release C into the atmosphere resulting in an aggravating climate change measure (Davidson & Janssens, 2006). Because the soil has a vital part to play in addressing global problems, the demand for soil information is increasing.

The growing demand for soil information in combination with the increase in available detailed satellite data has led to the development of Digital Soil Mapping (DSM) (McBratney, Mendonça Santos, & Minasny, 2003). DSM produces soil maps using soil mapping based on supervised machine learning (ML) algorithms or geostatistical methods like kriging to predict soil properties from soil point observations and environmental covariate layers that are typically derived from satellite imagery and digital elevation models. These covariate layers related to the five major soil-forming factors that were identified by Pendleton & Jenny, 1945 and formalised into a model for soil development. These factors are climate (cl), organisms (o), relief (r), parent material (p) and time (t), or 'CLORPT' and are widely used as input for DSM.

In many parts of the world, DSM has shifted from an academic pursuit to operational initiatives on both local (regional or national) (Hengl et al., 2015; Kempen, Brus, & de Vries, 2015) and global scale (Arrouays, Lagacherie, & Hartemink, 2017). SoilGrids is a DSM framework developed by ISRIC that provides global (world covering) scale prediction maps for a standard set of numeric soil properties (Bulk density of the fine earth fraction, Cation exchange capacity of the soil, Volumetric fraction of coarse fragments, Proportion of clay particles, Total nitrogen, Soil pH, Proportion of sand particles, Proportion of silt particles, Soil organic carbon content, Organic carbon density and Organic carbon stocks) at six standard depths intervals (0-5 cm, 5-15 cm 15-30 cm 30-60 cm 60-100 cm and 100-200 cm). Those predictions are based on a collection of worldwide soil point observations and remote sensing-based soil covariates (Hengl et al., 2017)(see 2.1, the SoilGrids framework). These maps are used in various initiatives, for instance, to fill in the gaps for the Global Soil Organic Carbon Map (FAO & ITPS, 2018), as a data source for assessing land degradation trends (UNCCD & The Global Mechanism, 2016) and as data input for ecological niche modelling of plant species (Velazco, Galvão, Villalobos, & De Marco, 2017).

Because of its global nature, SoilGrids might not represent local patterns of the spatial distribution of soil well or give accurate local predictions, for instance, for a specific country or region. This could be caused by the lack of soil point observations for that specific county/region or predictive relationships that are locally different from globally. To address this, it might be more accurate to calibrate a DSM model locally. Kempen et al., 2019 uses a locally fitted ML model to predict Soil Organic Carbon content (SOC) for Tanzania instead of a globally fitted ML model. This model very likely captures local predictive relationships much better than a globally calibrated model would, and will thus result in much more accurate predictions (Hand & Vinciotti, 2003). A local model selects covariates that are locally relevant. This selection might differ from a covariate set that is selected by a global model. The latter might not be optimal for a more local application. In this way, the model will be better tuned to local conditions. A negative side of this is that an extensive calibration dataset is needed to ensure there is enough calibration data available to calibrate a DSM model locally.

To provide more accurate local SoilGrids maps, one could consider serving the SoilGrids framework local data only (local soil samples and local covariates) and thereby make it a local model that has specifically tailored predictive relationships. Calibrating a local model requires more local data than calibrating a global model and may result in a patchwork of local models with sharp boundaries between them. If local data are available, then it can also be interesting to add these to the global model and analyse if this leads to locally improved (more accurate) predictions (Vitharana, Mishra, & Mapa, 2019). Therefore, this study aims to compare globally and locally calibrated SoilGrids models and assess the influence of adding local data to a globally calibrated SoilGrids model. To achieve this objective, three research questions will be answered.

1.1 Research questions

1. What is the model prediction performance of a globally calibrated SoilGrids model compared to a SoilGrids model calibrated on local soil data only?

2. What is the model prediction performance of the current SoilGrids model compared to a global SoilGrids model calibrated after adding local data?

3. How does the effect of adding local data on prediction accuracy depend on the size of the local dataset?

The methodology will be tested using Andhra Pradesh - India as case study area (chapter 2.5). The local SoilGrids model will be built according to the SoilGrids Framework, thereby using only soil observations from Andhra Pradesh and a local covariate feature selection. The soil properties chosen for this study are soil organic carbon content in % and soil pH in H2O.

2. Methodology

The research questions are answered using the SoilGrids framework as a basis. Chapter 2.1 describes the SoilGrids framework, which is used to answer the three research questions. Chapter 2.2, 2.3 and 2.4 each describes the method of a research question: what the model inputs and settings are, where predictions will be made and how the accuracy/influence of data of those predictions is determined. Chapter 2.5 explains the case study and chapter 2.6 finishes the methodology with the used materials and data.

2.1 The SoilGrids Framework

DSM often makes use of supervised machine learning (ML) algorithms to predict soil properties. Figure 1 shows the SoilGrids framework, which uses Random Forest (see appendix I, Theoretical background) as an ML algorithm. Each step in the framework is briefly explained below. See (Hengl et al., 2017) for a detailed step by step explanation of the SoilGrids DSM framework.

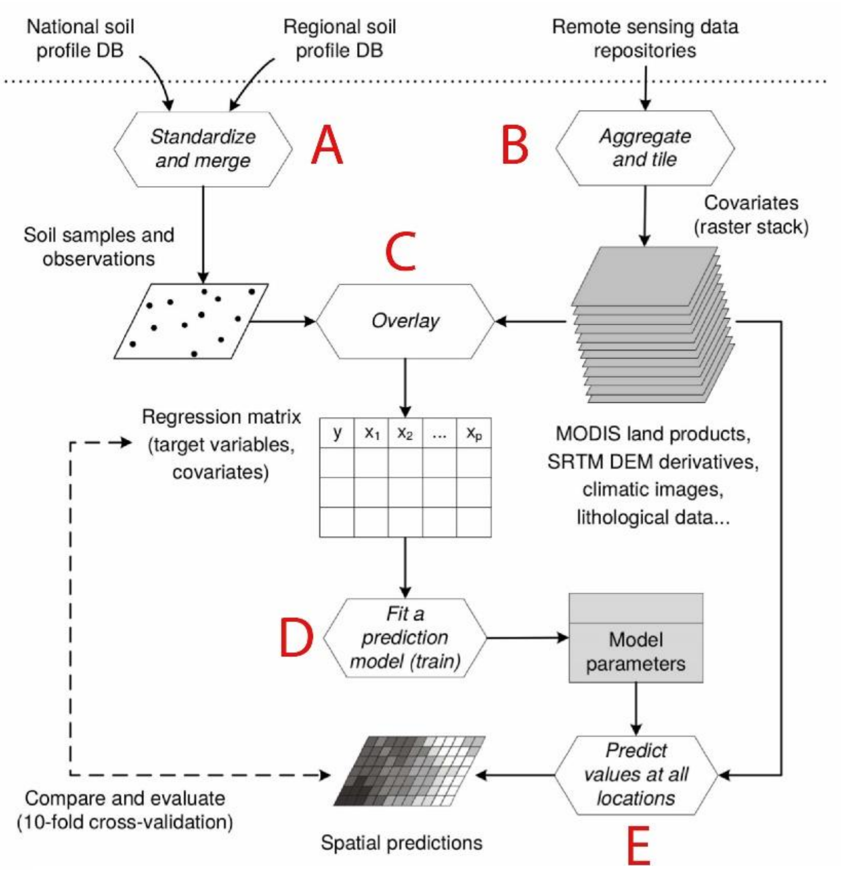

National soil profile DB
Regional soil profile DB
Remote sensing data repositories
Standardize and merge
A
B
Aggregate and tile
Covariates (raster stack)
Soil samples and observations
C
Overlay
Regression matrix (target variables, covariates)
y
x1
x2
...
xp
MODIS land products, SRTM DEM derivatives, climatic images, lithological data...
D
Fit a prediction model (train)
Model parameters
Predict values at all locations
Compare and evaluate (10-fold cross-validation)
Spatial predictions
E

Figure 1. SoilGrids statistical framework (Hengl et al., 2017).

A. Soil observations

The soil samples and observations dataset (part of step A, future explained in section 2.6 Data and materials) contains a compilation of soil profiles and sample data used for model calibration. The soil samples dataset is derived from soil observations made all over the world and samples analysed in the lab by multiple organisations. ISRIC collects geo-referenced soil profile data from the world, harmonises the data, merges datasets and serves the result via the World Soil Information Service (Batjes et al., 2017). SoilGrids soil profiles contain measured values of soil properties (e.g. pH in H2O, sand, silt and clay), sample *depth* and coordinates of the measured location. Besides the soil observations, the soil sample dataset may also include expert-based pseudo-observations. Some large areas that have extreme climatic conditions and/or have very restricted access are significantly under-sampled. To ensure that the model can represent those under-sampled areas, pseudo-observations are inserted and fill the gaps in the feature space so the dataset can be used for model training (Hengl et al., 2017).

B. Covariates

A covariate is a variable that is correlated with the soil property of interest. According to this definition, any variable that is measurable, considered to have a statistical relationship with the dependent variable and that is available at all observation and prediction points would qualify as a potential covariate. A covariate is thus a possible predictive or explanatory variable of the dependent variable (Fan, 2019). Hengl et al. (2017) list all the covariates used by SoilGrids. These include e.g. land cover classes (cultivated land, forests, grasslands, shrublands, wetlands, tundra, artificial surfaces and bare land cover), long-term averaged mean monthly hours under snow cover, global water table depth in meters, average soil and sedimentary-deposit thickness in meters. The full list of used covariates is shown in appendix II.

Covariates were generated using different remote sensing data repositories (e.g. MODIS land products), step B. Those data are stacked, so each location of the world has all covariate values *(see Section 2.6)*. This covariate stack is used to extract the regression matrix (see below) used for training data and used as input for the model predictions.

C. Regression matrix

To be able to calibrate the model, each soil observation needs to be associated with information about the covariates. A regression matrix was built by extracting all covariates collocated with the soil profiles using a spatial overlay operation, step C. In this regression matrix, the sample depth of the soil observations is used as *'depth'* covariate for model calibration.

D. Model calibration

Before the model is calibrated, first a correlation analyses and a random feature selection (RFE)(see appendix I, correlation analyses and RFE) are performed to gain the most optimal covariates to use in the Random Forest (RF, see appendix I; Random Forest) formula. RFE determines the covariate importance and the outcome of this function is a list with selected covariates which are most important for the RF predictions, without reducing the model performance. Next, the model parameters can be defined.

A machine learning algorithm learns patterns from existing data. RF learns parameters and structures directly from the training data and creates an ensemble of different tree models (Molnar, 2019). Hyperparameters are all model settings which cannot be learned directly from the training data. For SoilGrids the RF model hyperparameters which are set are mtry and num.trees. The hyperparameter mtry sets the number of covariables available for splitting at each tree node. The num.trees hyperparameter set the number of trees to grow. Larger number of trees produce more stable models and covariate importance estimates, but require more memory and longer run times (Liaw & Wiener, 2018). To estimate those hyperparameters, a random subset of the regression matrix (5 – 10% of the total size) is used to calibrate and validate a list of models where a predefined combination of hyperparameters was tested. The optimal hyperparameters of the RF model were defined by the model with the lowest RMSE.

The regression matrix was used to calibrate the random forest model, step D. Per soil property, a formula is defined, where: soil property is a function of all optimal covariates. The formula, regression matrix and hyperparameters together are used to calibrate the SoilGrids model. For each soil property, a separate model is calibrated.

E. Prediction & Validation

The fully calibrated RF model can be used to make predictions for any location and any depth where the covariates are known, Step E. The covariate raster stack built in step B is used as input data. ISRIC generates SoilGrids predictions at six standard depth intervals; 0-5 cm, 5-15 cm, 15-30 cm, 30-60 cm, 60-100 cm and 100-200 cm. To make predictions for a depth interval layer, the prediction depth is added as a covariate to the covariate stack (sample depth is not part of the covariate stack). The prediction depth is the centre point of the depth interval layer to predict for and is calculated using the following formula

$$\frac{top\ of\ a\ layer - bottom\ of\ a\ layer}{2} + bottom\ of\ a\ layer \qquad (1)$$

To determine the model performance (validation), the calibrated model was used to make predictions using 10-fold cross-validation (see appendix I, k-fold cross-validation. Each model was re-calibrated ten times using 90% of the data and predictions derived from the calibrated models are compared with observations of the remaining 10% to gain the model accuracy (Molnar, 2019). Assessments followed the same procedures as described in section 2.2.

2.1.1 SoilGrids rebuild

The original SoilGrids Framework was built in several different programs optimised for high-performance computing (HPC) and generation of tiled predictions (De Sousa, Poggio, Dawes, Kempen, & van den Bosch, 2020). To make this research executable in a non-HPC environment, it was decided to rebuild the SoilGrids framework completely in R. The SoilGrids framework was rebuilt as close as possible to the existing framework to minimise the influences on the model results. To be able to compare globally and locally calibrated SoilGrids models and assess the influence of adding local data to a globally calibrated SoilGrids model, there should not be any differences between the SoilGrids framework and the rebuilt DSM framework. Therefore, all model results were predicted using this remake of the SoilGrids framework.

2.2 Comparison of a global and local SoilGrids model

The global SoilGrids model, here called SG_{Global}, and the local SoilGrids model, here called SG_{Local}, were created using the SoilGrids framework for each soil property of interest. For the SG_{Global} model, global soil samples and global covariates were used to create the regression matrix, as shown in Table 1. The global soil sample dataset did not include the local soil samples used in the SG_{Local} model. For the covariates, I used the 129 covariates remaining after the correlation analysis (performed by ISRIC) as input for the RFE performed for each soil property model. The results of the RFE were used as covariate stack and as input for the model formula. The next step was to calibrating the model. The hyperparameters of the model were copied from the original SoilGrids, as the function to calculate those hyperparameters should be performed on an HPC and takes much of time (around ten days for all SoilGrids properties). The models should be as close as possible to the original SoilGrids and we assumed that for local calibration the hyperparameter results would not differ much from the global calibration results. Therefore, all models built during this research used the hyperparameters of the original SoilGrids. For SOC, mtry was set to 14 and num.trees to 250 for OC while for pH, mtry was set to 12 and num.trees to 150. With the hyperparameters set and the regression matrix complete, the model was calibrated and used for predicting. The model was used to make predictions for the local study area at a depth interval of interest and for the soil properties of interest.

The SG_{Local} model was created using local soil samples and the global covariates clipped to the local extent. The procedure of creating the SG_{Local} model was almost identical to SG_{Global}. The only difference was; in the regression matrix, the standard depth of the local soil samples and a random number between 1-10 (later used as fold) was added.

Table 1. SoilGrids model settings to compare a global and local model.

Model settings	SG_{Local}	SG_{Global}
Soil Observations	Local	Global
Used covariates	SG_{Local} RFE results	SG_{Global} RFE results
Prediction area	local study area	local study area
Soil Property	OC and soil pH	OC and soil pH
Prediction depth interval	5-15 cm	5-15 cm

Model comparison

The SG_{Global} and SG_{local} model were assessed by comparing the used covariates and their relative importance. The importance of the variable is calculated using the Gini Importance. The Gini importance calculates each covariate importance as the sum of the number of splits (across all tress) that include the covariate, proportionally to the number of samples (soil observations) it splits (Strobl, Malley, & Tutz, 2009). The result can be shown as a bar plot with the covariates on the y-axis and the relative importance of the covariates on the x-axis. To be able to compare the results, the x-axes of SG_{Global} was rescaled dividing the SG_{Global} variable importance by the result of equation 3.

$$\frac{SGGlobal\ soil\ observations}{SGLocal\ soil\ observations} \qquad (3)$$

Variable importance plots were used to assess whether global and local variable importance are different, indicating local patterns. The ranger package also reports model calibration fit via the R^2 based on out-of-bag (OOB) samples. Those statistics were also compared per model and per soil property.

Map comparison

The results of the SG_{Local} and SG_{Global} predictions were compared by plotting them individually and plotting the difference between the two prediction maps by subtracting the SG_{Global} results from the results SG_{Local}. A visual scan of the difference map was done to check for abnormalities, such as extremes, and the mean of the difference map was calculated to assess whether one model gives systematically higher or lower predictions. Next, descriptive statistics of both model predictions were calculated and compared.

Accuracy

The accuracy of the prediction performance of both models was assessed using a test data corresponding to a subset of the local soil observations dataset that was set aside for testing. Details are provided in Section 2.6. Accuracy was assessed separately for each of the two soil properties. The accuracy of the prediction performance was gained by calculating the root mean square error (RMSE) to get the overall accuracy (Eq. 4), the mean error (ME) to quantify the prediction bias (Eq. 5), the R2 to represent the fraction of explained variance (Eq. 6), and the prediction interval width as derived using QRF.

The RMSE and ME should be close to 0 for the best performance and indicate highest accuracy, as they represent the differences between the measured values and observed values. A model calibrates the data well if the differences between the observed values and the model's predicted values are small and unbiased. The R^2 is the fraction of the response variable variation that is explained by the model and it is expressed on a convenient 0 – 100% scale.

$$RMSE = \sqrt{\frac{1}{n}\sum_{i=1}^{n}(z(s_i) - \hat{z}(s_i))^2} \tag{4}$$

$$ME = \frac{1}{\mathrm{n}}\sum_{i=1}^{n} z(s_i) - \hat{z}(s_i) \tag{5}$$

where n is the total number of validation locations in the local study area. At each of these locations (s_i), the difference between the actual value ($z(s_i)$) and the predicted value ($\hat{z}(s_i)$) is computed.

$$R^2 = \left[1 - \frac{SSE}{SST}\right] \times 100 \tag{6}$$

where SSE is the sum of squared errors at validation points, and SST is the total sum of squares. An R^2 of 100 indicates a perfect model where the model explains 100 % of the variation.

Scatter density plots of the predicted against observed values along with 1:1 lines were plotted. The closer the predictions are to the 1:1 line, the more accurate the model is. Lastly, for the two models the performance statistics, descriptive statistics and scatter plots were compared to assess the differences between model performances and conclude which model, the SG_{Global} or the SG_{Local} was most accurate for the local study area.

2.3 Influence of new soil observations

To assess the influence of new local soil observations on the global model, the new local soil observations were added to the global soil observations. This resulted in a new SoilGrids model, called the SG_{Plus} model. SG_{Plus} was calibrated on a new regression matrix holding the same covariates as the SG_{Global} model and the soil observations of the SG_{Global} and SG_{Local} models, see table 2. For each soil property of interest, a prediction was made for all depth intervals of interest. The SG_{Global} model results of all three study areas were compared to SG_{Plus} model. The results of the SG_{Plus} and SG_{global} predictions were assessed by plotting the difference between the two prediction maps. This was done by subtracting SG_{Plus} results from the SG_{Global} results. Assessments followed the same procedures as described in section 2.2.

It is possible that adding local data not only influences the predictions in the local area but also elsewhere in the world. This may happen in areas that have comparable environmental conditions as the local area (i.e., areas that have comparable covariate values). To derive which parts of the world have similar soil-forming factors, the Homosoil concept (Miller, 2012) was used. The Homosoil method searches for the smallest taxonomic distance of the 'CLORPT' soil-forming factors between a reference area and the region of interest, in this case, the local area. This includes climate, physiography, and parent materials (Mallavan, Minasny, & McBratney, 2010). Because this method does not explicitly take all covariates of the SoilGrids model into account, two areas were selected to review the results. One area with a small taxonomic distance is selected (called the "std study area"), and one with a large taxonomic distance (called the "ltd study area"). The ltd study area was used as a reference area, I expected the std study area to show some deviation in the difference maps, while the ltd area should show very little to no deviation. If the ltd study area did show a large deviation, it might be because Homosoil did not take all covariates into account.

Table 2. SoilGrids model settings to determine the influence of new soil observations.

Model settings	SG_{Plus}	SG_{Global}
Soil Observations	Global + Local	Global
Used covariates	SG_{Global} RFE results	SG_{Global} RFE results
Prediction area	local, std & ltd study area	local, std & ltd study area
Soil Property	OC and soil pH	OC and soil pH
Prediction depth interval	0-5, 5-15 & 15-30 cm depth layer	0-5, 5-15 & 15-30 cm depth layer

2.4 Local data density

For traditional machine learning algorithms, accuracy typically increases according to a power-law (the more training data, the more accurate the model) and then reaches a plateau from whereon the accuracy of the predictions is just slightly changing. To analyse the influence of the local data density for the SG_{Global} model, the prediction performance was evaluated for different newly added local data sample sizes. The goal hereby is to gain insight into the accuracy grown of the SG_{Global} model for the local study area.

The local data samples were added to the SG_{Global} model in eight ascending steps (Table 3). The last step was the results of RQ2. The SG_{Global} model, including the new soil samples, is called $SG_{Plus}n$. The model was re-calibrated seven times with the original SG_{global} soil observations and the soil observations of the local area per ascending step (Table 4). The models are were used to make predictions for the local area and the local test dataset was used to gain the model accuracy. The results were presented as a learning curve. The prediction performance for the learning curve was calculated using the RMSE, calculated using from the test data.

Table 3. Number of added local sample data used for assessing the effect of local data density.

Run number	Number of new Soil samples
1	100
2	200
3	500
4	1000
5	2000
6	5000
7	10000
8	36898

Table 4. SoilGrids model settings to determine the influence of local data density.

Model settings	RQ3 $SG_{plus}n$
Soil Observations	Global + n local in ascending steps
Used covariates	SG_{Global} RFE results
Prediction area	local study area
Soil Property	Soil pH
Prediction depth interval	5-15 cm

2.5 Case study

The methods were tested using three different study areas. For the local study area, Andhra Pradesh, located in India (Figure 2), was chosen. This area was chosen because it represents a low sampling density area in SG_{Global} and new soil observations were present. To test the difference between a global and a local model, new local soil samples were needed for the local study area. Within ISRIC there were 506704 new local soil samples of Andhra Pradesh pre-processed and in the same layout as the SG_{global} soil samples ready to use. Nampula located in Mozambique was chosen as the std area. According to the Homosoil results (appendix III), this area is geographically most similar to the local study area. The Netherlands was chosen to represent the ltd study area. The Netherlands has a reasonable sample size in the SG_{Global} model and it is taxonomically distinct from Andhra Pradesh.

Andhra Pradesh

The state Andhra Pradesh is located in the south-west of India (between 77° and 84° 40' East and 12° 41' and 22° North) with a total surface area of 160,000 km^2 and it is the fourth-biggest state in India. The state can be divided into three different zones. The Coastal Plains in the east is bordered by the Bay of Bengal and has a coastline of around 972 km. The Western Pediplains have considerable height differences. The elevation ranges from 0 to > 600 m above mean sea level. The Eastern Ghats follow the Coastal Plains closely. One outstanding area is the hill range in the North-East part. Here the elevation attains a height of 600 to 1200 m (P.Sudhakar, Reddy, Prasad, SatyaKumar, & Rao, 2017). Temperatures range from 12° to 30°C in winter to 20° to 41°C in summer. The monsoon season, which starts in July and continues till September, is the most extreme season where the state receives heavy rainfall (1150 mm). The State is dominated by cropland with large forests in the northern part and in the centre of the south (Rao & Wanmali, 2018). Figure 2 shows the soil map of Andhra Pradesh. The northern part is dominated by Nitisols, With Regosols near the sea. The southern part of the area is a mixture of Leptosols, Luvisols and Vertisols (Pike, 2018).

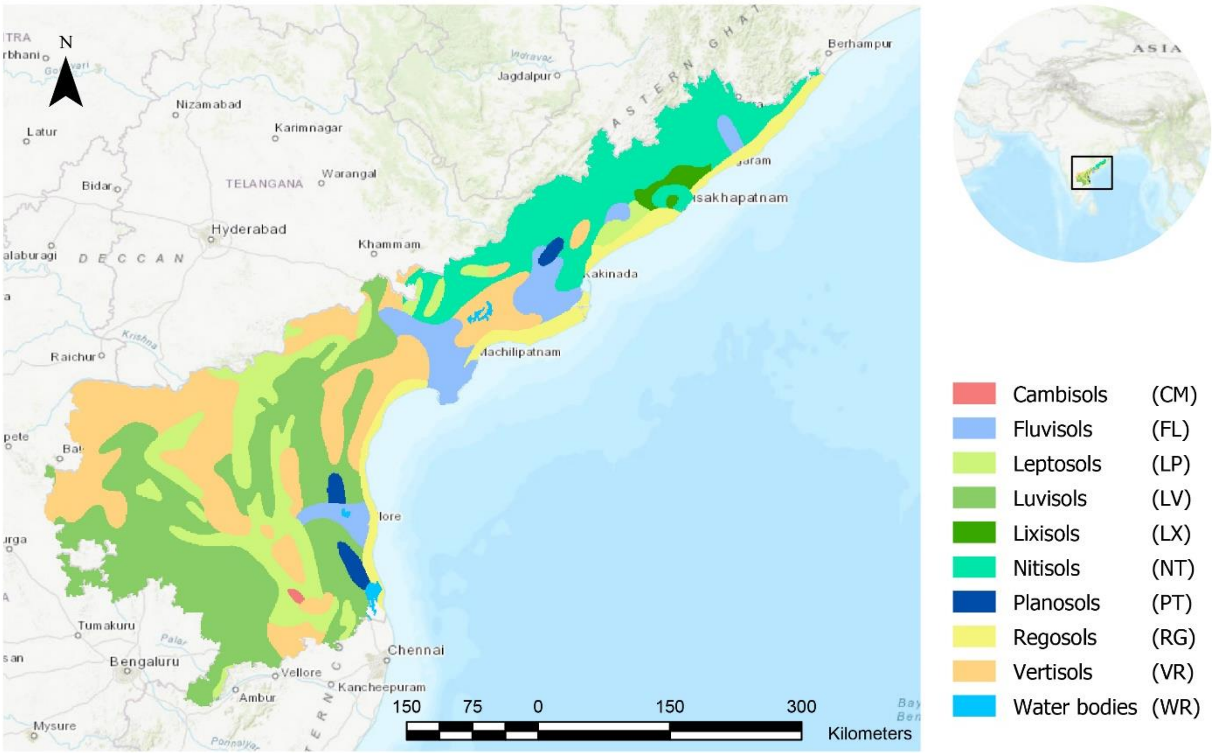

Figure 2. Distribution of major soil types in Andhra Pradesh – India (Maschinen et al., 2012).

Netherlands

The Netherlands has a total surface area of 33.883 km^2 and is located between the North Sea to the north and west, Germany to the east and Belgium to the south. Most of the terrain consists of coastal lowlands, river deltas and reclaimed land, with some hills in the south-east. The elevation ranges from -7m till 321 meters above sea level. The Netherlands has a mild, maritime climate with generally warm summers and gentle winters. There is no rainy season in the Netherlands. Rain occurs throughout the whole year with spring as the driest season (Rowen & Heslinga, 2020). The centre and west part of the Netherlands is covered with thick layers of silt and gravel transported from the European mountains by the rivers Rhine and Maas (Cambisols and Fluvisols). Clay (Gleysols) is deposited in the sheltered lagoons behind the coastal dunes (Regosols) and Luvisols are mainly found in the southern part of the Netherlands. The rest of the Netherlands is covered by sand (podzols) with some Histosols between the Fluvisols and Podzols (Figure 3) (Maschinen, Investition, Beschaffungen, Ersatzbeschaffungen, & Mittelherkunft, 2012).

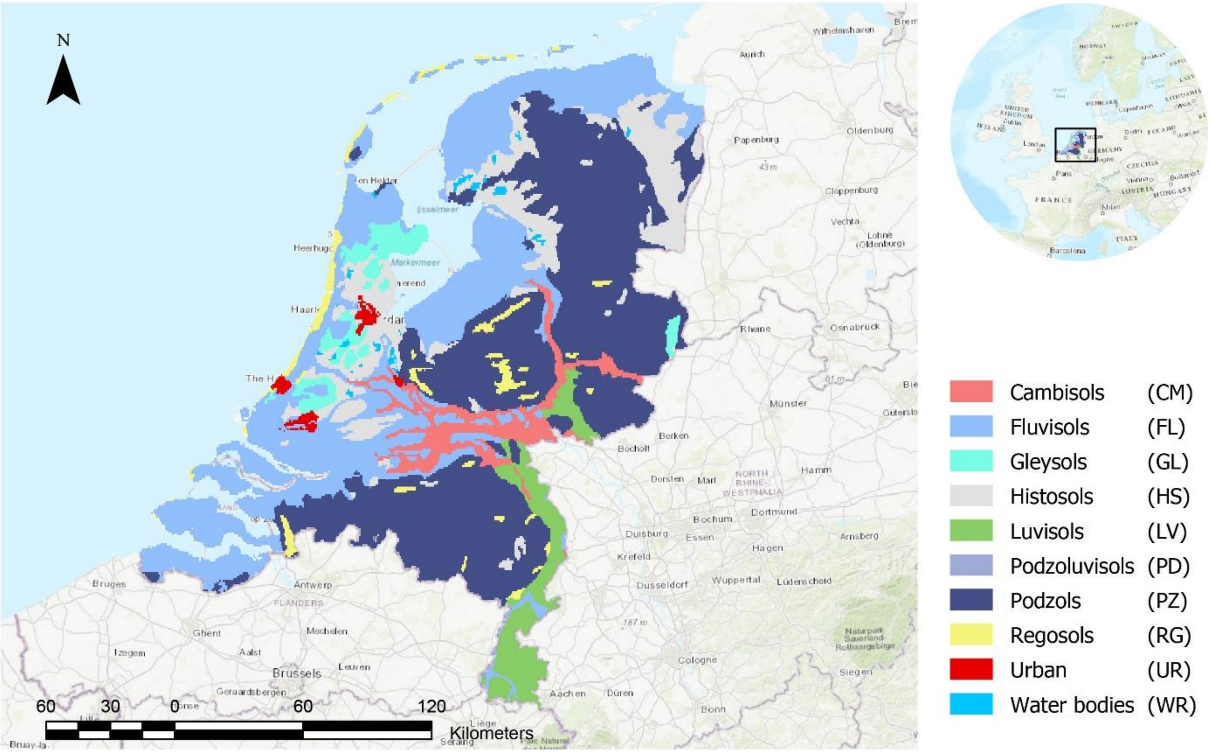

Figure 3. Distribution of major soil types in the Netherlands (Maschinen et al., 2012).

Nampula - Mozambique

Nampula is a province in the northern part of Mozambique and has a total area of 79.000 km². The Niassa Province borders Nampula to the north-west and west, the Zambezia Province to the south-west and the Indian Ocean is bordered to the east. The Ligonha River in the south-west of the area separates Nampula from Zambezia Province. In the west of are several hilly areas with mountains up to 1804m. Closer to the coastal area the land becomes less steep and near the coast, the rivers debouch into the Indian Ocean forming deltas at the northern and southern borders. The climate in Mozambique is tropical humid. There is a humid season from November to March and a dry season from April to October (Penvenne & Sheldon, 2020). Figure 4 shows the distribution of the major soil types in Nampula. The centre of the area is covered with Arenosols, with Lixisols to the east and west. The north-east of the area, from inland to the coast, is covered with Leptosols and Vertisols. The South-east of the area, also name from inland, is covered with Plansosols, Arenosols and Fluvisols (Maschinen et al., 2012).

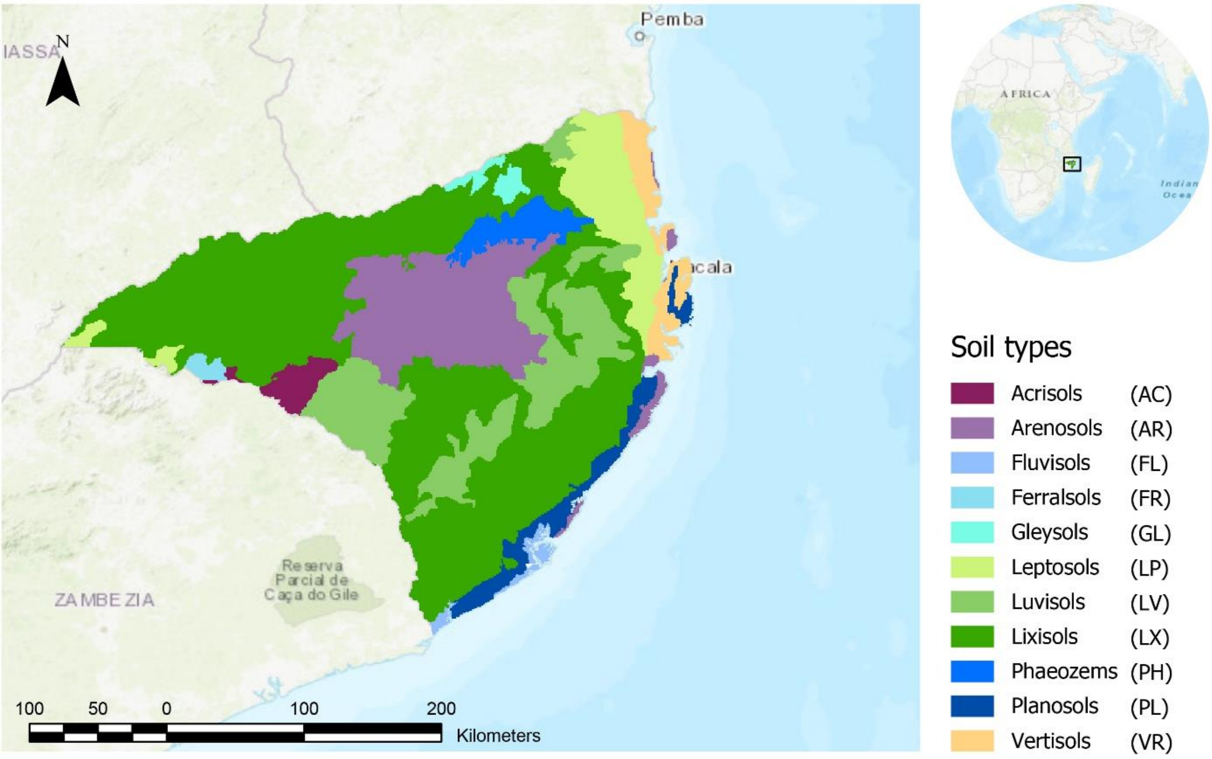

Figure 4. Distribution of major soil types in Nampula (Maschinen et al., 2012).

2.6 Data and materials

Three data sources were used in this research; soil sample data, a stack of covariate layers and the ESA land cover map. ISRIC provided all data, and therefore not much further pre-processing was needed.

SoilGrids Soil observations

The SoilGrids soil observations dataset is a compilation of hundred heterogeneous point datasets from all over the world that have been brought together in a standardised database (WoSIS). The WoSIS database itself is developed and maintained by ISRIC. The datasets which contribute to the final SoilGirds observations dataset are provided by several external soil-related organisations, governmental organisation and several databases available within ISRIC (e.g. WISE, AfSP and SCOTER) (Batjes et al., 2017).

For organic carbon, there are 152.350 records with soil sample locations and 602.979 soil observations in the Soil Sample dataset . For Soil pH, there are 150.798 records with soil sample data and 659.473 observation spread over all continents (see Figure 5). Not all observations are sampled observation. Besides the soil observations, the soil sample dataset also includes expert-based pseudo-observations. Some large areas that have extreme climatic conditions and/or have very restricted access are significantly under-sampled (e.g. Greenland, the Sahara or northern parts of Russia) (Hengl et al., 2017). Soil samples are a mix of profile data (described and sampled horizons) for fixed sample depths (de Sousa, n.d.).

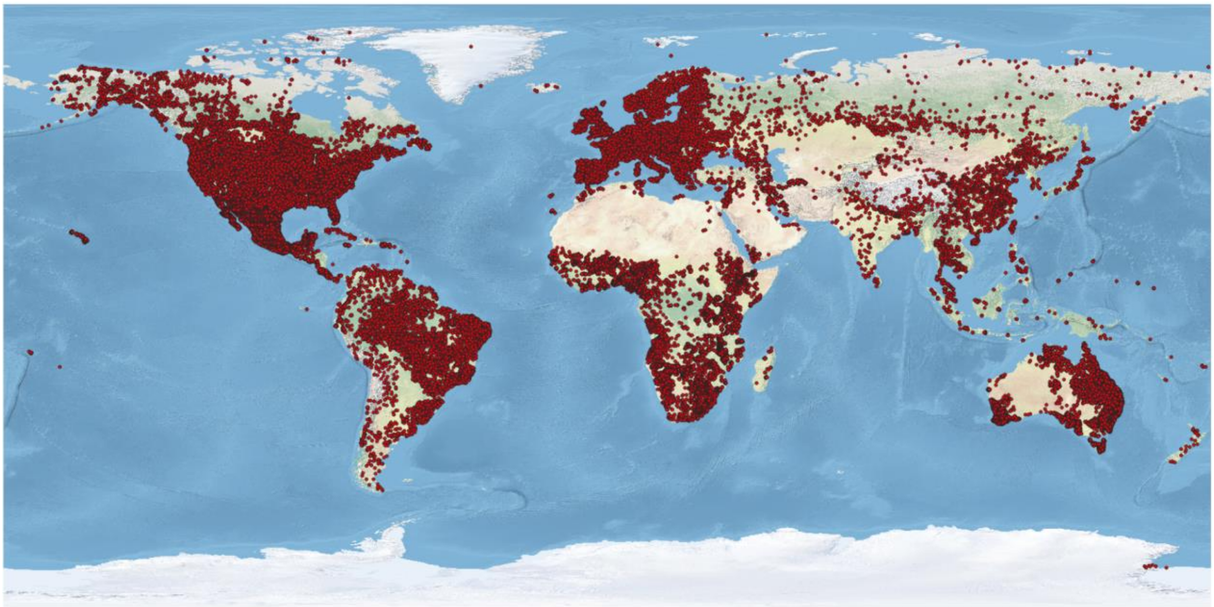

Figure 5. Locations of soil observations provided with the 'WoSIS September 2019 snapshot' (Batjes, Ribeiro, & Van Oostrum, 2020).

The soil data includes the profile location, sampling depth and the soil property values. An overview of the data is shown in table 5.

Table 5. Head of the global soil observations data.

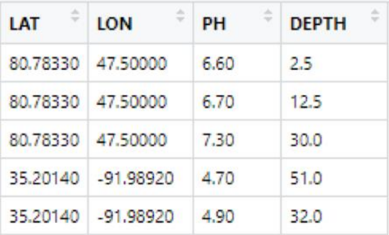

LAT	LON	PH	DEPTH
80.78330	47.50000	6.60	2.5
80.78330	47.50000	6.70	12.5
80.78330	47.50000	7.30	30.0
35.20140	-91.98920	4.70	51.0
35.20140	-91.98920	4.90	32.0

India soil observations

The India soil observations were derived from the Soil Health Card Scheme program. The Soil Health Card scheme is an initiative launched by the Government of India in 2015. Soil Health Cards were distributed to farmers all around India. A soil sample from the topsoil (0-15 cm depth) of the farmers' field was analysed in the lab on 12 parameters including soil pH and soil organic carbon content (Mishra, Nair, Singh, Gazeley, & Kapoor, 2015). These data were published as open data and downloaded by ISRIC. ISRIC pre-processed the data and harmonises it to the SoilGrids framework.

The India dataset represents 506704 soil sample locations covering the entire Andhra Pradesh region and represents profile location, and the soil property value (table 6). Because we wanted to assess the effect of adding new data and wanted to add a reasonable number of additional data points, only 10% of the data was used as training data and the remaining data as test data. To ensure that the spatial distribution of the data was retained during subsampling of the training data, the subsamples were based on a density estimate of the original observations. The r function Point process random subsample (pp.subsample) was used for this (Evans, 2018). The default settings of this model were used.

To merge the local (India) soil observations dataset and the SG_{Global} soil observations dataset , all covariates need a value for all locations. The column *'sample depth'* is not present in the India dataset and needed to be added. Because the soil observations in the India dataset are sampled at a sample depth between 0-15 cm, the average soil sample depth of 7.5 was used as sample depth for all soil samples.

Table 6. Head of the local soil observations data.

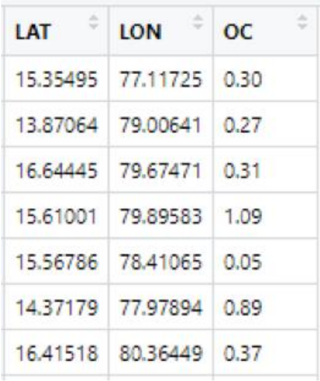

LAT	LON	OC
15.35495	77.11725	0.30
13.87064	79.00641	0.27
16.64445	79.67471	0.31
15.61001	79.89583	1.09
15.56786	78.41065	0.05
14.37179	77.97894	0.89
16.41518	80.36449	0.37

Soil properties and depths

The used soil properties for this research are; soil organic carbon (SOC) content in g/kg and soil pH in water. Organic carbon is together with pH, the best indicator of the health status of the soil structure (Maschinen et al., 2012). Therefore, the analysis was limited to these two soil properties.

This research focused on the 5-15 cm depth layer, as the new local soil sample data are enclosed in the selected depth interval. Research question 2 also focuses on the influence of new local soil samples on higher and lower depth intervals. Therefore, for research question 2; influence of new soil observations, the 0-5, 5-15 and 15-30 cm depth intervals are used, predicting at 2.5 cm, 10 cm and 22.5 cm depth.

Covariate stack

The original covariate stack consisted of 405 different covariates, which are primarily based on remote sensing data. These covariates were selected to represent factors of soil formation, according to Jenny, 1945. After the correlation analyses, performed by ISRIC, 129 covariates remained. Appendix II shows the table with all covariates and the description of their topic. All those covariates are stored in a raster stack with 250 x 250 m resolution and have the same spatial extent as the ESA land cover map

ESA land cover map

The global soil mask map derived from the latest ESA land cover map (Defourny, 2017) was used to mask out areas where no predictions of soil properties can be made because there is no soil present at these locations. Those areas were represented as NoData and turn up white in all maps. The classes Urban (code 190), inland water (code 210), glacier (code 220) and bare surface (code 200) were masked out as well (figure 5). No predictions are made for permanent ice areas since they are subject to extreme climatic conditions and therefore cannot be cultivated. The masked out areas are often under-represented in soil surveys, making it difficult to calibrate a reliable statistical model.

Statistical software

Analyses were conducted using freely available R software, which is a language and environment for statistical computing and graphics (The R Foundation, 2020). The advantage of using a scripting language is that the study is reproducible and reported in the scripts. The main Packages that were used during this research are shown in table 7.

Table 7. Used R libraries to create the results for the research.

Library	Usage
raster	manipulating and using calculations on raster data (Etten et al., 2020).
sp	manipulating and plotting spatial data (Hijmans et al., 2020).
caret	to create the random forest (ranger) and the RFE (Max et al., 2020).
tidyverse	gain RFE functionalities (Wickham, 2019).
devtools	Provide input data and functions to run the HomoSoil script (Hester, 2020).

3 Results

In this chapter, the results are described per research question. Results of modelling and mapping soil organic carbon and pH are provided separately, starting with the soil organic carbon results.

3.1 Comparison of a global and local SoilGrids model

The SG$_{Global}$ model and SG$_{Local}$ model were compared firstly by analysing the variables which were most important in explaining the soil property and by comparing model statistics. Next, the prediction maps and difference maps were assessed using descriptive statistics and visual comparison. Lastly, the accuracy of the map was evaluated based on scatter plots and RMSE, ME and R-squared.

3.1.1 Soil Organic Carbon content

Model comparison

Figure 6 shows the used covariates ranked by variable importance of the SG$_{Global}$ model. The full name of the covariates can be found in appendix II. From the 129 covariates presented to the RFE function, the SG$_{Global}$ model selected 45 covariates in total to represent the global area, while the SG$_{Local}$ model used 29 covariates. Both the global and the local model identified 29 identical covariates required to build an accurate model. What strikes is, from the top 4 covariates used by SG$_{Global,}$ the SG$_{Local}$ model used only one; total yearly radiation (CLM_WCL_SRCYRSUM). The remaining three global variables are, soil sample depth (DEPTH), SD yearly snowfall prob. at 500 m (CLM_ESA_SYRSTD) and annual temperature range (max temperature of the warmest month – min temperature of the coldest month) (CLM_WCL_BIO07). From the four most important covariates of SG$_{Local}$, two of them (total radiation for August; CLM_WCL_S08RAD and Digital Elevation model; MOR_ENV_DEMM) are also in the top 10 of the SG$_{Global}$ most important covariates. The other two, total monthly precipitation at 1 km for October (CLM_WCL_P10TOT) and precipitation of wettest quarter (CLM_WCL_BIO16), are in the bottom half of the SG$_{Global}$ covariate importance.

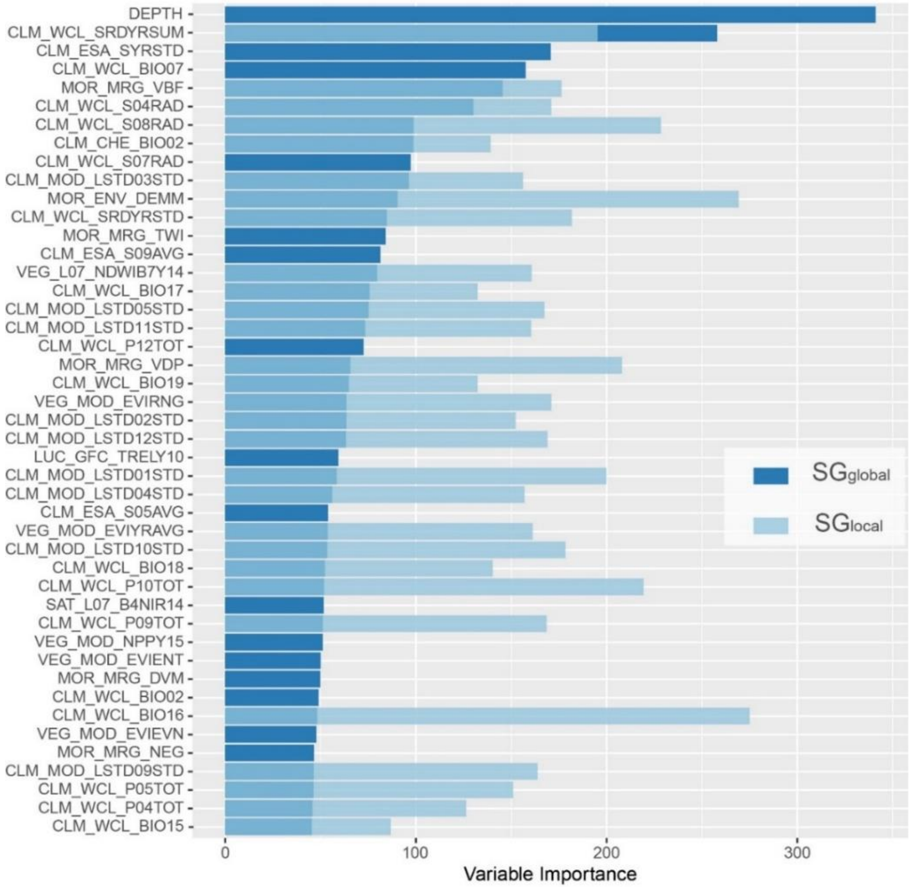

Figure 6. Variable importance of the SG$_{Global}$ and SG$_{Local}$ SOC models ranked by SG$_{Global}$ variable importance.

Map comparison

The SG_{Local} and SG_{Global} SOC prediction maps are shown on the right side of figure 7. The SG_{Local} map (top right) predicts SOC percentage between 0% and 1% SOC in the south with some higher predictions to the north. The SG_{Global} prediction map mainly shows predictions between 1.5% and 5% SOC, with some lower predictions in the south-west.

he differences map between the SG_{Global} and the SG_{Local} predictions is shown on the left side in Figure 7. Areas with relatively high SOC (between -2% and -3 % SOC difference) in the north correspond to forest areas and the areas in the south to mountain areas. For those areas the SG_{Global} model predicts a higher pH than the SG_{Local} model. Most other areas representing a difference between -0.5% and -1.5% SOC. This implies that the SG_{Global} model predicts higher SOC than the SG_{Local} model, which also shows op in Table 8. The mean difference is -0.41% SOC, revealing that SG_{Global} predicts overall higher SOC values. The absolute mean, which shows the mean deviation between the maps without taking into account which model predicts higher, is 1.41% SOC. If the observed statistics are compared to the predicted statistics of both models, SG_{Local} seems to do a better job.

Table 8. Descriptive statistics of the SOC models vs Observed values in Andhra Pradesh in % SOC.

	SG_{Local}	SG_{Global}	Observed	Difference SG_{Local} - SG_{Global}
Min.	0.07	0.76	0.02	-7.29
1st Qu.	0.42	1.59	0.32	-1.71
Median	0.53	2.01	0.49	-1.27
Mean	0.71	2.13	0.58	-0.41
3rd Qu.	0.68	2.51	0.72	-0.94
Max.	2.47	9.23	2.60	0.95
Abs Mean				1.41

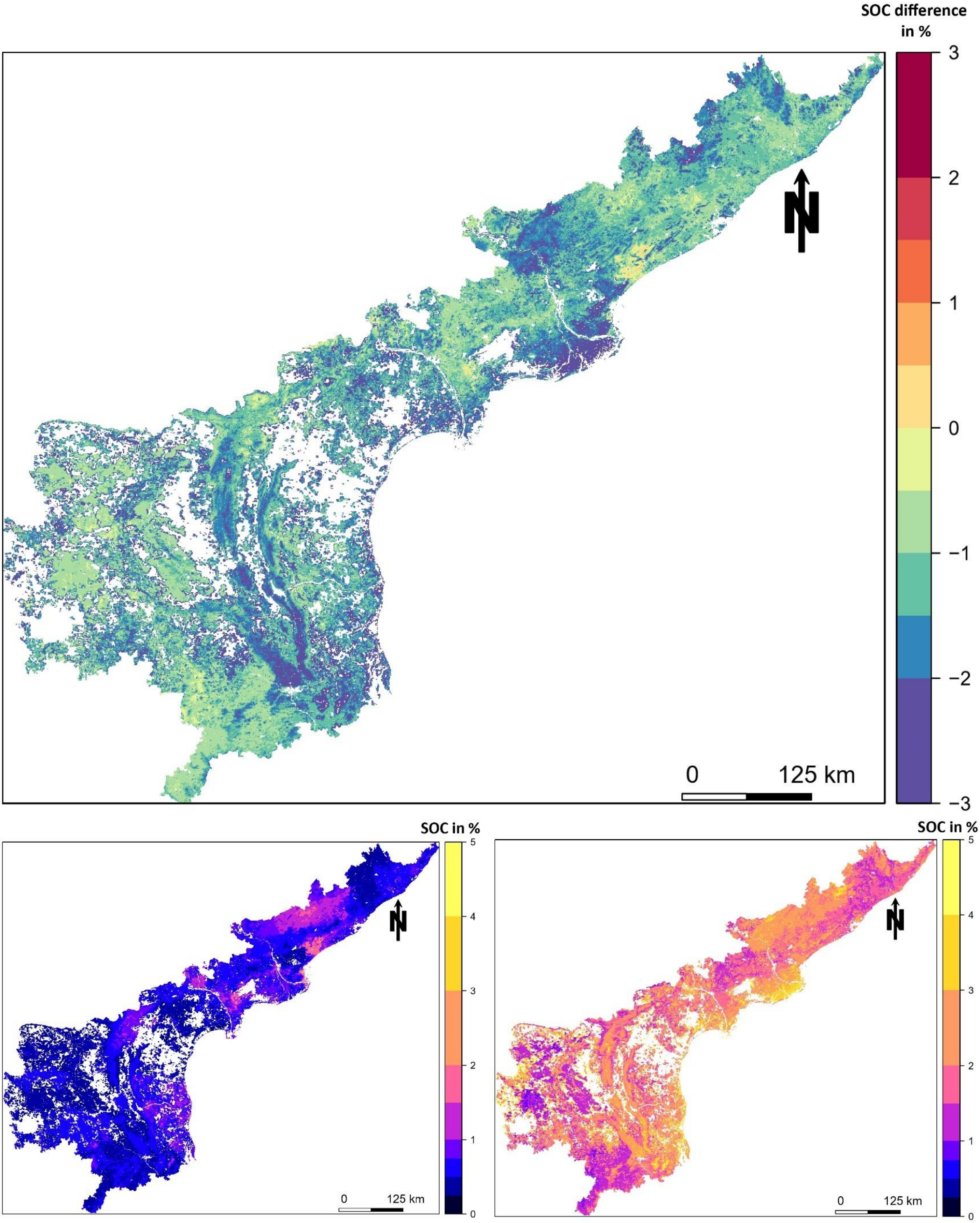

Figure 7. Soil pH prediction maps and difference map (top) of SG$_{Local}$ (bottom left) and SG$_{Global}$ (bottom right) for Andhra Pradesh - India.

Accuracy

To evaluate if SG_{Local} is more accurate than SG_{Global}, scatter plots of the model predictions for the Organic Carbon models (Figure 8) were made. These plots show the predicted values vs the observed values and a 1:1 line. The more the dots are aligned around the line, the closer the predicted values are to the observed values. The observed values are based on the testing dataset of India, hence the scatter plots and the descriptive statistics (Table 9) are only representative for Andhra Pradesh. The legend shows the number of predictions per plot-pixel.

The SG_{Global} scatter plot shows that most of the dots are below the 1:1 line, indicating that the model predicts higher SOC values than observed. The scatterplot modelled with global data only, shows the densest area for predicted SOC between 1.2% and 1.9% SOC, while the densest area for observed SOC values is between 1.2% and 2.2% SOC. This also shows in the descriptive statistics (Table 9), where SG_{Global} scores much higher for each validation metric. Therefore, the difference map shows more negative than positive values. The scatter plot of the SG_{Local} model is more around the 1:1 line.

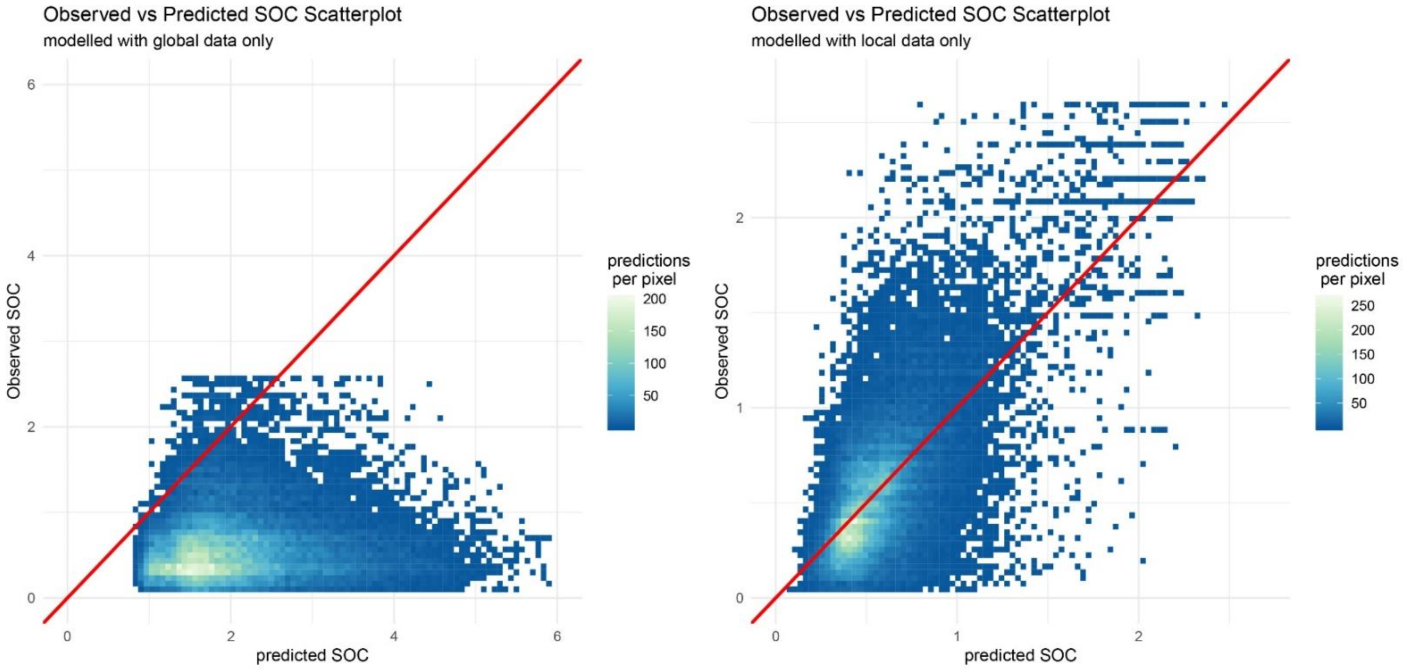

Figure 8. Scatterplots of the global (left) and local (right) SOC model.

Table 9. Descriptive statistics of the global and local SOC models with SOC in %.

	SG_{Local}	SG_{Global}
RMSE (% SOC)	0.286	1.720
ME	0.008	1.497
R^2 (% of the variation)	42.5	0.4

3.1.2 Soil pH

Model comparison

After the RFE for the soil pH models, the SG$_{Global}$ model selected 31 covariates and SG$_{Local}$ model selected 29 covariates (Figure 9). 23 covariates were identically selected in both models. The top five covariates of the SG$_{Global}$ model only have one covariate that was also selected for the SG$_{Local}$ model; total monthly precipitation at 1 km in April (CLM_WCLP04TOT). The other four were not selected; global 30m tree cover (LUC_GFC_TRELY10), soil sample depth (DEPTH), total monthly precipitation at 1 km in October (CLM_WCL_P10TOT) and precipitation of wettest quarter (CLM_WCL_BIO16). Of the four most interesting peeks in SG$_{Local}$, two are in the lowest 8 covariates of SG$_{Global}$; Total monthly precipitation at 1 km for September (CLM_WCL_P09TOT) and Precipitation of Warmest Quarter (CLM_WCL_BIO18). SG$_{Global}$ does not use one of the four most important covariates of the SG$_{Local}$ model; Bioclimatic zones: zone 32 (ECO_USG_Z32).

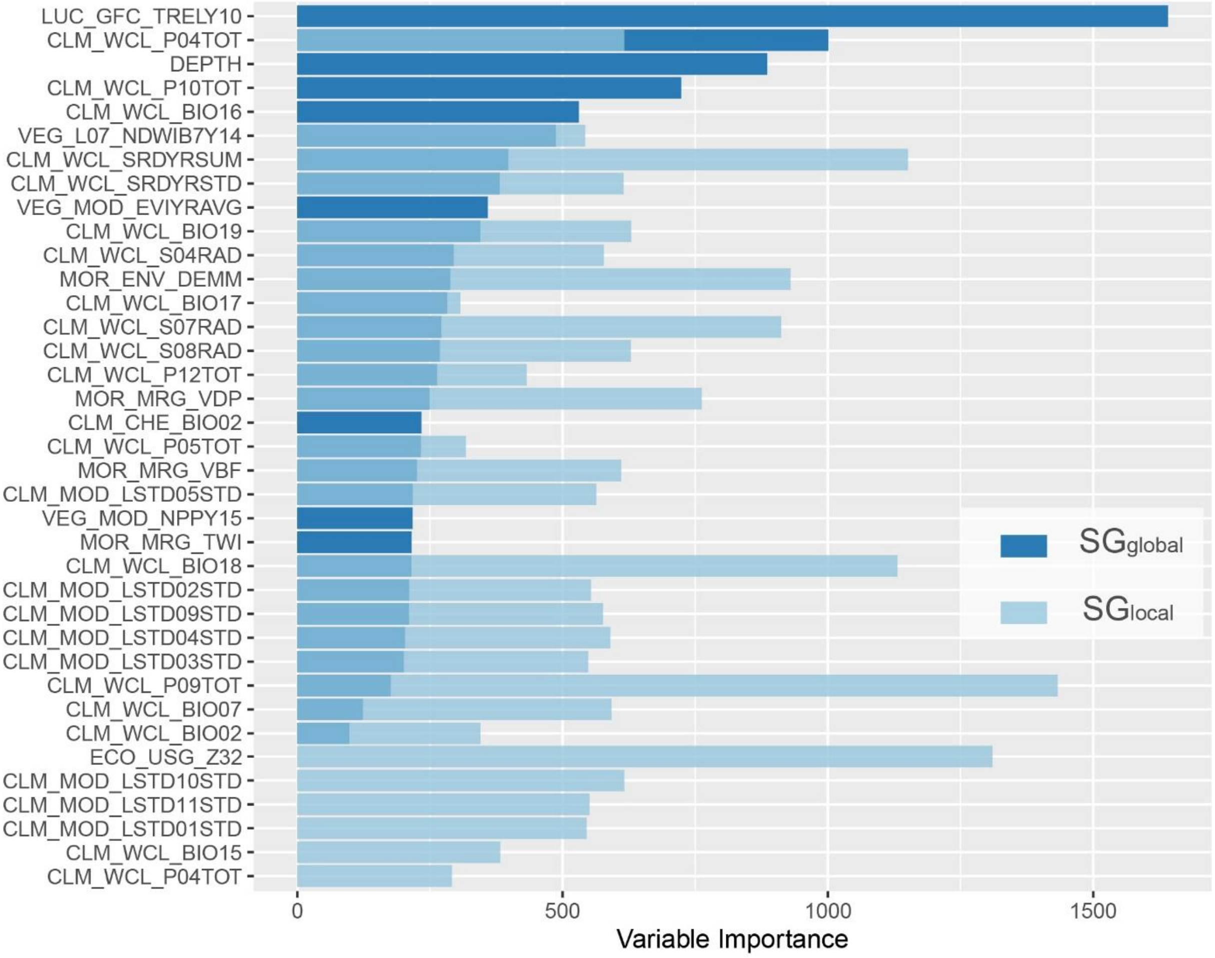

Figure 9. Variable importance of the global and local soil pH models.

Map comparison

The left map in Figure 10 shows the pH difference map between SG_{Local} minus SG_{Global}. The legend represents the difference between the two models in soil pH. Most of the map is represented by areas where SG_{Local} predicts a higher pH than SG_{Global}. This also shows in the mean of the descriptive statistics table (Table 10), where SG_{Global} has a mean of 6.73 pH and SG_{Local} a mean of 7.37 pH. Other descriptive statistics show that the SG_{Global} and SG_{Local} model predicts 0.64 and 0.38 pH higher than the minimum soil observation. The maximum pH predicted with the SG_{Global} model is 0.9 pH lower than the maximum prediction of soil pH, while SG_{Local} has a 0.07 pH difference.

Table 10. Descriptive statistics of the Soil pH models vs Observed values in Andhra Pradesh.

	SG_{Local}	SG_{Global}	Observed	Difference SG_{Local} - SG_{Global}
Min.	5.18	5.44	4.80	-1.81
1st Qu.	7.01	6.46	6.90	0.24
Median	7.29	6.80	7.41	0.51
Mean	7.37	6.73	7.38	0.52
3rd Qu.	7.79	7.05	7.90	0.81
Max.	9.05	8.01	9.12	2.22
Abs Mean				0.56

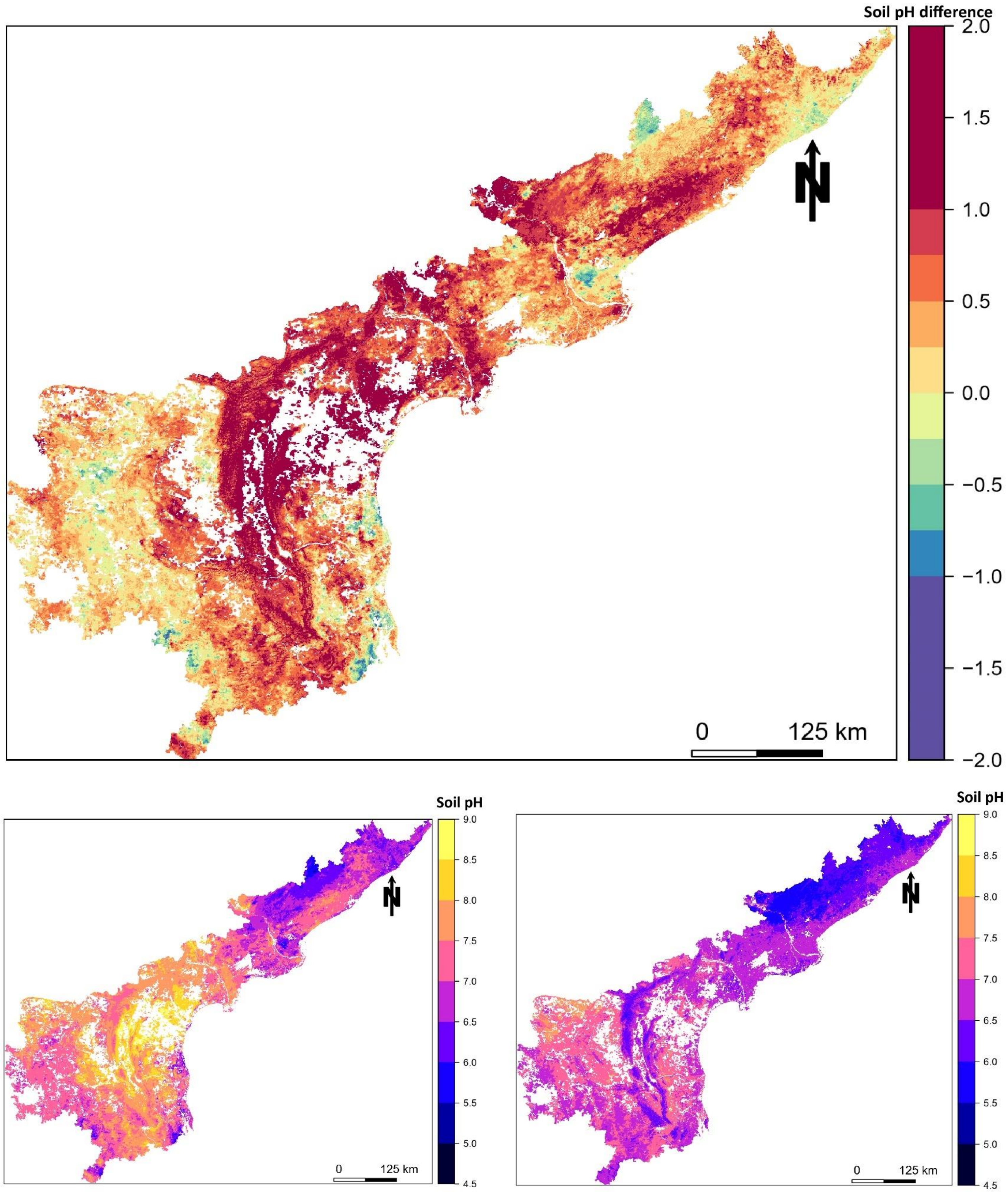

Figure 10. Soil pH prediction maps and difference map (top) of SG_{Local} (left) and SG_{Global} (right) for Andhra Pradesh.

Accuracy

Figure 11 shows scatter plots of the SG$_{\text{Global}}$ and SG$_{\text{Local}}$ models. Note that the observed values are based on the testing dataset of India, meaning that the scatter plots and the statistics are only representative for Andhra Pradesh. The scatter plot modelled with global data shows that the densest point area lies above the 1:1 line, meaning the model predicts lower soil pH values than observed. This also shows in the descriptive statistics (Table 10) where the SG$_{\text{Global}}$ model prediction mean is 0.85 pH units lower than the observed value mean.

The scatter plot modelled with local data only is close to the 1:1 line. The predicted values below 7.5 pH diverge a bit below the 1:1 line, indicating that the model predicts too high pH values, while the predicted values above 7.5 pH diverge a bit above the 1:1 line, indicating the model predicts too low. This also shows in the descriptive statistics (Table 11), the minimum value is higher than the observed value, while the maximum predictive value is lower than the observed value.

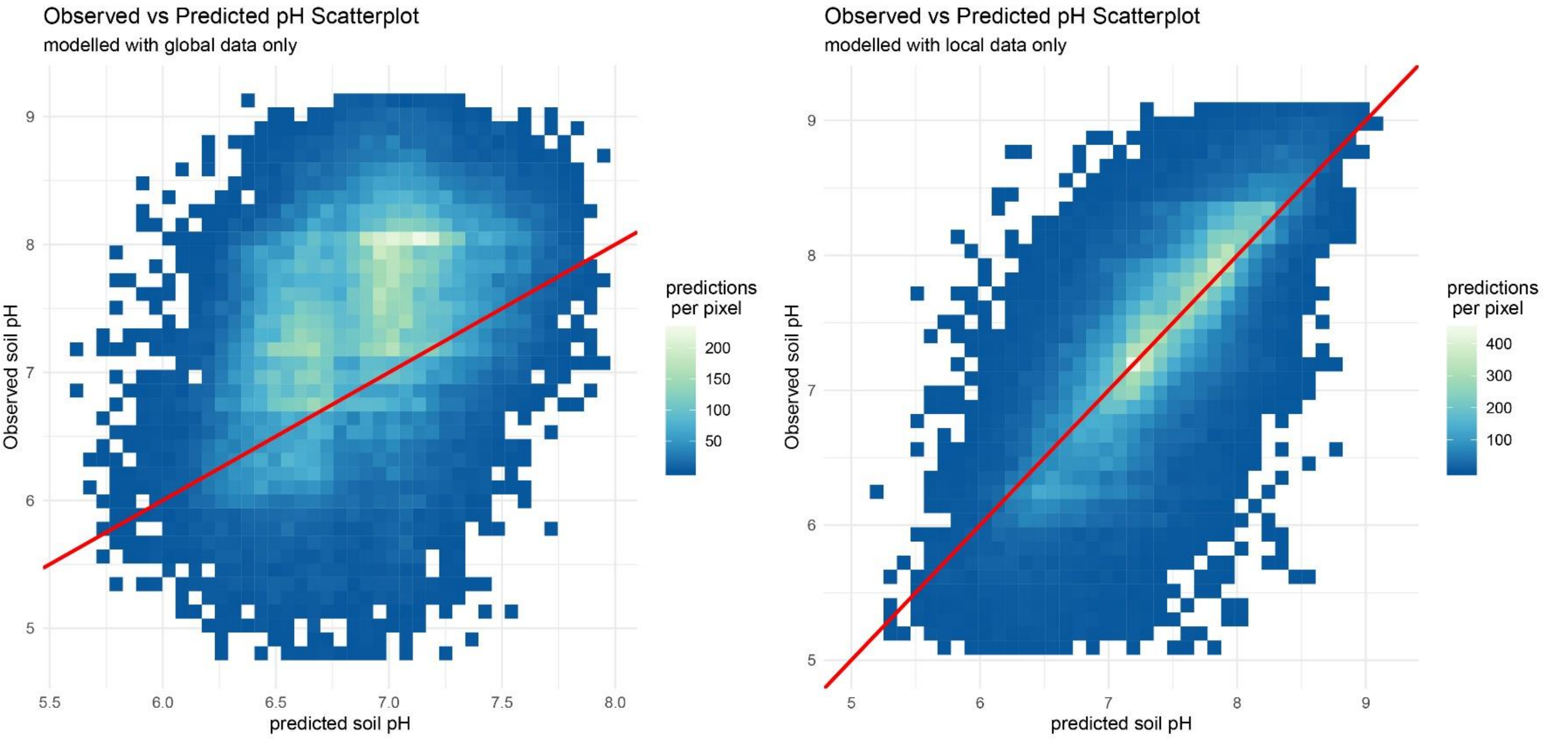

Figure 11. Scatterplots of the global (left) and local (right) soil pH model.

Table 11. Descriptive statistics of the local and Global soil pH models.

	SG$_{\text{Local}}$	SG$_{\text{Global}}$
RMSE (soil pH)	0.467	0.837
ME	-0.001	-0.490
R^2 (% of the variation)	59.1	14.6

3.2 Influence of new soil observations

For each study area, the difference maps between SG$_{plus}$ and SG$_{Global}$ (SG$_{plus}$ minus SG$_{Global}$) are shown per soil property at three different depths. The main highlights per study area and soil property are stated, starting with Andhra Pradesh, then Nampula and ending with The Netherlands. The section starts with the model statistics and variable importance.

3.2.1 model comparison

Figure 12 shows the variable importance for the SG$_{Global}$ and SG$_{Plus}$ models for SOC. Both models use the same RFE selected covariates, but the importance deviates. In the top four most important covariates from the SG$_{Global}$ models the CLM_WCL_SRDYRSUM (Total Yearly Solar radiation at 1 km), CLM_ESA_SYRST (SD yearly snowfall prob. at 500 m) and CLM_WCL_BIO07 (annual temperature range; maximum temp of the warmest month minus minimum temp of the coldest month) deviate most.

Table 12 shows the OOB error statistics for the SG$_{Global}$ and SG$_{Plus}$ models. The OOB error is based on all global observations. The RMSE is lower for the SG$_{Plus}$ model and the ME is even significantly lower for the SG$_{Plus}$. The R2 however is almost equal.

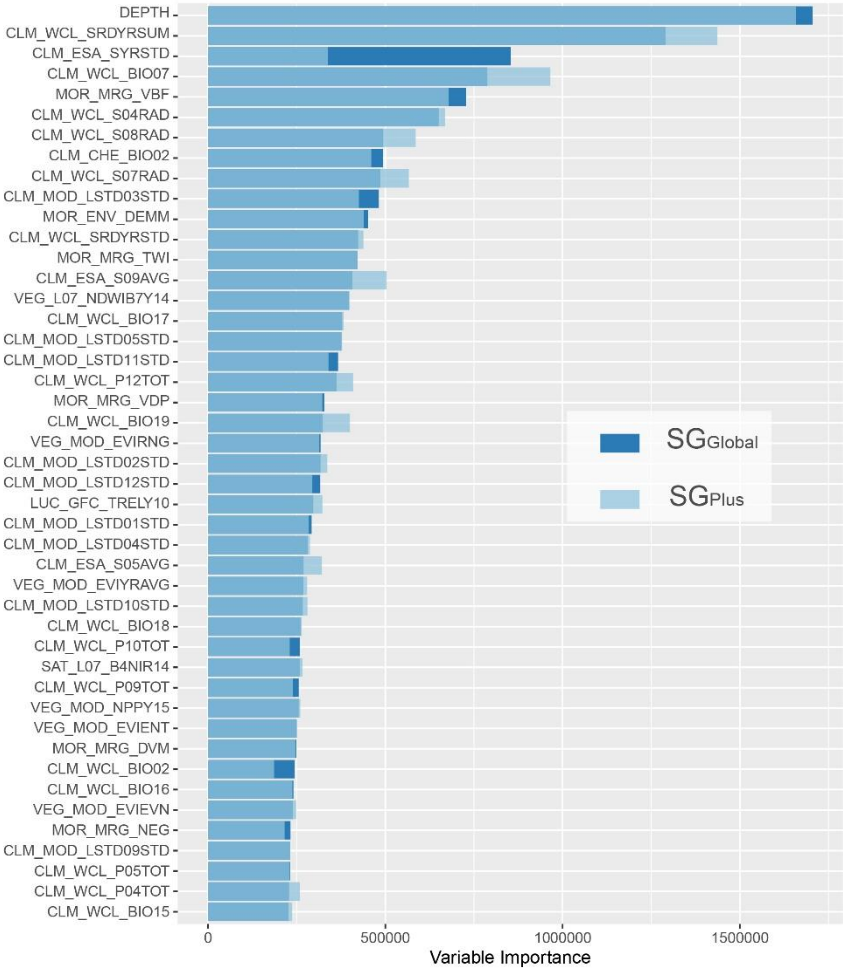

Figure 12. Variable importance of the SG$_{Global}$ and SG$_{Plus}$ SOC models based on the variable importance ranking of SG$_{Global}$.

Table 12. OOB statistics for SG$_{Global}$ and SG$_{Plus}$ for SOC (%).

	SG$_{Global}$	SG$_{Plus}$
RMSE (% SOC)	3.056	2.950
ME	9.341	8.704
R^2 (% of the variation)	71.7	72.1

Figure 12 shows the variable importance for the SG_{Global} and SG_{Plus} models for soil pH. Both models use the same RFE selected covariates, but the importance deviates. From the six most deviation covariate importance, five are the top five most important covariates from the SGGlobal model. Those covariates are; LUC_GFC_TRELY10 (Global 30m Tree Cover), Depth (sample depth), CLM_WCL_P04TOT (Total monthly precipitation at 1 km for April), CLM_WCL_P10TOT (Total monthly precipitation at 1 km for October) and CLM_WCL_BIO16 (Precipitation of Wettest Quarter). The other deviating covariate is CML_WCL_BI09 (Mean Temperature of Driest Quarter).

Table 12 shows the OOB error statistics for the SG_{Global} and SG_{Plus} models. All model statistics are almost equal for both models, but the SG_{Plus} model scores slightly better.

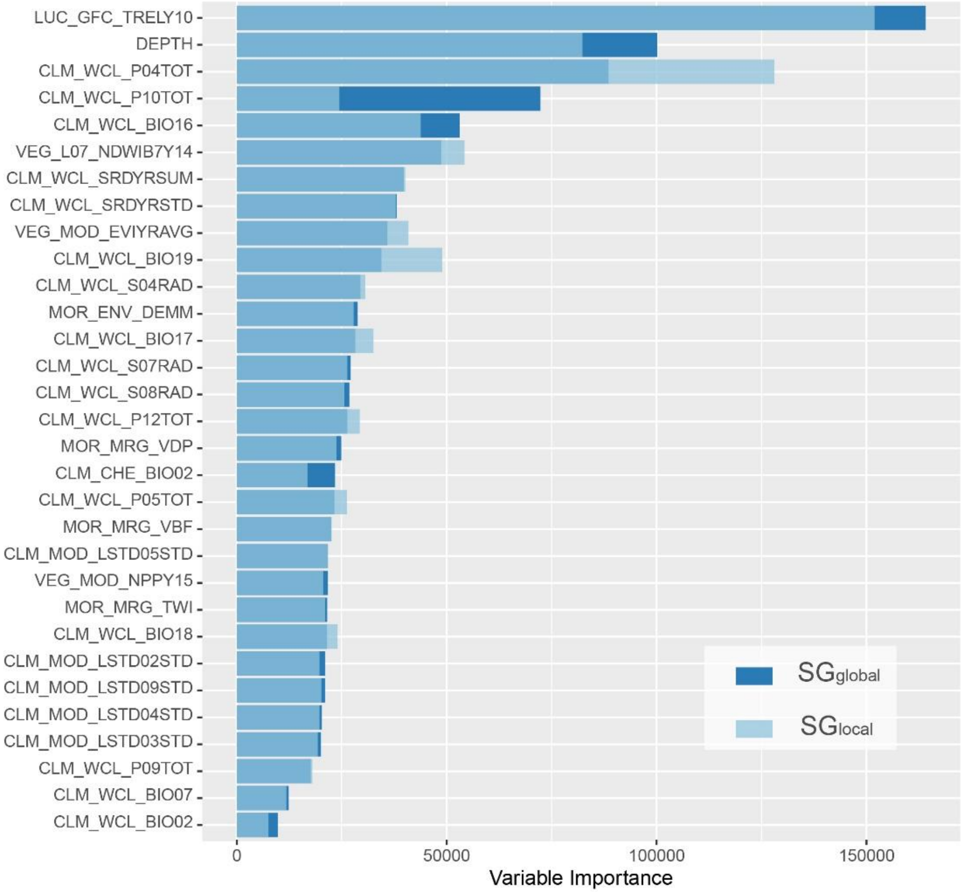

Figure 13.Variable importance of the SG_{Global} and SG_{Plus} soil pH models.

Table 13. OOB statistics for SG_{Global} and SG_{Plus} for soil pH.

	SG_{Global}	SG_{Plus}
RMSE (pH)	0.539	0.535
MSE	0.290	0.286
R^2 (% of variation)	0.842	0.842

3.2.2 Andhra Pradesh

Organic Carbon

The 0-5 cm depth map (left map of Figure 14) shows mainly areas with a difference between 0% and -1% SOC. In the centre of the area and in the south-west part, the difference is between -1% and -3% SOC. In the south-east part, the difference is between 1% and 2% SOC. This also shows in the statistics table (Table 14) where the difference between the SG_{Plus} and the SG_{Global} mean is 0.35% SOC, the least difference of all three SOC depth maps. The minimum and median are similar, while the maximum deviates around 1% SOC.

The 5-15 cm depth map (middle map of Figure 14) shows mainly areas with a difference between -2% and -3% SOC. This means the SG_{Global} model predicts higher SOC values than the SG_{Plus} model. This also shows in the statistics table, where the mean of SG_{Plus} is 0.71% SOC, and the mean of SG_{Global} is 2.13 % SOC. This is the highest mean difference between all three SOC depth maps.

The 15-30 cm depth map (right map of Figure 14) shows mainly areas with a deviation between 0% and -1% SOC. The southern part of the area shows a deviation between -1% till -2% SOC, with in northern part a small area representing a difference between 0.5% and 1.5% SOC. The statistics table also shows that the SG_{Global} predictions are higher than the SG_{Local} predictions, though the mean difference is smaller than the 5-15 cm depth map.

Table 14. Statistics table of SOC (%) in Andhra Pradesh – India.

	0 - 5 cm		5 - 15 cm		15 - 30 cm	
	SG_{Plus}	**SG_{Global}**	**SG_{Plus}**	**SG_{Global}**	**SG_{Plus}**	**SG_{Global}**
Min.	0.76	0.89	0.08	0.76	0.17	0.58
Median	2.37	2.75	0.63	2.01	0.76	1.43
Mean	2.55	2.90	0.71	2.13	0.84	1.59
Max.	11.1	10.00	7.22	9.23	7.26	9.34

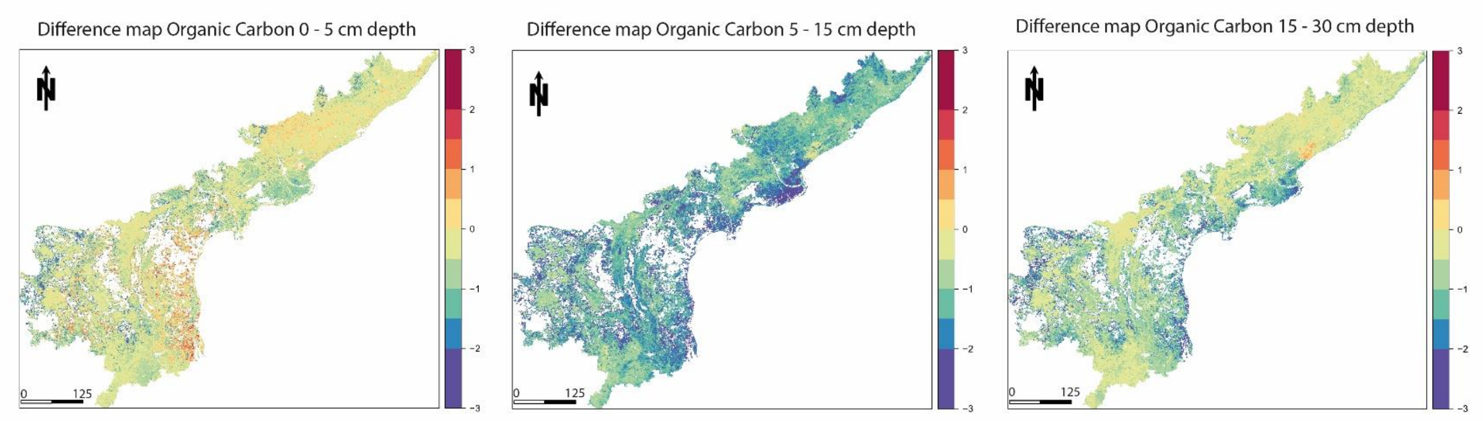
Difference map Organic Carbon 0 - 5 cm depth
Difference map Organic Carbon 5 - 15 cm depth
Difference map Organic Carbon 15 - 30 cm depth
N
0
125
3
2
1
0
−1
−2
−3

Figure 14. Difference maps of SOC (%) for three interval depths.

Soil pH

Figure 15 shows the difference maps of soil pH for Andhra Pradesh. The difference maps for al depths show similar patterns, where the 0-5 cm depth map has the least deviation, meaning the difference between the model results is lower. The 5-15 cm and 15 – 30 cm depth maps have the most deviation, meaning the difference between the model results is larger. The largest difference areas, where the $\mathrm{SG}_{\mathrm{Plus}}$ model predicts higher, are located in the centre of the difference maps. Closer to the borders, the difference gets less and there are some areas near the border where the $\mathrm{SG}_{\mathrm{Global}}$ predicts higher soil pH. Table 15 shows that all the differences between de statistics are largest for the 5-15 cm depth map and smallest for the 0-5 cm depth map. The median, mean and max are for all $\mathrm{SG}_{\mathrm{Plus}}$ models at all tree depths higher than the $\mathrm{SG}_{\mathrm{Global}}$ model.

Table 15. Statistics table of soil pH for Andhra Pradesh – India.

	0 - 5 cm		5 - 15 cm		15 - 30 cm	
	$\mathrm{SG}_{\mathrm{Plus}}$	**$\mathrm{SG}_{\mathrm{Global}}$**	**$\mathrm{SG}_{\mathrm{Plus}}$**	**$\mathrm{SG}_{\mathrm{Global}}$**	**$\mathrm{SG}_{\mathrm{Plus}}$**	**$\mathrm{SG}_{\mathrm{Global}}$**
Min.	5.24	5.47	5.18	5.44	5.20	5.41
Median	7.22	6.75	7.29	6.80	7.28	6.85
Mean	7.15	6.70	7.26	6.73	7.25	6.77
Max.	8.69	7.00	9.05	8.01	8.97	7.92

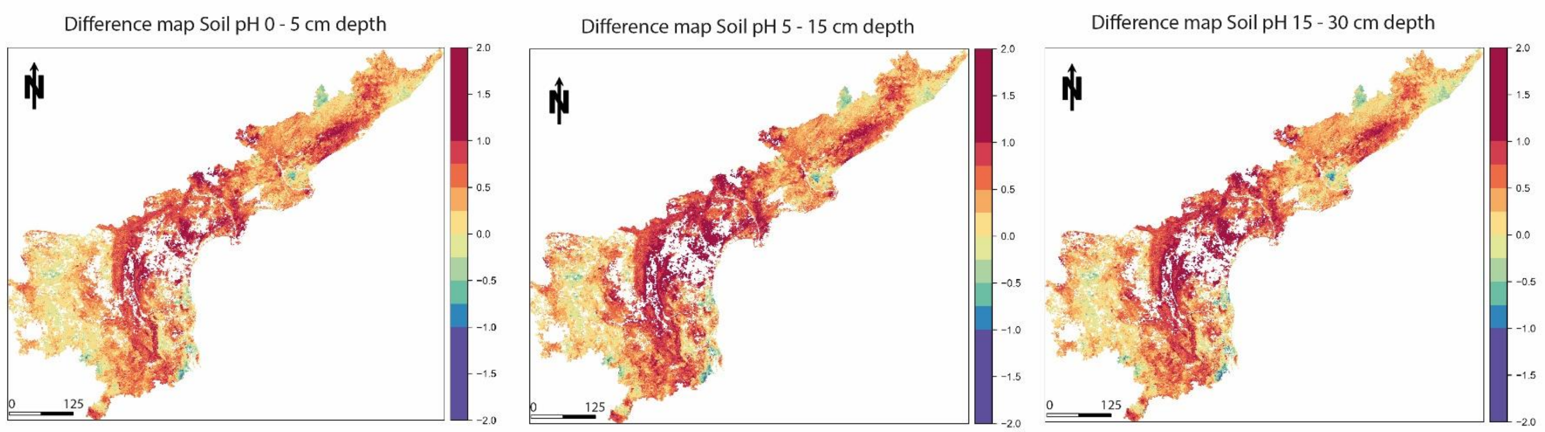
Difference map Soil pH 0 - 5 cm depth
Difference map Soil pH 5 - 15 cm depth
Difference map Soil pH 15 - 30 cm depth
N
0
125
2.0
1.5
1.0
0.5
0.0
−0.5
−1.0
−1.5
−2.0

Figure 15. Difference maps of soil pH for three interval depths, Andhra Pradesh – India.

3.2.3 Nampula

Organic Carbon

Figure 16 shows the results for Organic Carbon in Nampula. Overall, the three depth maps do not show substantial differences. In the 0 - 5 cm depth map, the most considerable difference is located in the north-east and south-eastern part of the area (near the coast). In the north-eastern part of the area, there is a small strip where the deviation is between -1% and -1.5% SOC. In the south-eastern part of the area, there is a small area where the deviation is between 1% and 2% SOC.

At the eastern border of the 5-15 cm depth difference map, there is a deviation between -1% and -3% SOC. In the southern point of the study area, there is a deviation between 0.5% and 1% SOC. In the 16 – 30 cm depth map, the same areas show the most considerable differences, where the deviation in the south is more spread. The statistic table for Organic Carbon (Table 16) also shows that the deviation between the two models for all depths is small. The maximum mean deviation is 0.5% SOC, and the min, max and median for each model and depth are almost equal.

Table 16. Statistical table of SOC (%) in Nampula – Mozambique.

	0 - 5 cm		5 - 15 cm		15 - 30 cm	
	SG_{Plus}	SG_{Global}	SG_{Plus}	SG_{Global}	SG_{Plus}	SG_{Global}
Min.	0.73	0.73	0.34	0.33	0.40	0.34
Median	1.57	1.54	1.31	1.28	1.05	1.02
Mean	1.70	1.66	1.38	1.36	1.13	1.08
Max.	13.63	15.96	9.08	12.34	7.94	9.17

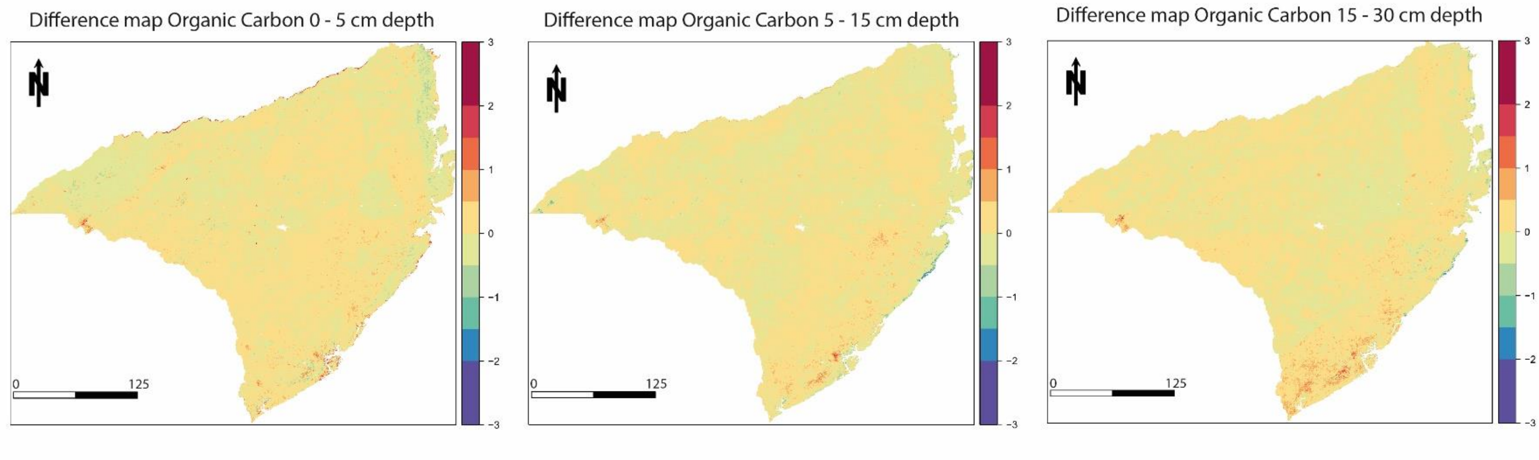
Difference map Organic Carbon 0 - 5 cm depth
Difference map Organic Carbon 5 - 15 cm depth
Difference map Organic Carbon 15 - 30 cm depth
N
0
125
3
2
1
0
-1
-2
-3

Figure 16. Difference maps of SOC (%) for three interval depths, Nampula – Mozambique.

Soil pH

Figure 17 shows that the difference map for soil pH for all three depth is almost equal. The areas with a difference higher than 0.25 pH show near the east border a slightly bigger area in the 15-30 cm depth map than the 0-5 cm depth map, but the areas with a difference higher than 0.25 pH in the western part of the area shows less dark red in the 15-30 cm depth map. This also shows in the statistic table for soil pH (Table 17), the mean of all predictions is equal for 0-5 and 5-15 cm depth and differs 0.01 pH of 15-30 cm depth.

Table 17. Statistical table of soil pH in Nampula – Mozambique.

	0 - 5 cm		5 - 15 cm		15 - 30 cm	
	SG$_{Plus}$	**SG$_{Global}$**	**SG$_{Plus}$**	**SG$_{Global}$**	**SG$_{Plus}$**	**SG$_{Global}$**
Min.	5.13	5.19	5.13	5.15	5.08	5.08
Median	6.07	6.07	6.06	6.06	6.04	6.03
Mean	6.08	6.08	6.07	6.07	6.05	6.04
Max.	7.62	7.62	7.72	7.66	7.70	7.65

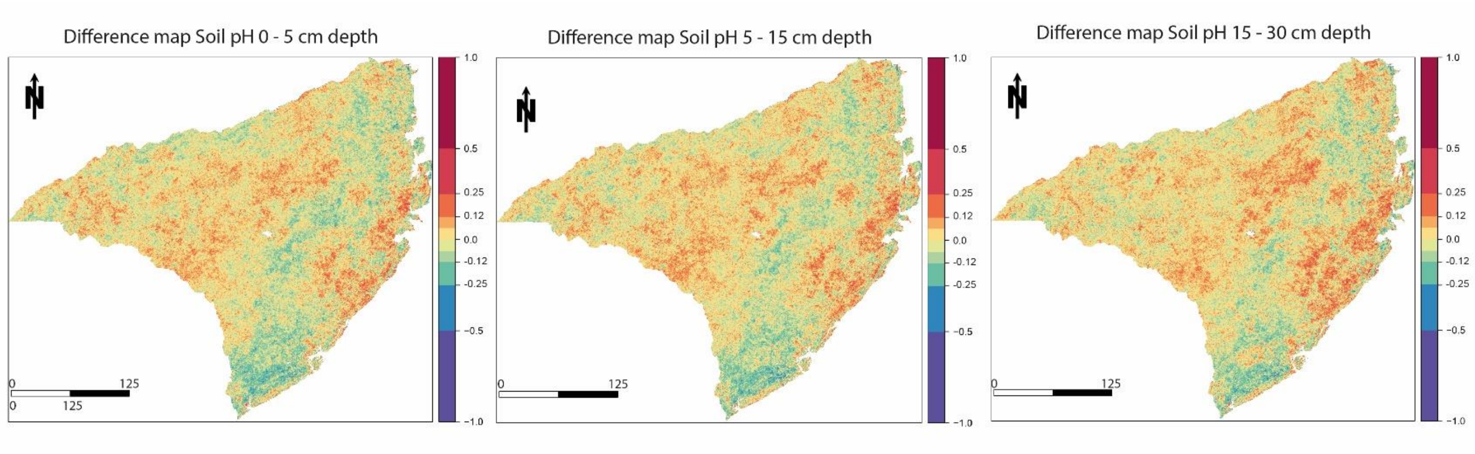

Difference map Soil pH 0 - 5 cm depth

Difference map Soil pH 5 - 15 cm depth

Difference map Soil pH 15 - 30 cm depth

Figure 17. Difference maps of soil pH for three interval depths, Nampula – Mozambique.

3.2.4 Netherlands

Organic Carbon

The 0-5 depth difference map (Figure 18, left map) shows big areas with large differences in the northern and north-eastern part of the area and some in the western part, where the SG_{Plus} model predicts between -1.5% and -2% SOC higher. The centre and southern part of the area show a significant amount of pixels indicating that the SG_{Global} model predicts higher SOC values than the SG_{Local} model. The statistics table (Table 18) also shows that the means are quite similar, but a slightly higher mean for SG_{Plus}; SG_{Plus} 9.82% and SG_{Global} 9.40% SOC.

The 5-15 cm Organic Carbon difference map shows an area of predominantly large differences (between 1.5% and 3% SOC) in the northern part of the Netherlands. This indicates that the SG_{Plus} model predicts higher Organic Carbon than the SG_{Global} model. Compared to the 0-5 and 15-30 cm depth maps, this prediction maps shows the least deviation, indicating that the model predictions are close to each other. The means of both maps are similar.

The 15-30 cm depth map shows bigger areas with higher negative differences (between -2% and -3% SOC) than the other depth maps. Those areas indicate that SG_{Global} predicts a higher SOC %. Only the centre and southern part of the area show small dense areas of positive prediction values, which indicates that the SG_{Global} model predicts higher SOC values that the SG_{Plus} model. The statistics table shows that the median and mean both are around 1 % higher for SG_{Global} than for $SG_{Local.}$

Table 18. Statistical table of SOC (%) in the Netherlands.

	0 - 5 cm		5 - 15 cm		15 - 30 cm	
	SG_{Plus}	**SG_{Global}**	**SG_{Plus}**	**SG_{Global}**	**SG_{Plus}**	**SG_{Global}**
Min.	1.90	1.88	1.23	1.16	0.61	0.53
Median	9.88	9.41	5.09	4.85	6.63	7.49
Mean	9.82	9.40	5.48	5.18	7.11	8.11
Max.	37.71	36.18	36.78	34.87	42.44	43.66

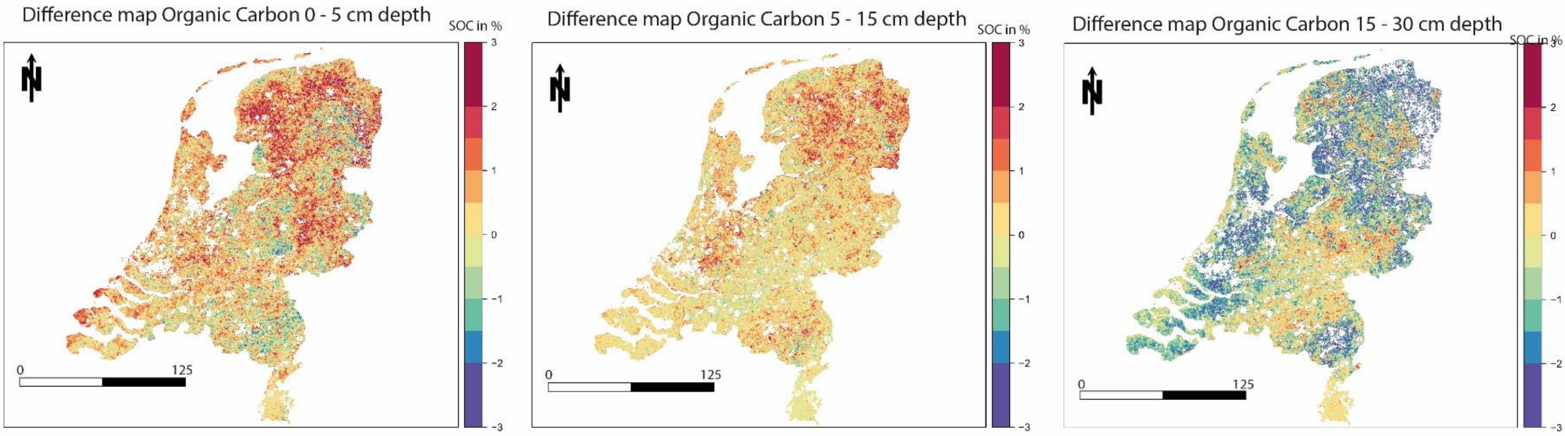

Difference map Organic Carbon 0 - 5 cm depth

Difference map Organic Carbon 5 - 15 cm depth

Difference map Organic Carbon 15 - 30 cm depth

Figure 18. Difference maps of soil SOC (%) for three interval depths in the Netherlands.

Soil pH

The 0-5 cm depth map (Figure 19, left map) shows the most diverge results of the three difference maps. Equally spread over the entire area, there are clusters of high difference areas (between 0.25 and 1 pH) and areas with low differences (around 0.0 pH). In between there are some outliers till -1 pH. Still, the overrepresented deviation between 0.5 and 1 pH indicates that the SG_{Plus} model predicts higher pH values than the SG_{Global} model. The statistical table (Table 19) only shows a difference of 0.04 pH in the mean of the predictions.

The difference maps for 5-15 cm and 15-30 cm depth (Figure 19, middle and right map) are quite similar. There is a cluster of high deviation (0.5 pH till 1.0 pH) near the western part, but no future outstanding areas with high differences. The rest of the area deviates between 0.5 pH and -0.5 pH deviation. The statistics table shows no significant differences between the two models.

Table 19. Statistical table of soil pH in the Netherlands.

	0 - 5 cm		5 - 15 cm		15 - 30 cm	
	SG_{Plus}	**SG_{Global}**	**SG_{Plus}**	**SG_{Global}**	**SG_{Plus}**	**SG_{Global}**
Min.	3.69	3.69	3.75	3.74	3.82	3.79
Median	5.98	5.99	6.01	6.01	7.61	5.99
Mean	5.94	5.90	6.13	6.12	6.11	6.11
Max.	8.18	8.13	8.07	8.05	7.26	9.34

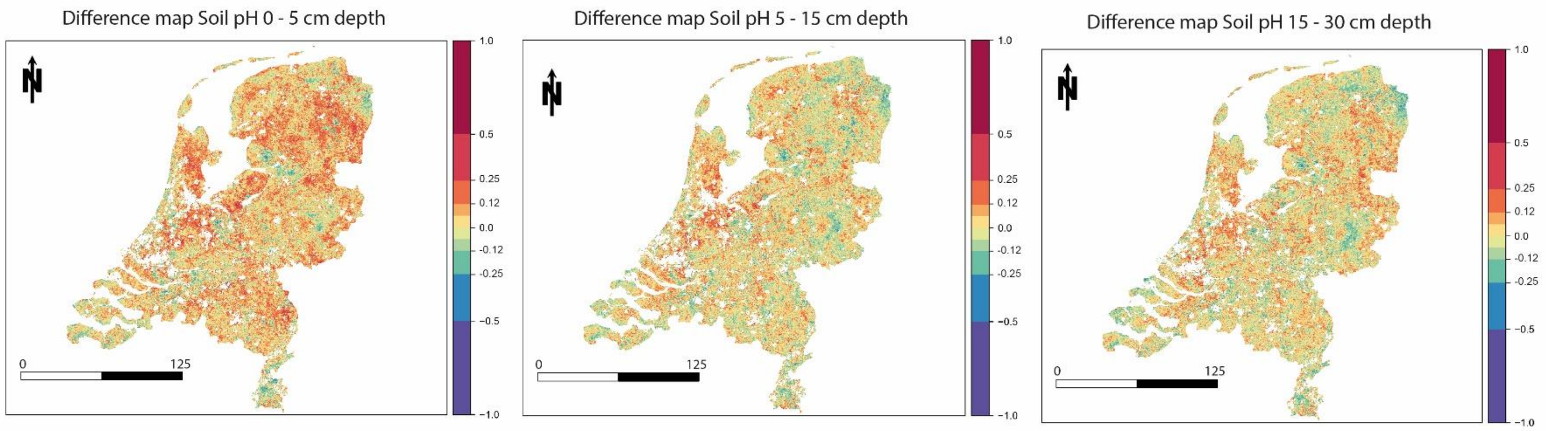
Difference map Soil pH 0 - 5 cm depth
Difference map Soil pH 5 - 15 cm depth
Difference map Soil pH 15 - 30 cm depth
N
0
125
1.0
0.5
0.25
0.12
0.0
-0.12
-0.25
−0.5
−1.0

Figure 19. Difference maps between SGPlus and SGGlobal of soil pH for three interval depths – the Netherlands.

3.3 Local data density

Figure 21 shows a series of maps where, with each step, the amount of new local soil observations added to the $\mathrm{SG}_{\text{Gloabl}}$ model increases. The maps show the difference between the $\mathrm{SG}_{\text{plus}}n$ model and the $\mathrm{SG}_{\text{Global}}$ model. For each map predicted with more local observations as the previous one, the difference between the two models becomes larger. This starts at the centre of the area and spreads out more to the North and South. Most parts of the map contain deviation that indicate that the $\mathrm{SG}_{\text{plus}}n$ model predicts a higher soil pH than the $\mathrm{SG}_{\text{Global}}$ model (from 0 till -2). Still there are a few areas, mainly in the south near the borders and some in the north, where the $\mathrm{SG}_{\text{Global}}$ model predicts higher.

Table 20 shows the model statistics for each prediction map and the observed values. Hereby noting that the observed values are randomly taken soil observations (around 37.000) and therefore do not cover the entire study area. It might be possible that the real minimum and maximum differ from the one stated here, but it gives a general overview of minimum values for min and max are. Figure 20 shows how the statistics slowly move closer to the observed values as n increases, lifting steeper at the beginning of let line and flattening around n2000.

Table 20. Descriptive statistics of $\mathrm{SG}_{Plus}n$ models, compared to the SG_{Global} predictions and observed values all predicted for Andhra Pradesh for the soil property soil pH.

	n100	n200	n500	n1000	n2000	n5000	n10000	n36898	SGGlobal	Observed
Min.	5.34	5.50	5.37	5.41	5.31	5.43	5.15	5.18	5.44	4.8
Median	7.11	7.17	7.21	7.02	7.25	7.26	7.29	7.29	6.80	7.41
Mean	7.00	7.07	7.13	7.14	7.21	7.22	7.25	7.26	6.73	7.38
Max.	8.54	8.38	8.60	8.69	8.73	8.81	8.91	9.05	8.01	9.12
abs. Mean diff	0.28	0.35	0.40	0.42	0.48	0.50	0.54			

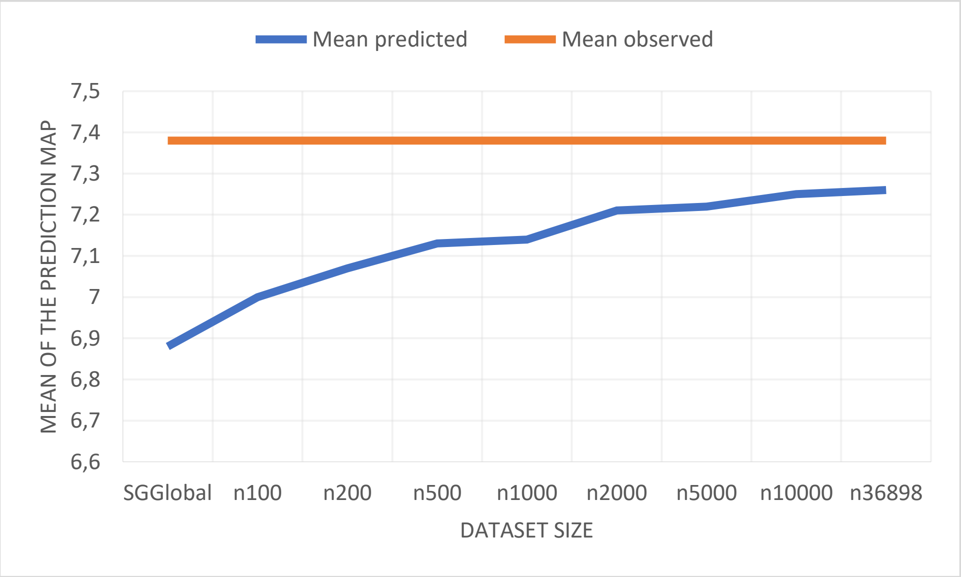

Figure 20. Learning curve of the predicted mean of the SGPlusn model with respect to the mean observed soil observations, for soil pH in Andhra Pradesh – India, with the size of the dataset used for calibrating the model.

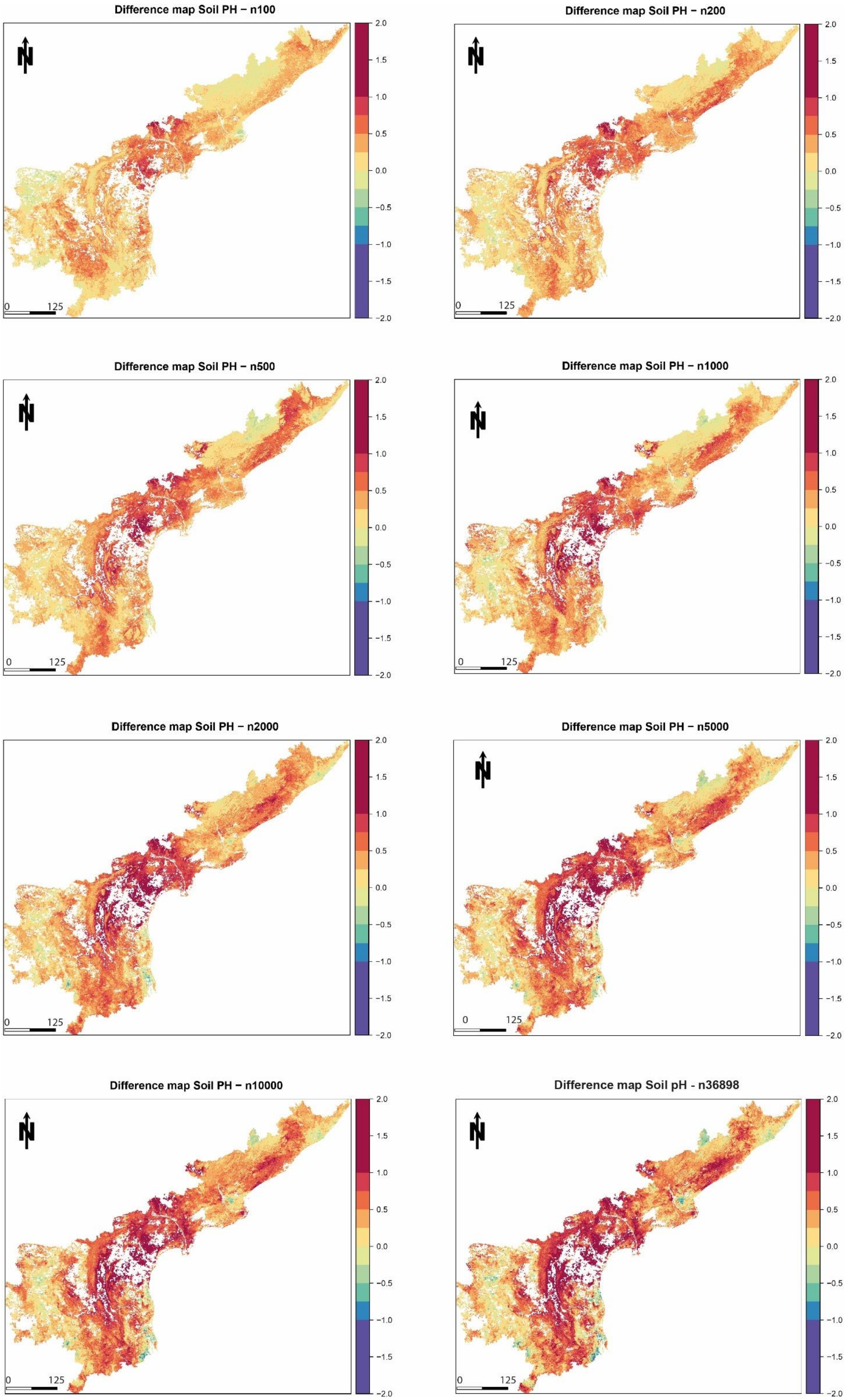
Difference map Soil PH – n100

Difference map Soil PH – n200

Difference map Soil PH – n500

Difference map Soil PH – n1000

Difference map Soil PH – n2000

Difference map Soil PH – n5000

Difference map Soil PH – n10000

Difference map Soil pH - n36898

Figure 21. Difference maps with ascending new data samples used for calibrating the model for soil pH in Andhra Pradesh – India.

4 Discussion

This chapter briefly discusses all results, additional clarification is given to conflicting results and unexpected findings. Hereafter the limitations of the study are explained, and the chapter ends by summarising the importance of some results.

4.1 Comparison of a global and local SoilGrids model

Figure 7 and 10 show the SOC and soil pH prediction results of the SG_{Global} and SG_{Local}. For each soil property the prediction results are of SG_{Global} deviate from the SG_{Local} model, which resulted in a deviation map with large deviations. Figures 8 and 11 and Tables 9 and 11 imply that the SG_{Local} model is a better model than the SG_{Global} model to make predictions for the Andhra Pradesh study area. The scatterplots of the SG_{Local} model are closer to the 1:1 line, the RMSE, ME are closer to 0 and R-squared is higher for SG_{Local}. Tifafi et al. (2018) also showed large differences between the globally calibrated SoilGrids predictions and local reference data.

There could be two reasons, or a combination of both options, why SG_{Local} predicts better for Andhra Pradesh then SG_{Global}. Firstly, the SG_{Local} model uses other covariates which are better suited for Andhra Pradesh. Secondly, the number of soil observations to predict SOC and soil pH in the SG_{Global} model are not representative enough to make accurate predictions for Andhra Pradesh. Even if there are only four soil observations present for Andhra Pradesh in the SG_{Global} model, other soil observations with covariates equal to Andhra Pradesh in feature space, might compensate for the lack of local soil observations but they have to be present in the SG_{Global} model and have similar covariates.

To analyse if the number of local soil observations causes the difference between SG_{Global} and SG_{Global}, the SG_{Plus} model results (Table 14 for SOC and Table 15 for soil pH) were compared to the SG_{Global} model results (as the SG_{Plus} model contains the SG_{Global} and SG_{Local} soil observations and uses the same covariates as the SG_{Global} model). Tables 12 and 14 show the statistics for the tree SOC models and Tables 13 and 15 show the statistics for the soil pH models, all at the 5-15 cm depth interval. Those statistics show that for both models, the RMSE, ME and R^2 of the SG_{Plus} model are significantly improved in comparison with the SG_{Global} model. Other researches also showed that adding more data to an RF model improves the prediction accuracy (Caubet et al. 2019; Fassnacht et al., 2014). All together, we can conclude that most of the extreme deviation between the SG_{Global} and SG_{Local} model has to do with the number of local soil samples in the training data. Still, the SG_{Local} model predictions are slightly better compared to the SG_{Plus} model. This difference is the result of global modelling or local modelling. Influences might be from the global soil observations in SG_{Global} model or the locally selected covariates from the SG_{Local} model, as those are the only two differences between the models. To tell if the locally selected covariates have an influence on the difference between SG_{Global} and SG_{Local} model, the variable importance for both models are compared.

An interesting finding in the variable importance comparison between the SG_{Global} and SG_{Local} models is that the variable importance of both models is very different for both soil pH and SOC (Figure 6 for SOC and Figure 9 for soil pH). The variable importance is only meaningful if the model fits the data well (Ando, 2014). Here the models are calibrated at a different scale. The SG_{Global} model predicts soil properties for a global scale quite well. However, when we only look at a local scale, the model does not perform very well. Therefore, the variable Importance of the SG_{Global} model does not tell us much for local scale. The Variable importance of the SG_{Local} model, on the other hand, really shows what covariates are important for the local scale. Especially for the soil pH model covariates differ between a globally calibrated model and a locally calibrated model. Research of (Ando, 2014; Bolourchi, Moradi, Demirel, & Uysal, 2018) all show that selecting representative covariates is essential for an accurate prediction of local patterns. An example of a possible local pattern is shown in the SG_{Local} prediction map of Figure 10 (bottom maps). The northeast part of SG_{Local} map shows more deviation in soil pH than the SG_{Global} prediction map. This may be explained by the deviation in variable importance between the two models. Based on this information we can also assume that the difference between the SG_{Plus} and SG_{Local} which was not explained by the new local soil samples is explained by the covariates.

Another interesting observation in Table 8 is that the minimum difference between SG_{Global} and SG_{Local} model is extremely high, namely -7.29 % SOC. This while the min and max SOC % are 0.07 and 2.47 for SG_{Local} and 0.76 and 9.23 for SG_{Global}. When looking at the histogram of the occurrence (Figure 21) of prediction values, it is clear that predictions above 5.0 % SOC only occur in a few cases and therefore, do not influence further results.

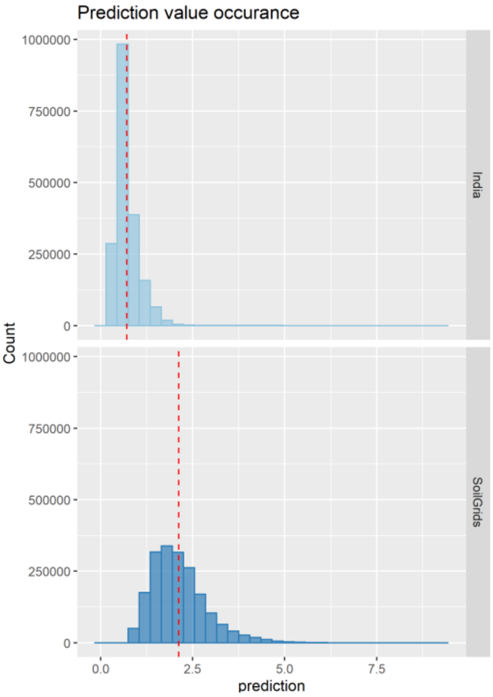

Figure 22. Prediction value Occurrence for SG_{Local} and SG_{Global} for SOC.

4.2 Influence of new soil observations

One thing I expected is that adding more local data points to a model would improve the accuracy of a random forest model for the local area. The results of RQ1 show that more local points indeed improved the accuracy of the local study area for both soil properties. I also expected that the std study area (Nampula) would show substantial differences and the ltd study area (the Netherlands) would show little to no differences when adding new datapoints. However, the opposite occurred, especially for the SOC models. The std study area showed little to no differences for SOC predictions after adding new local data in India, while the ltd study area showed substantial differences. This does not necessarily mean that other ltd and std areas also show this deviation. To see other areas also show this deviation future research is needed (see section 5.4) Also unexpected is that the 0 -5 cm and 5-15 cm depth interval layers show more deviation than the 5-10 cm depth interval layer, while this is the depth interval for which new local soil samples where added. The soil pH model showed for both Nampula and the Netherlands visually the same amount of deviation. The mean of all maps stayed the same however. To find out what caused the deviation, the SOC results of the Netherlands were compared to other studies and the variable importance plot was examined.

Because the SOC maps for the Netherlands have the largest differences between the two models, the results were compared to other work. Figure 19 Shows the SOC maps based on two different data sources in % SOC. Even if both maps look different at first sight, there are some similar patterns in the data. All values predicted higher than 11.63% SOC (dark brown) show up in the same areas with similar patterns. And at the centre of the map (the Veluwe) show similar patterns. The Costal area and the south-west of the area both show uniform colours, although the right map predicts lower than 1.74 % SOC and the left map predicts values between 1.74% and 2.91 % SOC.

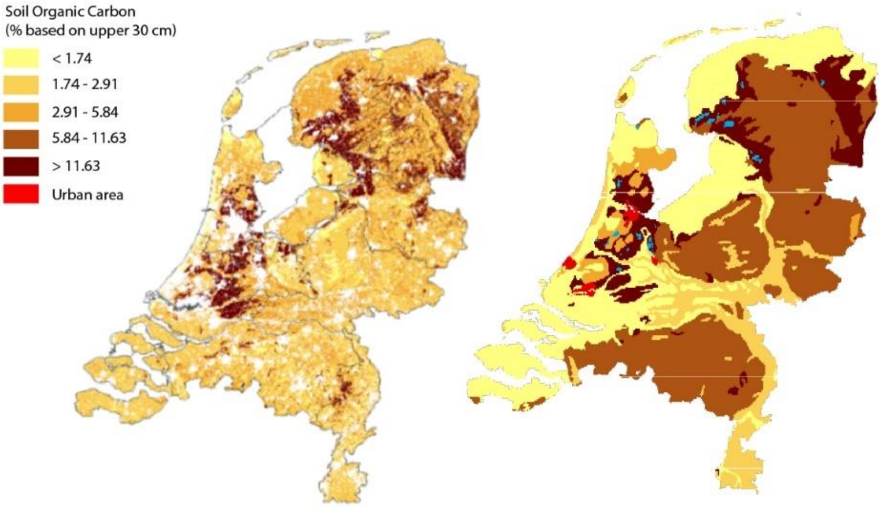

Figure 23. Estimated SOC (%) for 0 - 30 cm depth layer in the Netherlands according to two different sources. Left: Dutch soil map, land use map and LSK data (Lesschen et al., 2012) and right HWSD based on soil types (figure 3) from Hiederer & Köchy, 2012.. The legend represents the SOC % for both maps.

The maps in Figure 23 show the SOC in % for the depth interval layer of 0 – 30. To be able to compare the SG$_{Global}$ and SG$_{Plus}$ maps to those maps the weighted mean of the prediction maps for both models was calculated and plotted (Figure 24). When comparing the SG$_{Global}$ and SG$_{Plus}$ maps in Figure 24, both maps seem almost similar, while the difference maps show a lot of deviation (Figure 18). This probably happened because the 0-5cm and 5-15cm interval depth maps show mainly positive difference, while the 15-30 cm depth map mainly shows a negative difference, neutralising each other in the weighted mean map of figure 24. When comparing figure 24 to the maps shown in Figure 23, the predicted values higher than 11.63 % SOC seem to follow the same patterns in all four maps. The north-west part of the area shows different prediction values for both maps in figure 23 and the maps in figure 24. Figure 24 Show a predicted value between 5.84% SOC and 11.63% SOC while the maps of figure 23 show a predicted value lower than 1.74% SOC and between 2.91 and 5.84% SOC. The south-east part of the area shows for figure 24 a predicted value lower than 1.74% SOC, the lowest predictions of the area. All together, the comparison did not show any explanation why both SOC models deviated so much.

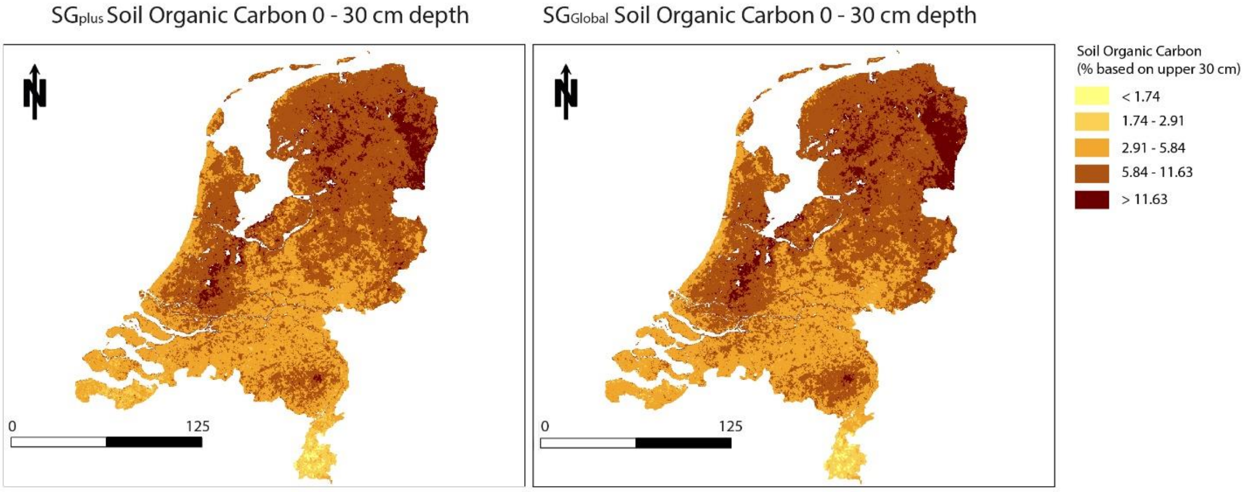
SG$_{plus}$ Soil Organic Carbon 0 - 30 cm depth

SG$_{Global}$ Soil Organic Carbon 0 - 30 cm depth

Figure 24. Estimated SOC (%) for 0 - 30 depth interval layer in the Netherlands according to the SG$_{Plus}$ model (left) and the SG$_{Global}$ model (right).

The comparison of the variable importance of SG_{Plus} and SG_{Global} resulted in something interesting. Figures 12 and 13 show the variable importance of SOC and soil pH. The SG_{Plus} showed different variable importance after adding the local soil observations to the model for both soil properties. The soil pH models showed the least deviation in variable importance and in OOB statistics. The deviation between the Soil pH maps was also smaller for all areas. The differences in variable importance probably caused the deviation between the models in Nampula and the Netherlands but do not explain why prediction results in the Netherlands deviated more than in Nampula. To examine why exactly the Netherlands showed higher differences, future research is needed (see 5.1; recommendations).

4.3 local data density

The results of the local data density analyses (Figure 22 and 23 and Table 21) show that adding more local observations increased the deviation between the $SG_{Plus}n$ model and the SG_{Global} model. From this we can tell that increasingly adding more local soil observations has a tremendous effect on the local predictions. The descriptive statistics of adding more local soil observations is also shown in Table 21, where Figure 23 shows the course of the mean predictions. Even though the minimum and maximum fluids when new soil samples are added, the median, mean and absolute mean difference all move slowly to the observed values. It is interesting to see that the mean prediction course starts off lifting steeper at the beginning of the line and flattens around n2000. This confirms our expectations that accuracy typically increases according to a power-law (the more training data, the more accurate the model) and then reaches a plateau from whereon the accuracy of the predictions is just slightly changing. Although accuracy is here measured as the mean and median of the predictions and not as RMSE, ME or R^{2}. It is interesting that even when a large number of new soil observations are added, the statistics in Table 21 do not reach the observed values. When the results of the comparison of a global and a local SoilGrids model (Table 11; the descriptive statistics of the Soil pH models vs Observed values in Andhra Pradesh), especially the SG_{Local} results, are compared to the $SG_{Plus}n36898$ and observed values, it is interesting to see what the influence of locally selected covariates is. Since SG_{Local} is calibrated using all local soil observations and uses local covariates, and $SG_{Plus}n36898$ is calibrated also using all local soil observations but uses globally selected covariates, the difference between the two model statistics (mean of 7.37 pH for $SG_{Local,}$ 7.26 pH for $SG_{Plus}n36898$ and 7.38 as observed mean pH) is the influence of locally selected covariates.

4.4 limitations of this study

For this study, it was not tested how many soil observations were already in the SG_{Global} dataset with a small taxonomic distance to the soil observations in Andhra Pradesh and Nampula. This may influence how extreme the differences between the SG_{Global} and SG_{Local} are. The more std soil observations there are in SG_{Global}, the smaller the differences will be between the models.

It was also not tested what the influence of adding clustered data to the SoilGrids model has. Research showed that for other machine learning models, well-distributed sampling methods have a huge influence on the accuracy of the results (Caubet et al., 2019). Even if RF does not take sampling locations into account and is well known for its ability to handle skewed data and small numbers of observations, it might increase the accuracy of the model. To test this, further research is needed.

Because the SoilGrids DSM model was rebuilt, this may have caused some small deviations in the results. The original SoilGrids DSM predictions were compared with the SG_{Global} results for the 5-15 cm depth layer for SOC and soil pH. It was expected that the results would be almost similar, but there was a large difference between the two prediction maps. Even when the original trained SoilGrids DSM model was used to make predictions for the Andhra Pradesh study area, there was a deviation between the original and the rebuilt model results. A possible reason for this may be differences in the covariate stack used to make predictions. Due to time limits, this was not investigated. This could possibly influence the prediction results when being compared to other study results, but since the same data were used to build all SoilGrids DSM models, this did not influence the comparison between models.

It might happen that the covariates selected after the correlation analyses and RFE are still correlated. This was not taken into account during the interpretation of the results. If there is still a correlation between covariates, RF will randomly select one of the covariates as important and the other as less important. When two models each pick the other covariate as important, this will result in a differing variable importance plot.

The accuracy of the model results for the local data density research question is now measured in the mean of the prediction map. To gain better insight in the accuracy, it is better to use the RMSE or R^2. For the interpretation of this research, the mean was good enough, however the RMSE might show different results.

5 Conclusions and recommendations

This study aim was to compare globally and locally calibrated SoilGrids models and assess the influence of adding local data to a globally calibrated SoilGrids model. To achieve this objective, the three research questions are answered in this chapter. This chapter ends with recommendations for future study.

5.1 Comparison of a global and local SoilGrids model

The SG_{Global} and the SG_{Local} model differ in each aspect considered in the comparison. In the model comparison, map comparison and accuracy, the SG_{Local} model performed better than the SG_{Global} model. This was due to the local soil samples used to calibrate SG_{Local} and the locally performed RFE. Together they caused the changes to the covariates selection and covariate importance for the random forest predictions, which had a direct effect on the accuracy.

5.2 Influence of new soil observations

When the local soil observations were added to the global model, the accuracy of the predictions increased substantially. It was expected that the areas close in covariate feature space would benefit most from local soil observations and the areas distant in feature space would benefit least. Results showed that it was not the case. In this research, the area distant in covariate feature space showed more deviation than the area close in feature space. Future research is needed to find out why the distant area showed such deviation. The OOB model statistics showed that adding the local soil observations had a positive influence on the model accuracy on predictions around the entire globe. To tell if the new local samples also had a positive influence on Nampula and the Netherlands specific, a test dataset is needed for future research.

5.3 Effect of local data density

The effect of adding local data on prediction accuracy first increased steadily as the size of the local data increased and then flattened off. This shows that the first set of new local data samples has the biggest effect on the local prediction accuracy and that adding more local soil observations to the model keeps increasing model the accuracy, but there is a tremendous amount of local soil samples needed to slowly rise the accuracy until it completely flattens out. From this point, only calibration with locally selected covariates can increase the model accuracy.

5.4 Recommendations

SoilGrids implementation

This study shows that it is important to realise that adding new data observations to the globally calibrated SoilGrids model influences model results in areas close in feature space, but also areas distant in feature space, according to the Homosoil principle. The OOB model statistics showed that adding local data did influence the model accuracy all over the globe in a positive way. Therefore, global modelling has its benefits, as soil observations from the entire globe can be used to make predictions for a local area. However, Other researches have shown that at some point having a good covariate selection is more important than having more available soil samples (Fassnacht et al., 2014). To make even more accurate predictions with a SoilGrids model, a combination between locally selected covariates and global soil observations can be used to make predictions for a local area. To find out if this combination is technical feasible, what the best local area size is and how to deal with border areas, future research is needed.

Influence of local data on other areas

The differences in variable importance probably caused the deviation between the models in Nampula and the Netherlands but did not explain why prediction results in the Netherlands deviated more than in Nampula. There was no logical explanation of why adding local data had such a high effect on areas which we expected to be far in feature space and such little effect on areas close in feature space. It might be that the selected areas from the Homosoil script were not as close in feature space as expected. The Homosoil script uses other covariates to select regions (based on Euclidean distance) than the covariates used for modelling. To find out if this was the case, a different selection method should be used to select the std and ltd study areas. The research report of A. Schoneveld, 2020 shows that Euclidean distance is not always the best method to calculate the distance in feature space and that other methods such as the Manhattan may calculate feature space distance better. Besides, could It be useful to introduce more study areas to investigate whether the deviation in the ltd and std study area will occur in different areas with different environmental conditions. For further research, more study areas may give further insights into how new local soil samples influences other areas.

Another possibility to find out why adding local data had such a high effect on predictions in the Netherlands, is analysing which variables have the most effect on the predictive model by performing a sensitivity analyses. To explain the relationship between model variables and predictions .. presents a method to look inside the black box of RF. It computes the contribution of each covariate to the RF model. The GINI variable importance used during this study is, according to Palczewska, 2013 often insufficient for the complete understanding of the relationship between covariates and the predicted value. Kuz'min et all., 2011 propose a new technique to calculate the contribution of a covariate. In this method, feature contribution is computed separately for each prediction and provides detailed information about relationships between variables and the predicted value (Palczewska, Palczewski, Marchese Robinson, & Neagu, 2013).

P. Grover, 2017 presents a methods to find for a given data point and associated prediction, which covariables (or combinations of covariables) explain this specific prediction. They use the *treeinterpreter* package in Python to show the sorted list of bias (mean of data at starting node) and individual node contributions for a given prediction (Grover, 2017). This local interpretation determines which covariables are used to come to that final prediction. This can be used to find out which covariates contributed most to the predictions with the largest deviation in all study areas. If the covariates used for the predictions in the Netherlands show similarity to the covariates used for predictions in Andhra Pradesh, then it could be an explanation why the predictions in the Netherlands show such high deviation.

6. References

Ando. (2014). Selecting good features. *Diving into Data, part III:* Retrieved from http://blog.datadive.net/selecting-good-features-part-iii-random-forests/

Arrouays, D., Lagacherie, P., & Hartemink, A. E. (2017). Digital soil mapping across the globe. *Geoderma Regional*. https://doi.org/10.1016/j.geodrs.2017.03.002

Batjes, N. H., Ribeiro, E., & Van Oostrum, A. (2020). Standardised soil profile data to support global mapping and modelling (WoSIS snapshot 2019). *Earth System Science Data*, *12*(1), 299–320. https://doi.org/10.5194/essd-12-299-2020

Batjes, N. H., Ribeiro, E., Van Oostrum, A., Leenaars, J., Hengl, T., & Mendes De Jesus, J. (2017). WoSIS: Providing standardised soil profile data for the world. *Earth System Science Data*, *9*(1), 1–14. https://doi.org/10.5194/essd-9-1-2017

Bickelhaupt, D. (2020). Soil pH; What it means. *SUNY, College of Environmental Science and Forestry*. Retrieved from https://www.esf.edu/pubprog/brochure/soilph/soilph.htm

Bolourchi, P., Moradi, M., Demirel, H., & Uysal, S. (2018). *Random Forest Feature Selection for SAR-ATR*. https://doi.org/10.1109/UKSim.2018.0002

Bouma, J., Montanarella, L., & Evanylo, G. (2019). The challenge for the soil science community to contribute to the implementation of the UN Sustainable Development Goals. *Soil Use and Management*, (March), 1–9. https://doi.org/10.1111/sum.12518

Breiman, L. (2001). Random Forest. *Machine Learning Proces*, 5–32. Retrieved from https://link.springer.com/content/pdf/10.1023%2FA%3A1010933404324.pdf

Brownlee, J. (2019). A Gentle introduction to k-fold Cross-validation. *Statistics*. Retrieved from https://machinelearningmastery.com/k-fold-cross-validation/

Caubet, M., Román Dobarco, M., Arrouays, D., Minasny, B., & Saby, N. P. A. (2019). Merging country, continental and global predictions of soil texture: Lessons from ensemble modelling in France. *Geoderma*. https://doi.org/10.1016/j.geoderma.2018.09.007

Davidson, E. A., & Janssens, I. A. (2006). Temperature sensitivity of soil carbon decomposition and feedbacks to climate change. *Nature*, *440*(7081), 165–173. https://doi.org/10.1038/nature04514

de Sousa, L. (n.d.). How were the spatial predictions generated? Retrieved October 18, 2019, from https://www.isric.org/explore/soilgrids/faq-soilgrids#What_is_SoilGrids

De Sousa, L., Poggio, L., Dawes, G., Kempen, B., & van den Bosch, H. (2020). *Computational Infrastructure of SoilGrids 2.0*. https://doi.org/10.1007/978-3-030-39815-6_3

Defourny, P. (2017). *Land Cover CCI*. Retrieved from maps.elie.ucl.ac.be/CCI/viewer/download/ESACCI-LC-Ph2-PUGv2_2.0.pdf

Etten, J. Van, Sumner, M., Cheng, J., Bevan, A., Bivand, R., Busetto, L., … Wueest, R. (2020). *Package "raster."* Retrieved from https://github.com/rspatial/raster/issues/

Evans, J. S. (2018). pp.subsample. *RDocumentation*. Retrieved from https://www.rdocumentation.org/packages/spatialEco/versions/1.1-1/topics/pp.subsample

Fan, S. (2019). Covariate. In *Encyclopedia of Research Design* (Neil J. Sa, pp. 285–287). https://doi.org/https://dx.doi.org/10.4135/9781412961288

FAO, & ITPS. (2018). *Global Soil Organic Carbon Map (GSOCmap) Technical Report*. Retrieved from http://esdac.jrc.ec.europa.eu/content/global-soil-organic-carbon-estimates

Fassnacht, F. E., Hartig, F., Latifi, H., Berger, C., Hernández, J., Corvalán, P., & Koch, B. (2014). Importance of sample size, data type and prediction method for remote sensing-based estimations of aboveground forest biomass. *Remote Sensing of Environment*. https://doi.org/10.1016/j.rse.2014.07.028

Frankenfield, J. (2018). Machine Learning. *Investopedia*. Retrieved from https://www.investopedia.com/terms/m/machine-learning.asp

Griffin, E., & Edwards, T. (2019). *What is soil organic carbon*. Retrieved from https://www.agric.wa.gov.au/measuring-and-assessing-soils/what-soil-organic-carbon

Grover, P. (2017). Intuitive Interpretation of Random Forest. *Data Institute*, *Data Insti*. Retrieved from https://medium.com/usf-msds/intuitive-interpretation-of-random-forest-2238687cae45

Hand, D. J., & Vinciotti, V. (2003). Local versus global models for classification problems: Fitting models where it matters. *American Statistician*, *57*(2), 124–131. https://doi.org/10.1198/0003130031423

Hengl, T., De Jesus, J. M., Heuvelink, G. B. M., Gonzalez, M. R., Kilibarda, M., Blagotić, A., … Kempen, B. (2017). SoilGrids250m: Global gridded soil information based on machine learning. In *PLoS ONE* (Vol. 12). https://doi.org/10.1371/journal.pone.0169748

Hengl, T., Heuvelink, G. B. M., Kempen, B., Leenaars, J. G. B., Walsh, M. G., Shepherd, K. D., … Tondoh, J. E. (2015). Mapping soil properties of Africa at 250 m resolution: Random forests significantly improve current predictions. *PLoS ONE*, *10*(6), 1–26. https://doi.org/10.1371/journal.pone.0125814

Hester, J. (2020). *package "Devtools."* Retrieved from https://www.rdocumentation.org/packages/devtools/versions/1.13.6

Hiederer, R., & Köchy, M. (2012). Global soil organic carbon estimates and thharmoniseded world soil database. In *EUR 25225EN, Luxembourg*. https://doi.org/10.2788/13267

Hijmans, R., Sumner, M., Macqueen, D., Lemon, J., Brien, J. O., & Rourke, J. O. (2020). *Package ' sp .'* Retrieved from https://cran.r-project.org/web/packages/sp/sp.pdf

Jobbágy, E., & Jackson, R. (2000). The Vertical Distribution of Soil Organic Carbon and Its Relation to Climate and Vegetation. *ECOLOGICAL APPLICATIONS*, *10*, 423–436. https://doi.org/10.2307/2641104

Kempen, B., Brus, D. J., & de Vries, F. (2015)Operationalisingng digital soil mapping for nationwide updating of the 1:50,000 soil map of the Netherlands. *Geoderma*. https://doi.org/10.1016/j.geoderma.2014.11.030

Kempen, B., Dalsgaard, S., Kaaya, A. K., Chamuya, N., Ruipérez-González, M., Pekkarinen, A., & Walsh, M. G. (2019). Mapping topsoil organic carbon concentrations and stocks for Tanzania. *Geoderma*, *337*(June 2018), 164–180. https://doi.org/10.1016/j.geoderma.2018.09.011

Koch, A., Mcbratney, A., Adams, M., Field, D., Hill, R., Crawford, J., … Zimmermann, M. (2013). Soil Security: Solving the Global Soil Crisis. *Global Policy*, *4*(4), 434–441. https://doi.org/10.1111/1758-5899.12096

Kopittke, P. M., Menzies, N. W., Wang, P., McKenna, B. A., & Lombi, E. (2019). Soil and the intensification of agriculture for global food security. *Environment International*, *132*, 105078. https://doi.org/https://doi.org/10.1016/j.envint.2019.105078

Kuhn, M. (2009). *Variable Selection Using the caret package*. Retrieved from https://r-forge.r-project.org/scm/viewvc.php/*checkout*/pkg/caret/inst/doc/caretSelection.pdf?revision=77&root=caret&pathrev=90

Kuz'min, V., Polishchuk, P., Artemenko, A., & Andronati, S. (2011). Interpretation of QSAR Models Based on Random Forest Methods. *Molecular Informatics*, *30*. https://doi.org/10.1002/minf.201000173

Lesschen, J. P., Heesmans, H. I. M., Mol-Dijkstra, J. P., van Doorn, A., Verkaik, E., den, W., & Kuikman, P. (2012). *Mogelijkheden voor koolstofvastlegging in de Nederlandse landbouw en natuur*.

Liaw, A., & Wiener, M. (2018). Breiman and Cutler's Random Forests for Classification and Regression. *CRAN*, 29. Retrieved from https://cran.r-project.org/web/packages/randomForest/randomForest.pdf

Mallavan, B., Minasny, B., & McBratney, A. (2010). *Digital Soil Mapping. Progress in Soil Science*. https://doi.org/https://doi.org/10.1007/978-90-481-8863-5_12

Maschinen, B., Investition, A., Beschaffungen, G., Ersatzbeschaffungen, B., & Mittelherkunft, S. (2012). *Harmonized World Soil Database*. Retrieved from https://library.wur.nl/isric/fulltext/isricu_i29850_001.pdf

Max, A., Wing, J., Weston, S., Williams, A., Keefer, C., Engelhardt, A., … Kuhn, M. M. (2020). *Package ' caret .'* Retrieved from https://cran.r-project.org/web/packages/caret/caret.pdf

McBratney, A. B., Mendonça Santos, M. L., & Minasny, B. (2003). On digital soil mapping. In *Geoderma* (Vol. 117). https://doi.org/10.1016/S0016-7061(03)00223-4

Meinshausen, N. (2006). Quantile Regression Forests. *Machine Learning Research*, *7*(3), 983–999. https://doi.org/10.1111/j.1541-0420.2010.01521.x

Miller, B. A. (2012). The Need to Continue Improving Soil Survey Maps. *Soil Horizons*, *53*(3), 11. https://doi.org/10.2136/sh12-02-0005

Mishra, J. P., Nair, D., Singh, R., Gazeley, U., & Kapoor, R. (2015). *Improving the Soil Health Card Scheme*. 1–8. Retrieved from https://static1.squarespace.com/static/5b7cc54eec4eb7d25f7af2be/t/5c745123f9619af62c469c2b/1551126823002/Policy+Brief_FINAL_High+Quality_25th+Feb.pdf

Molnar, C. (2019). Interpretable Machine Learning. Retrieved October 9, 2019, from https://christophm.github.io/interpretable-ml-book/index.html

Mosaic. (2020). Soil pH. Retrieved from https://www.agric.wa.gov.au/measuring-and-assessing-soils/what-soil-organic-carbon

Palczewska, A., Palczewski, J., Marchese Robinson, R., & Neagu, D. (2013). *Interpreting random forest models using a feature contribution method*.

P.Sudhakar, Reddy, M. B., Prasad, K. M., SatyaKumar, Y., & Rao, D. S. (2017). *Ground Water Year Book 2016-2017 Andhra Pradesh State*. 101.

Pendleton, R. L., & Jenny, H. (1945). Factors of Soil Formation: A System of Quantitative Pedology. In *Geographical Review* (Vol. 35). https://doi.org/10.2307/211491

Penvenne, J. M., & Sheldon, K. (2020). Mozambique. *Encyclopædia Britannica*. Retrieved from https://www.britannica.com/place/Mozambique

Pike, J. (2018). Andhra Pradesh - Geography. Retrieved October 11, 2019, from GlobalSecurity website: https://www.globalsecurity.org/military/world/india/andhra-pradesh-geography.htm

Rao, C., & Wanmali, S. (2018). Andhra Pradesh. *Encyclopædia Britannica*. Retrieved from https://www.britannica.com/place/Andhra-Pradesh

Rowen, H., & Heslinga, M. W. (2020). Netherlands. *Encyclopædia Britannica*. Retrieved from https://www.britannica.com/place/Netherlands

Sanchez, P. A., Ahamed, S., Carré, F., Hartemink, A. E., Hempel, J., Huising, J., … Zhang, G. L. (2009). Digital soil map of the world. *Science*, *325*(5941), 680–681. https://doi.org/10.1126/science.1175084

Schoneveld, A. C. (2020). *Added value of synthetic profiles*. 71.

Strobl, C., Malley, J., & Tutz, G. (2009). An introduction to recursive partitioning: Rationale, application, and characteristics of classification and regression trees, bagging, and random forests. *Psychological Methods*, Vol. 14, pp. 323–348. https://doi.org/10.1037/a0016973

The R Foundation. (2020). Introduction to R. Retrieved from https://www.r-project.org/about.html

Tifafi, M., Guenet, B., & Hatté, C. (2018). Large Differences in Global and Regional Total Soil Carbon Stock Estimates Based on SoilGrids, HWSD, and NCSCD: Intercomparison and Evaluation Based on Field Data From USA, England, Wales, and France. *Global Biogeochemical Cycles*, *32*(1), 42–56. https://doi.org/10.1002/2017GB005678

UNCC, & The Global Mechanism. (2016). *Land Degradation Neutrality Target Setting – A Technical Guide*. (May), 1–68.

Velazco, S. J. E., Galvão, F., Villalobos, F., & De Marco, P. (2017). Using worldwide edaphic data to model plant species niches: An assessment at a continental extent. *PLoS ONE*, *12*(10), 1–24. https://doi.org/10.1371/journal.pone.0186025

Vitharana, U. W. A., Mishra, U., & Mapa, R. B. (2019). National soil organic carbon estimates can improve global estimates. *Geoderma*. https://doi.org/10.1016/j.geoderma.2018.09.005

Wickham, H. (2019). *Package ‘ tidyverse .’* 1–5. Retrieved from https://cran.r-project.org/web/packages/tidyverse/tidyverse.pdf

Yiu, T. (2019). Understanding Ranodom Forst. *Towards Data Science*. Retrieved from https://towardsdatascience.com/understanding-random-forest-58381e0602d2

Appendix

I Theoretical background

K-fold Cross-validation

Cross-validation is a resampling procedure used to estimate the accuracy of a machine learning model on unseen data. The parameter called k refers to the number of groups that a data sample will be split into. K-fold cross-validation shuffles the dataset randomly and splits the dataset into k groups (Brownlee, 2019). Each model ire-calibrateded 10 times using 90% of the data and predictions derived from the calibrated models are compared with observations of the remaining 10% (de Sousa, n.d.). If k is set to 10, there will be 10 different test and training sets which are used to estimate the model accuracy. The dataset can be divided into k-groups by using folds. The dataset is equally divided and each data value in a fold is assigned the fold number (between 0 and k). The training dataset is used to calibrate the model and make predictions. Those predictions are evaluated on the corresponding test datasets. All the runs together arsummariseded and represent the accuracy of a model.

Random Forest

SoilGrids maps are produced using automated soil mapping based on the machine learning algorithm Random Forest (RF). RF has a simple yet powerful concept. It consists of a large number of individual decision trees that operate as a group. A simple example of a decision tree is shown in figure 25 Each time the path splits into two is called a node, and the question asked is based on the covariates (e.g. *is red?* Is probably based on the covariate; number colour and *is underlined?* On the covariate that tells if a number is underlined or not). At a node observations are split, observations that meet the criteria go down the Yes branch and ones that don't go down the No branch. At each node the model will ask: What covariate will allow me to split the observations in a way that the 'Yes' groups are as different from each other as possible and the members of each resulting subgroup are as similar to each other as possible (Yiu, 2019)? The hyperparameter mtry sets the number of covariables available for splitting at each tree node. The ntree hyperparameter set the number of trees to grow. Larger number of trees produce more stable models and covariate importance estimates, but require more memory and longer run times (Liaw & Wiener, 2018).

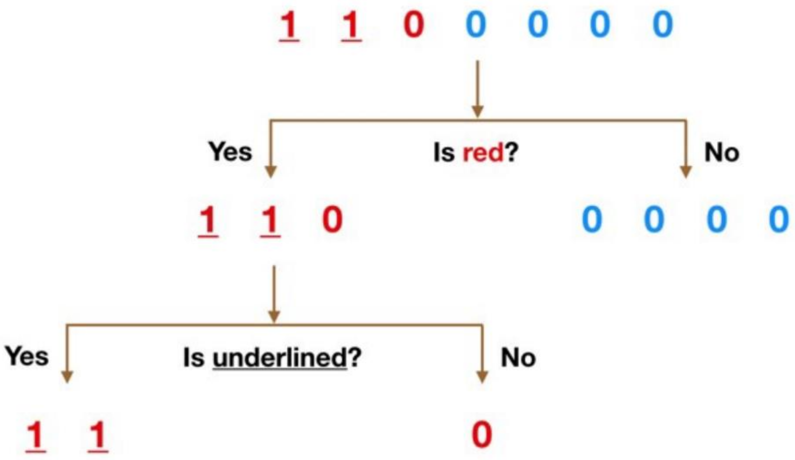

Figure 25. Random Forest decision tree example to predict numbers and their colours (Yiu, 2019).

Each decision tree is trained on a different data subset, where sampling is done with replacement and uses a different covariates subset to reduce correlation between trees. All individual decision trees are then used to make predictions (Breiman, 2001). The conditional mean of all those predictions is used to get the final RF regression prediction (Meinshausen, 2006). Because there is a low correlation between the trees, trees can produce ensemble predictions that are more accurate than any of the individual predictions. All trees together overcome errors of individual trees.

correlation analyses

For this research, it is important to use covariates which also have a low correlation. Reducing the number of covariates used in a model reduces calculation time and processing power needed. Besides, keeping two covariates which are highly correlated, can lead to incorrect conclusions when interpreting the variable importance. When a dataset has two highly correlated feature, RF can pick any of those covariates as important predictor and the other as not important, with no concrete preference for which covariate. If the RF models we want to compare in this study both pick another covariate as main predictor, conclusions based on that variable importance are then incorrect (Ando, 2014). correlation analyses assessed bi-variate correlations between covariates with the Pearson correlation coefficient. If this coefficient was larger than 0.85, then one of the correlated covariates was excluded randomly.

RFE

Variables with high importance have a significant impact on the model prediction values. On the other side, variables with low importance might be omitted from a model, making model calibration and prediction simpler and faster.

Automatic feature selection methods can be was used to identify attributes covariates that are and are not required to build an accurate model to be used. An automatic method for feature selection provided by the caret R package is called Recursive Feature Elimination or RFE. RFE builds n models with different subsets of a dataset and states the most important variables based on the GINI index (see chapter 2.2 model comparison) (Kuhn, 2009). SoilGrids uses n = 4 to determine the covariates. This results in four differently selected covariate tables. If a covariate occurs in all those covariate tables, this covariate is selected for the final model. When the amount number of selected covariates for the final model is less than 25% of the input covariable, also the covariates that occurs three times are used in the final model (de Sousa, n.d.).

Table 22 and table 23 show the OOB accuracy of the SG_{Local} model before and after the RFE. This shows that you can remove *x* variables that are not that significant and have similar or better performance in with much shorter training time.

Table 22. SOC (%) OOB statistics for the SG_{Local} model.

	All covariates	RFE covariates
RMSE	0.29	0.29
MSE	0.08	0.08
R^2	0.42	0.42

Table 23. soil pH OOB statistics for the SG_{Local} model.

	All covariates	RFE covariates
RMSE	0.48	0.47
MSE	0.23	0.22
R^2	0.58	0.59

OOB error

Each tree in the Random Forest is trained on a subset of the data, which is sampled with replacement from the original data. This results in around ~2/3 of distinct observations in each tree. The out-of-bag error is calculated on all the observations, but for calculating each row’s error, the method only considers trees that have not seen this row during training. This is similar to evaluating the model on a validation set.

Soil Properties - soil pH and Soil Organic Carbon.

Organic Carbon is together with pH, the best simple indicator of the health status of the soil. Moderate to high amounts of organic carbon are associated with fertile soils with a good structure (Maschinen et al., 2012). Soil organic carbon (SOC) is the largest carbon (C) stock in most terrestrial ecosystems, containing approximately 2344 Gt of organic C globally (Davidson & Janssens, 2006). Moreover, soil irecogniseded as the second largest C pool after the oceans and one of the most important components of the biosphere, delivering major ecosystem services and functions (Ogle & Paustian, 2005). SOC refers only to the carbon component of organic compounds. The main influences of the amount of SOC are soil type, climate and land/soil management. Where for soil, clay binds to organic matter, helping it from being decomposed, while sandy soils are coarse-textured which causes SOC to be rapidly decomposed. For climate SOC increase with rainfall, this is because increasing rainfall supports plant growth. Temperature also plays a part as decreasing temperatures slow the decomposer of SOC. Because SOC mainly exist in the top 0-10 cm of soils, land and soil management can have a big influence of SOC. Deforestation for example lay SOC bare for erosion, and transfers soil down the slope into the lower parts of the landscape, leaving the slope with low SOC content and the lower parts with increased soc content (Griffin & Edwards, 2019).

The acidity or alkalinity of a substance is measured in pH units, a scale running from 0 to 14. A Soil pH lower than 7 is a high acidity soil, a pH of 7 is neutral and a pH higher than 7 is a high alkalinity soil. Most cultivated plants enjoy slightly acidic conditions with a pH of about 6.5. but some plants grow best under slightly acidic conditions (Mosaic, 2020). There are three main reasons when soil tends to become acidic. First is rainwater. Soils formed under low rainfall conditions tend to be natural as rainwater leaches basic ions away. Soils formed under conditions of high annual rainfall are more acidic than are soils formed under more arid conditions. Second is nitrogefertilisersrs. Intensive farming can result in soil acidification over a number of years with nitrogefertilisersrs or manures. Last main influencer of soil pH are plants. Decomposing organic matter and root respiration release Carbon dioxide which dissolves in soil water to form a weak organic acid (Bickelhaupt, 2020).

II Covariates explanation

FULL_CODE	DESCRIPTION
CLM_CHE_BIO02	Mean diurnal range [Â°C] at 1 km (based on CHELSA climate surfaces).
CLM_CHE_BIO04	Temperature seasonality at 1 km (based on CHELSA climate surfaces).
CLM_CHE_BIO07	Temperature Annual Range [Â°C] at 1 km (based on CHELSA climate surfaces).
CLM_CHE_BIO08	Mean Temperature of wettest quarter at 1 km (based on CHELSA climate surfaces).
CLM_CHE_BIO09	Mean Temperature of driest quarter [Â°C] at 1 km (based on CHELSA climate surfaces).
CLM_CHE_BIO13	Precipitation of wettest month [mm] at 1 km (based on CHELSA climate surfaces).
CLM_CHE_BIO14	Precipitation of driest month [mm] at 1 km (based on CHELSA climate surfaces).
CLM_CHE_P01AVG	Mean monthly precipitation at 1 km (based on CHELSA climate surfaces) for January.
CLM_CHE_P02AVG	Mean monthly precipitation at 1 km (based on CHELSA climate surfaces) for February.
CLM_CHE_P03AVG	Mean monthly precipitation at 1 km (based on CHELSA climate surfaces) for March.
CLM_CHE_P04AVG	Mean monthly precipitation at 1 km (based on CHELSA climate surfaces) for April.
CLM_CHE_P05AVG	Mean monthly precipitation at 1 km (based on CHELSA climate surfaces) for May.
CLM_CHE_P06AVG	Mean monthly precipitation at 1 km (based on CHELSA climate surfaces) for June.
CLM_CHE_P07AVG	Mean monthly precipitation at 1 km (based on CHELSA climate surfaces) for July.
CLM_CHE_P08AVG	Mean monthly precipitation at 1 km (based on CHELSA climate surfaces) for August.
CLM_CHE_P09AVG	Mean monthly precipitation at 1 km (based on CHELSA climate surfaces) for September.
CLM_CHE_P10AVG	Mean monthly precipitation at 1 km (based on CHELSA climate surfaces) for October.
CLM_CHE_P11AVG	Mean monthly precipitation at 1 km (based on CHELSA climate surfaces) for November.
CLM_CHE_P12AVG	Mean monthly precipitation at 1 km (based on CHELSA climate surfaces) for December.
CLM_CHE_PYRSUM	Total annual precipitation at 1 km (based on CHELSA climate surfaces).
CLM_CHE_T01MIN	Minimum monthly temperature at 1 km (based on CHELSA Climate) for January.
CLM_CHE_T02MIN	Minimum monthly temperature at 1 km (based on CHELSA Climate) for February.
CLM_CHE_T03MIN	Minimum monthly temperature at 1 km (based on CHELSA Climate) for March.
CLM_CHE_T04MIN	Minimum monthly temperature at 1 km (based on CHELSA Climate) for April.
CLM_CHE_T05MIN	Minimum monthly temperature at 1 km (based on CHELSA Climate) for May.
CLM_CHE_T06MIN	Minimum monthly temperature at 1 km (based on CHELSA Climate) for June.
CLM_CHE_T07MIN	Minimum monthly temperature at 1 km (based on CHELSA Climate) for July.
CLM_CHE_T08MIN	Minimum monthly temperature at 1 km (based on CHELSA Climate) for August.
CLM_CHE_T09MIN	Minimum monthly temperature at 1 km (based on CHELSA Climate) for September.
CLM_CHE_T10MIN	Minimum monthly temperature at 1 km (based on CHELSA Climate) for October.
CLM_CHE_T11MIN	Minimum monthly temperature at 1 km (based on CHELSA Climate) for November.
CLM_CHE_T12MIN	Minimum monthly temperature at 1 km (based on CHELSA Climate) for December.
CLM_CHE_TYRMIN	Yearly averages of minimum monthly temperatures at 1 km (based on CHELSA Climate)
CLM_ESA_S01AVG	Mean monthly snowfall prob. at 500 m (based on MODIS snow product) for January.
CLM_ESA_S02AVG	Mean monthly snowfall prob. at 500 m (based on MODIS snow product) for February.
CLM_ESA_S03AVG	Mean monthly snowfall prob. at 500 m (based on MODIS snow product) for March.
CLM_ESA_S04AVG	Mean monthly snowfall prob. at 500 m (based on MODIS snow product) for April.
CLM_ESA_S05AVG	Mean monthly snowfall prob. at 500 m (based on MODIS snow product) for May.
CLM_ESA_S06AVG	Mean monthly snowfall prob. at 500 m (based on MODIS snow product) for June.
CLM_ESA_S07AVG	Mean monthly snowfall prob. at 500 m (based on MODIS snow product) for July.
CLM_ESA_S08AVG	Mean monthly snowfall prob. at 500 m (based on MODIS snow product) for August.
CLM_ESA_S09AVG	Mean monthly snowfall prob. at 500 m (based on MODIS snow product) for September.
CLM_ESA_S10AVG	Mean monthly snowfall prob. at 500 m (based on MODIS snow product) for October.
CLM_ESA_S11AVG	Mean monthly snowfall prob. at 500 m (based on MODIS snow product) for November.
CLM_ESA_S12AVG	Mean monthly snowfall prob. at 500 m (based on MODIS snow product) for December.
CLM_ESA_SYRAVG	Mean yearly snowfall prob. at 500 m (based on MODIS snow product)
CLM_ESA_SYRSTD	SD yearly snowfall prob. at 500 m (based on MODIS snow product)
CLM_MOD_CC01AVG	Long-term averaged monthly cloud cover Jan
CLM_MOD_CC02AVG	Long-term averaged monthly cloud cover Feb
CLM_MOD_CC03AVG	Long-term averaged monthly cloud cover Mar
CLM_MOD_CC04AVG	Long-term averaged monthly cloud cover Apr
CLM_MOD_CC05AVG	Long-term averaged monthly cloud cover May
CLM_MOD_CC06AVG	Long-term averaged monthly cloud cover Jun
CLM_MOD_CC07AVG	Long-term averaged monthly cloud cover Jul
CLM_MOD_CC08AVG	Long-term averaged monthly cloud cover Aug
CLM_MOD_CC09AVG	Long-term averaged monthly cloud cover Sep
CLM_MOD_CC10AVG	Long-term averaged monthly cloud cover Oct
CLM_MOD_CC11AVG	Long-term averaged monthly cloud cover Nov
CLM_MOD_CC12AVG	Long-term averaged monthly cloud cover Dec
CLM_MOD_CCSC	Cloud cover seasonality concentration
CLM_MOD_CCYRAVG	Long-term averaged mean cloud cover
CLM_MOD_LSTD01AVG	Long-term averaged mean monthly surface temperature (daytime) MODIS January. Derived using a stack of MOD11A2 LST images.
CLM_MOD_LSTD01STD	Long-term s.d. of the monthly surface temperature (daytime) MODIS January. Derived using a stack of MOD11A2 LST images.
CLM_MOD_LSTD02AVG	Long-term averaged mean monthly surface temperature (daytime) MODIS February. Derived using a stack of MOD11A2 LST images.
CLM_MOD_LSTD02STD	Long-term s.d. of the monthly surface temperature (daytime) MODIS February. Derived using a stack of MOD11A2 LST images.
CLM_MOD_LSTD03AVG	Long-term averaged mean monthly surface temperature (daytime) MODIS March. Derived using a stack of MOD11A2 LST images.
CLM_MOD_LSTD03STD	Long-term s.d. of the monthly surface temperature (daytime) MODIS March. Derived using a stack of MOD11A2 LST images.
CLM_MOD_LSTD04AVG	Long-term averaged mean monthly surface temperature (daytime) MODIS April. Derived using a stack of MOD11A2 LST images.
CLM_MOD_LSTD04STD	Long-term s.d. of the monthly surface temperature (daytime) MODIS April. Derived using a stack of MOD11A2 LST images.
CLM_MOD_LSTD05AVG	Long-term averaged mean monthly surface temperature (daytime) MODIS May. Derived using a stack of MOD11A2 LST images.
CLM_MOD_LSTD05STD	Long-term s.d. of the monthly surface temperature (daytime) MODIS May. Derived using a stack of MOD11A2 LST images.
CLM_MOD_LSTD06AVG	Long-term averaged mean monthly surface temperature (daytime) MODIS June. Derived using a stack of MOD11A2 LST images.
CLM_MOD_LSTD06STD	Long-term s.d. of the monthly surface temperature (daytime) MODIS June. Derived using a stack of MOD11A2 LST images.
CLM_MOD_LSTD07AVG	Long-term averaged mean monthly surface temperature (daytime) MODIS July. Derived using a stack of MOD11A2 LST images.
CLM_MOD_LSTD07STD	Long-term s.d. of the monthly surface temperature (daytime) MODIS July. Derived using a stack of MOD11A2 LST images.
CLM_MOD_LSTD08AVG	Long-term averaged mean monthly surface temperature (daytime) MODIS August. Derived using a stack of MOD11A2 LST images.
CLM_MOD_LSTD08STD	Long-term s.d. of the monthly surface temperature (daytime) MODIS August. Derived using a stack of MOD11A2 LST images.
CLM_MOD_LSTD09AVG	Long-term averaged mean monthly surface temperature (daytime) MODIS September. Derived using a stack of MOD11A2 LST images.
CLM_MOD_LSTD09STD	Long-term s.d. of the monthly surface temperature (daytime) MODIS September. Derived using a stack of MOD11A2 LST images.
CLM_MOD_LSTD10AVG	Long-term averaged mean monthly surface temperature (daytime) MODIS October. Derived using a stack of MOD11A2 LST images.
CLM_MOD_LSTD10STD	Long-term s.d. of the monthly surface temperature (daytime) MODIS October. Derived using a stack of MOD11A2 LST images.
CLM_MOD_LSTD11AVG	Long-term averaged mean monthly surface temperature (daytime) MODIS November. Derived using a stack of MOD11A2 LST images.
CLM_MOD_LSTD11STD	Long-term s.d. of the monthly surface temperature (daytime) MODIS November. Derived using a stack of MOD11A2 LST images.
CLM_MOD_LSTD12AVG	Long-term averaged mean monthly surface temperature (daytime) MODIS December. Derived using a stack of MOD11A2 LST images.
CLM_MOD_LSTD12STD	Long-term s.d. of the monthly surface temperature (daytime) MODIS December. Derived using a stack of MOD11A2 LST images.
CLM_MOD_LSTDYRAVG	Long-term averaged mean annual surface temperature (daytime) MODIS. Derived using a stack of MOD11A2 LST images.
CLM_MOD_LSTDYRSTD	Long-term s.d. of the monthly surface temperature (daytime) MODIS Yealry. Derived using a stack of MOD11A2 LST images.

CLM_MOD_LSTN01AVG	Long-term averaged mean monthly surface temperature (nighttime) MODIS January. Derived using a stack of MOD11A2 LST images.
CLM_MOD_LSTN01STD	Long-term s.d. of the monthly surface temperature (nighttime) MODIS January. Derived using a stack of MOD11A2 LST images.
CLM_MOD_LSTN02AVG	Long-term averaged mean monthly surface temperature (nighttime) MODIS February. Derived using a stack of MOD11A2 LST images.
CLM_MOD_LSTN02STD	Long-term s.d. of the monthly surface temperature (nighttime) MODIS February. Derived using a stack of MOD11A2 LST images.
CLM_MOD_LSTN03AVG	Long-term averaged mean monthly surface temperature (nighttime) MODIS March. Derived using a stack of MOD11A2 LST images.
CLM_MOD_LSTN03STD	Long-term s.d. of the monthly surface temperature (nighttime) MODIS March. Derived using a stack of MOD11A2 LST images.
CLM_MOD_LSTN04AVG	Long-term averaged mean monthly surface temperature (nighttime) MODIS April. Derived using a stack of MOD11A2 LST images.
CLM_MOD_LSTN04STD	Long-term s.d. of the monthly surface temperature (nighttime) MODIS April. Derived using a stack of MOD11A2 LST images.
CLM_MOD_LSTN05AVG	Long-term averaged mean monthly surface temperature (nighttime) MODIS May. Derived using a stack of MOD11A2 LST images.
CLM_MOD_LSTN05STD	Long-term s.d. of the monthly surface temperature (nighttime) MODIS May. Derived using a stack of MOD11A2 LST images.
CLM_MOD_LSTN06AVG	Long-term averaged mean monthly surface temperature (nighttime) MODIS June. Derived using a stack of MOD11A2 LST images.
CLM_MOD_LSTN06STD	Long-term s.d. of the monthly surface temperature (nighttime) MODIS June. Derived using a stack of MOD11A2 LST images.
CLM_MOD_LSTN07AVG	Long-term averaged mean monthly surface temperature (nighttime) MODIS July. Derived using a stack of MOD11A2 LST images.
CLM_MOD_LSTN07STD	Long-term s.d. of the monthly surface temperature (nighttime) MODIS July. Derived using a stack of MOD11A2 LST images.
CLM_MOD_LSTN08AVG	Long-term averaged mean monthly surface temperature (nighttime) MODIS August. Derived using a stack of MOD11A2 LST images.
CLM_MOD_LSTN08STD	Long-term s.d. of the monthly surface temperature (nighttime) MODIS August. Derived using a stack of MOD11A2 LST images.
CLM_MOD_LSTN09AVG	Long-term averaged mean monthly surface temperature (nighttime) MODIS September. Derived using a stack of MOD11A2 LST images.
CLM_MOD_LSTN09STD	Long-term s.d. of the monthly surface temperature (nighttime) MODIS September. Derived using a stack of MOD11A2 LST images.
CLM_MOD_LSTN10AVG	Long-term averaged mean monthly surface temperature (nighttime) MODIS October. Derived using a stack of MOD11A2 LST images.
CLM_MOD_LSTN10STD	Long-term s.d. of the monthly surface temperature (nighttime) MODIS October. Derived using a stack of MOD11A2 LST images.
CLM_MOD_LSTN11AVG	Long-term averaged mean monthly surface temperature (nighttime) MODIS November. Derived using a stack of MOD11A2 LST images.
CLM_MOD_LSTN11STD	Long-term s.d. of the monthly surface temperature (nighttime) MODIS November. Derived using a stack of MOD11A2 LST images.
CLM_MOD_LSTN12AVG	Long-term averaged mean monthly surface temperature (nighttime) MODIS December. Derived using a stack of MOD11A2 LST images.
CLM_MOD_LSTN12STD	Long-term s.d. of the monthly surface temperature (nighttime) MODIS December. Derived using a stack of MOD11A2 LST images.
CLM_MOD_LSTNYRAVG	Long-term averaged mean annual surface temperature (nighttime) MODIS. Derived using a stack of MOD11A2 LST images.
CLM_MOD_LSTNYRSTD	Long-term s.d. of the monthly surface temperature (nighttime) MODIS Yealry. Derived using a stack of MOD11A2 LST images.
CLM_MOD_PWV01	Long-term averaged mean monthly MODIS Precipitable Water Vapor in cm for months January and February. Derived using a stack of MOD05_L2 monthly images from NEO.
CLM_MOD_PWV03	Long-term averaged mean monthly MODIS Precipitable Water Vapor in cm for months March and April. Derived using a stack of MOD05_L2 monthly images from NEO.
CLM_MOD_PWV05	Long-term averaged mean monthly MODIS Precipitable Water Vapor in cm for months May and June. Derived using a stack of MOD05_L2 monthly images from NEO.
CLM_MOD_PWV07	Long-term averaged mean monthly MODIS Precipitable Water Vapor in cm for months July and August. Derived using a stack of MOD05_L2 monthly images from NEO.
CLM_MOD_PWV09	Long-term averaged mean monthly MODIS Precipitable Water Vapor in cm for months September and October. Derived using a stack of MOD05_L2 monthly images from NEO.
CLM_MOD_PWV11	Long-term averaged mean monthly MODIS Precipitable Water Vapor in cm for months November and December. Derived using a stack of MOD05_L2 monthly images from NEO.
CLM_WCL_BIO01	BIO1 = Annual Mean Temperature
CLM_WCL_BIO02	BIO2 = Mean Diurnal Range (Mean of monthly (max temp - min temp))
CLM_WCL_BIO03	BIO3 = Isothermality (BIO2/BIO7) (* 100)
CLM_WCL_BIO04	BIO4 = Temperature Seasonality (standard deviation *100)
CLM_WCL_BIO05	BIO5 = Max Temperature of Warmest Month
CLM_WCL_BIO06	BIO6 = Min Temperature of Coldest Month
CLM_WCL_BIO07	BIO7 = Temperature Annual Range (BIO5-BIO6)
CLM_WCL_BIO08	BIO8 = Mean Temperature of Wettest Quarter
CLM_WCL_BIO09	BIO9 = Mean Temperature of Driest Quarter
CLM_WCL_BIO10	BIO10 = Mean Temperature of Warmest Quarter
CLM_WCL_BIO11	BIO11 = Mean Temperature of Coldest Quarter
CLM_WCL_BIO12	BIO12 = Annual Precipitation
CLM_WCL_BIO13	BIO13 = Precipitation of Wettest Month
CLM_WCL_BIO14	BIO14 = Precipitation of Driest Month
CLM_WCL_BIO15	BIO15 = Precipitation Seasonality (Coefficient of Variation)
CLM_WCL_BIO16	BIO16 = Precipitation of Wettest Quarter
CLM_WCL_BIO17	BIO17 = Precipitation of Driest Quarter
CLM_WCL_BIO18	BIO18 = Precipitation of Warmest Quarter
CLM_WCL_BIO19	BIO19 = Precipitation of Coldest Quarter
CLM_WCL_P01TOT	Total monthly precipitation at 1 km (based on WorldCim v2 Climate) for January.
CLM_WCL_P02TOT	Total monthly precipitation at 1 km (based on WorldCim v2 Climate) for February.
CLM_WCL_P03TOT	Total monthly precipitation at 1 km (based on WorldCim v2 Climate) for March.
CLM_WCL_P04TOT	Total monthly precipitation at 1 km (based on WorldCim v2 Climate) for April.
CLM_WCL_P05TOT	Total monthly precipitation at 1 km (based on WorldCim v2 Climate) for May.
CLM_WCL_P06TOT	Total monthly precipitation at 1 km (based on WorldCim v2 Climate) for June.
CLM_WCL_P07TOT	Total monthly precipitation at 1 km (based on WorldCim v2 Climate) for July.
CLM_WCL_P08TOT	Total monthly precipitation at 1 km (based on WorldCim v2 Climate) for August.
CLM_WCL_P09TOT	Total monthly precipitation at 1 km (based on WorldCim v2 Climate) for September.
CLM_WCL_P10TOT	Total monthly precipitation at 1 km (based on WorldCim v2 Climate) for October.
CLM_WCL_P11TOT	Total monthly precipitation at 1 km (based on WorldCim v2 Climate) for November.
CLM_WCL_P12TOT	Total monthly precipitation at 1 km (based on WorldCim v2 Climate) for December.
CLM_WCL_S01RAD	Solar radiation at 1 km (based on WorldCim v2 Climate) for January.
CLM_WCL_S02RAD	Solar radiation at 1 km (based on WorldCim v2 Climate) for February.
CLM_WCL_S03RAD	Solar radiation at 1 km (based on WorldCim v2 Climate) for March.
CLM_WCL_S04RAD	Solar radiation at 1 km (based on WorldCim v2 Climate) for April.
CLM_WCL_S05RAD	Solar radiation at 1 km (based on WorldCim v2 Climate) for May.
CLM_WCL_S06RAD	Solar radiation at 1 km (based on WorldCim v2 Climate) for June.
CLM_WCL_S07RAD	Solar radiation at 1 km (based on WorldCim v2 Climate) for July.
CLM_WCL_S08RAD	Solar radiation at 1 km (based on WorldCim v2 Climate) for August.
CLM_WCL_S09RAD	Solar radiation at 1 km (based on WorldCim v2 Climate) for September.
CLM_WCL_S10RAD	Solar radiation at 1 km (based on WorldCim v2 Climate) for October.
CLM_WCL_S11RAD	Solar radiation at 1 km (based on WorldCim v2 Climate) for November.
CLM_WCL_S12RAD	Solar radiation at 1 km (based on WorldCim v2 Climate) for December.
CLM_WCL_SRDYRAVG	Average Yearly Solar radiation at 1 km (based on WorldCim v2 Climate).
CLM_WCL_SRDYRSTD	SD Yearly Solar radiation at 1 km (based on WorldCim v2 Climate).
CLM_WCL_SRDYRSUM	Total Yearly Solar radiation at 1 km (based on WorldCim v2 Climate).
CLM_WCL_T01AVG	Average monthly temperature at 1 km (based on WorldCim v2 Climate) for January.
CLM_WCL_T01MAX	Maximum monthly temperature at 1 km (based on WorldCim v2 Climate) for January.
CLM_WCL_T01MIN	Minimum monthly temperature at 1 km (based on WorldCim v2 Climate) for January.
CLM_WCL_T02AVG	Average monthly temperature at 1 km (based on WorldCim v2 Climate) for February.
CLM_WCL_T02MAX	Maximum monthly temperature at 1 km (based on WorldCim v2 Climate) for February.
CLM_WCL_T02MIN	Minimum monthly temperature at 1 km (based on WorldCim v2 Climate) for February.
CLM_WCL_T03AVG	Average monthly temperature at 1 km (based on WorldCim v2 Climate) for March.
CLM_WCL_T03MAX	Maximum monthly temperature at 1 km (based on WorldCim v2 Climate) for March.
CLM_WCL_T03MIN	Minimum monthly temperature at 1 km (based on WorldCim v2 Climate) for March.
CLM_WCL_T04AVG	Average monthly temperature at 1 km (based on WorldCim v2 Climate) for April.

CLM_WCL_T04MAX	Maximum monthly temperature at 1 km (based on WorldCim v2 Climate) for April.
CLM_WCL_T04MIN	Minimum monthly temperature at 1 km (based on WorldCim v2 Climate) for April.
CLM_WCL_T05AVG	Average monthly temperature at 1 km (based on WorldCim v2 Climate) for May.
CLM_WCL_T05MAX	Maximum monthly temperature at 1 km (based on WorldCim v2 Climate) for May.
CLM_WCL_T05MIN	Minimum monthly temperature at 1 km (based on WorldCim v2 Climate) for May.
CLM_WCL_T06AVG	Average monthly temperature at 1 km (based on WorldCim v2 Climate) for June.
CLM_WCL_T06MAX	Maximum monthly temperature at 1 km (based on WorldCim v2 Climate) for June.
CLM_WCL_T06MIN	Minimum monthly temperature at 1 km (based on WorldCim v2 Climate) for June.
CLM_WCL_T07AVG	Average monthly temperature at 1 km (based on WorldCim v2 Climate) for July.
CLM_WCL_T07MAX	Maximum monthly temperature at 1 km (based on WorldCim v2 Climate) for July.
CLM_WCL_T07MIN	Minimum monthly temperature at 1 km (based on WorldCim v2 Climate) for July.
CLM_WCL_T08AVG	Average monthly temperature at 1 km (based on WorldCim v2 Climate) for August.
CLM_WCL_T08MAX	Maximum monthly temperature at 1 km (based on WorldCim v2 Climate) for August.
CLM_WCL_T08MIN	Minimum monthly temperature at 1 km (based on WorldCim v2 Climate) for August.
CLM_WCL_T09AVG	Average monthly temperature at 1 km (based on WorldCim v2 Climate) for September.
CLM_WCL_T09MAX	Maximum monthly temperature at 1 km (based on WorldCim v2 Climate) for September.
CLM_WCL_T09MIN	Minimum monthly temperature at 1 km (based on WorldCim v2 Climate) for September.
CLM_WCL_T10AVG	Average monthly temperature at 1 km (based on WorldCim v2 Climate) for October.
CLM_WCL_T10MAX	Maximum monthly temperature at 1 km (based on WorldCim v2 Climate) for October.
CLM_WCL_T10MIN	Minimum monthly temperature at 1 km (based on WorldCim v2 Climate) for October.
CLM_WCL_T11AVG	Average monthly temperature at 1 km (based on WorldCim v2 Climate) for November.
CLM_WCL_T11MAX	Maximum monthly temperature at 1 km (based on WorldCim v2 Climate) for November.
CLM_WCL_T11MIN	Minimum monthly temperature at 1 km (based on WorldCim v2 Climate) for November.
CLM_WCL_T12AVG	Average monthly temperature at 1 km (based on WorldCim v2 Climate) for December.
CLM_WCL_T12MAX	Maximum monthly temperature at 1 km (based on WorldCim v2 Climate) for December.
CLM_WCL_T12MIN	Minimum monthly temperature at 1 km (based on WorldCim v2 Climate) for December.
CLM_WCL_V01APR	water vapor pressure at 1 km (based on WorldCim v2 Climate) for January.
CLM_WCL_V02APR	water vapor pressure at 1 km (based on WorldCim v2 Climate) for February.
CLM_WCL_V03APR	water vapor pressure at 1 km (based on WorldCim v2 Climate) for March.
CLM_WCL_V04APR	water vapor pressure at 1 km (based on WorldCim v2 Climate) for April.
CLM_WCL_V05APR	water vapor pressure at 1 km (based on WorldCim v2 Climate) for May.
CLM_WCL_V06APR	water vapor pressure at 1 km (based on WorldCim v2 Climate) for June.
CLM_WCL_V07APR	water vapor pressure at 1 km (based on WorldCim v2 Climate) for July.
CLM_WCL_V08APR	water vapor pressure at 1 km (based on WorldCim v2 Climate) for August.
CLM_WCL_V09APR	water vapor pressure at 1 km (based on WorldCim v2 Climate) for September.
CLM_WCL_V10APR	water vapor pressure at 1 km (based on WorldCim v2 Climate) for October.
CLM_WCL_V11APR	water vapor pressure at 1 km (based on WorldCim v2 Climate) for November.
CLM_WCL_V12APR	water vapor pressure at 1 km (based on WorldCim v2 Climate) for December.
CLM_WCL_W01SPD	Wind speed at 1 km (based on WorldCim v2 Climate) for January.
CLM_WCL_W02SPD	Wind speed at 1 km (based on WorldCim v2 Climate) for February.
CLM_WCL_W03SPD	Wind speed at 1 km (based on WorldCim v2 Climate) for March.
CLM_WCL_W04SPD	Wind speed at 1 km (based on WorldCim v2 Climate) for April.
CLM_WCL_W05SPD	Wind speed at 1 km (based on WorldCim v2 Climate) for May.
CLM_WCL_W06SPD	Wind speed at 1 km (based on WorldCim v2 Climate) for June.
CLM_WCL_W07SPD	Wind speed at 1 km (based on WorldCim v2 Climate) for July.
CLM_WCL_W08SPD	Wind speed at 1 km (based on WorldCim v2 Climate) for August.
CLM_WCL_W09SPD	Wind speed at 1 km (based on WorldCim v2 Climate) for September.
CLM_WCL_W10SPD	Wind speed at 1 km (based on WorldCim v2 Climate) for October.
CLM_WCL_W11SPD	Wind speed at 1 km (based on WorldCim v2 Climate) for November.
CLM_WCL_W12SPD	Wind speed at 1 km (based on WorldCim v2 Climate) for December.
ECO_USG_BIOCLZ	Bioclimatic zones based on the USGS's A New Map of Global Ecological Land Units.
ECO_USG_Z01	Bioclimatic zones based on the USGS's A New Map of Global Ecological Land Units.
ECO_USG_Z02	Bioclimatic zones based on the USGS's A New Map of Global Ecological Land Units.
ECO_USG_Z03	Bioclimatic zones based on the USGS's A New Map of Global Ecological Land Units.
ECO_USG_Z04	Bioclimatic zones based on the USGS's A New Map of Global Ecological Land Units.
ECO_USG_Z05	Bioclimatic zones based on the USGS's A New Map of Global Ecological Land Units.
ECO_USG_Z06	Bioclimatic zones based on the USGS's A New Map of Global Ecological Land Units.
ECO_USG_Z07	Bioclimatic zones based on the USGS's A New Map of Global Ecological Land Units.
ECO_USG_Z08	Bioclimatic zones based on the USGS's A New Map of Global Ecological Land Units.
ECO_USG_Z09	Bioclimatic zones based on the USGS's A New Map of Global Ecological Land Units.
ECO_USG_Z10	Bioclimatic zones based on the USGS's A New Map of Global Ecological Land Units.
ECO_USG_Z11	Bioclimatic zones based on the USGS's A New Map of Global Ecological Land Units.
ECO_USG_Z12	Bioclimatic zones based on the USGS's A New Map of Global Ecological Land Units.
ECO_USG_Z13	Bioclimatic zones based on the USGS's A New Map of Global Ecological Land Units.
ECO_USG_Z14	Bioclimatic zones based on the USGS's A New Map of Global Ecological Land Units.
ECO_USG_Z15	Bioclimatic zones based on the USGS's A New Map of Global Ecological Land Units.
ECO_USG_Z16	Bioclimatic zones based on the USGS's A New Map of Global Ecological Land Units.
ECO_USG_Z17	Bioclimatic zones based on the USGS's A New Map of Global Ecological Land Units.
ECO_USG_Z18	Bioclimatic zones based on the USGS's A New Map of Global Ecological Land Units.
ECO_USG_Z19	Bioclimatic zones based on the USGS's A New Map of Global Ecological Land Units.
ECO_USG_Z20	Bioclimatic zones based on the USGS's A New Map of Global Ecological Land Units.
ECO_USG_Z21	Bioclimatic zones based on the USGS's A New Map of Global Ecological Land Units.
ECO_USG_Z22	Bioclimatic zones based on the USGS's A New Map of Global Ecological Land Units.
ECO_USG_Z23	Bioclimatic zones based on the USGS's A New Map of Global Ecological Land Units.
ECO_USG_Z24	Bioclimatic zones based on the USGS's A New Map of Global Ecological Land Units.
ECO_USG_Z25	Bioclimatic zones based on the USGS's A New Map of Global Ecological Land Units.
ECO_USG_Z26	Bioclimatic zones based on the USGS's A New Map of Global Ecological Land Units.
ECO_USG_Z27	Bioclimatic zones based on the USGS's A New Map of Global Ecological Land Units.
ECO_USG_Z28	Bioclimatic zones based on the USGS's A New Map of Global Ecological Land Units.
ECO_USG_Z29	Bioclimatic zones based on the USGS's A New Map of Global Ecological Land Units.
ECO_USG_Z30	Bioclimatic zones based on the USGS's A New Map of Global Ecological Land Units.
ECO_USG_Z31	Bioclimatic zones based on the USGS's A New Map of Global Ecological Land Units.
ECO_USG_Z32	Bioclimatic zones based on the USGS's A New Map of Global Ecological Land Units.
ECO_USG_Z33	Bioclimatic zones based on the USGS's A New Map of Global Ecological Land Units.
ECO_USG_Z34	Bioclimatic zones based on the USGS's A New Map of Global Ecological Land Units.
ECO_USG_Z35	Bioclimatic zones based on the USGS's A New Map of Global Ecological Land Units.
ECO_USG_Z36	Bioclimatic zones based on the USGS's A New Map of Global Ecological Land Units.
ECO_USG_Z37	Bioclimatic zones based on the USGS's A New Map of Global Ecological Land Units.

ECO_USG_Z38	Bioclimatic zones based on the USGS's A New Map of Global Ecological Land Units.
ECO_USG_Z39	Bioclimatic zones based on the USGS's A New Map of Global Ecological Land Units.
GEO_DAC_ASS	Average soil and sedimentary-deposit thickness in meters. Estimated using physical landform models.
GEO_GLM_L01	based on the global lithology map
GEO_GLM_L02	based on the global lithology map
GEO_GLM_L03	based on the global lithology map
GEO_GLM_L04	based on the global lithology map
GEO_GLM_L05	based on the global lithology map
GEO_GLM_L06	based on the global lithology map
GEO_GLM_L07	based on the global lithology map
GEO_GLM_L08	based on the global lithology map
GEO_GLM_L09	based on the global lithology map
GEO_GLM_L10	based on the global lithology map
GEO_GLM_L11	based on the global lithology map
GEO_GLM_L13	based on the global lithology map
GEO_GLM_L14	based on the global lithology map
GEO_GLM_L15	based on the global lithology map
GEO_GLM_L16	based on the global lithology map
GEO_USG_QUA	
LUC_ESA_LCE	ESA land cover map 2010
LUC_ESA_LC5	ESA land cover map 2015
LUC_ESA_L000	ESA land cover map 2010 class L000
LUC_ESA_L010	ESA land cover map 2010 class L010
LUC_ESA_L011	ESA land cover map 2010 class L011
LUC_ESA_L012	ESA land cover map 2010 class L012
LUC_ESA_L020	ESA land cover map 2010 class L020
LUC_ESA_L030	ESA land cover map 2010 class L030
LUC_ESA_L040	ESA land cover map 2010 class L040
LUC_ESA_L050	ESA land cover map 2010 class L050
LUC_ESA_L060	ESA land cover map 2010 class L060
LUC_ESA_L061	ESA land cover map 2010 class L061
LUC_ESA_L062	ESA land cover map 2010 class L062
LUC_ESA_L070	ESA land cover map 2010 class L070
LUC_ESA_L071	ESA land cover map 2010 class L071
LUC_ESA_L072	ESA land cover map 2010 class L072
LUC_ESA_L080	ESA land cover map 2010 class L080
LUC_ESA_L081	ESA land cover map 2010 class L081
LUC_ESA_L082	ESA land cover map 2010 class L082
LUC_ESA_L090	ESA land cover map 2010 class L090
LUC_ESA_L100	ESA land cover map 2010 class L100
LUC_ESA_L110	ESA land cover map 2010 class L110
LUC_ESA_L120	ESA land cover map 2010 class L120
LUC_ESA_L121	ESA land cover map 2010 class L121
LUC_ESA_L122	ESA land cover map 2010 class L122
LUC_ESA_L130	ESA land cover map 2010 class L130
LUC_ESA_L140	ESA land cover map 2010 class L140
LUC_ESA_L150	ESA land cover map 2010 class L150
LUC_ESA_L152	ESA land cover map 2010 class L152
LUC_ESA_L153	ESA land cover map 2010 class L153
LUC_ESA_L160	ESA land cover map 2010 class L160
LUC_ESA_L170	ESA land cover map 2010 class L170
LUC_ESA_L180	ESA land cover map 2010 class L180
LUC_ESA_L190	ESA land cover map 2010 class L190
LUC_ESA_L200	ESA land cover map 2010 class L200
LUC_ESA_L201	ESA land cover map 2010 class L201
LUC_ESA_L202	ESA land cover map 2010 class L202
LUC_ESA_L220	ESA land cover map 2010 class L220
LUC_GFC_BARLY10	Global 30m Bare Ground (circa 2010)
LUC_GFC_TRELY10	Global 30m Tree Cover (circa 2010)
LUC_GLC_C01	Cultivated land cover for year 2010 based on GlobCover30
LUC_GLC_C02	Forests cover for year 2010 based on GlobCover30
LUC_GLC_C03	Grasslands cover for year 2010 based on GlobCover30
LUC_GLC_C04	Shrublands cover for year 2010 based on GlobCover30
LUC_GLC_C05	Wetland cover for year 2010 based on GlobCover30
LUC_GLC_C07	Tundra cover for year 2010 based on GlobCover30
LUC_GLC_C08	Artificial Surfaces cover for year 2010 based on GlobCover30
LUC_GLC_C09	Bareland cover for year 2010 based on GlobCover30
LUC_GLC_C01t	Binary: Cultivated land cover for year 2010 based on GlobCover30
LUC_GLC_C02t	Binary: Forests cover for year 2010 based on GlobCover30
LUC_GLC_C03t	Binary: Grasslands cover for year 2010 based on GlobCover30
LUC_GLC_C04t	Binary: Shrublands cover for year 2010 based on GlobCover30
LUC_GLC_C05t	Binary: Wetland cover for year 2010 based on GlobCover30
LUC_GLC_C07t	Binary: Tundra cover for year 2010 based on GlobCover30
LUC_GLC_C08t	Binary: Artificial Surfaces cover for year 2010 based on GlobCover30
LUC_GLC_C09t	Binary: Bareland cover for year 2010 based on GlobCover30
LUC_LDS_MNG	Landsat-based estimated distrubution of Mangroves published in Giri et al. (2011)
MOR_ENV_DEME	DEM based on 100 m resolution from EarthEnv-DEM90. No additional post-processing has been applied to remove vegetation and filter noise.
MOR_ENV_DEMM	Merged elevation based on 100 m resolution DEMs from ViewfinderPanoramas SRTM DEM, SRTMGL3, and GMTED2010.
MOR_MRG_CRD	Local downslope Curvature based on DEMMRG5 derived in SAGA GIS.
MOR_MRG_CRU	Local upslope Curvature based on DEMMRG5 derived in SAGA GIS.
MOR_MRG_CRV	Downslope Curvature based on DEMMRG5 derived in SAGA GIS.
MOR_MRG_DV2	Deviation from Mean Value (surface roughness) based on DEMMRG5. Derived in SAGA GIS using a 13 by 13 search radius.
MOR_MRG_DVM	Deviation from Mean Value (surface roughness) based on DEMMRG5. Derived in SAGA GIS using a 9 by 9 search radius.
MOR_MRG_MRN	Melton Ruggedness Number derived in SAGA GIS
MOR_MRG_NEG	Negative Topographic Openness based on DEMMRG5
MOR_MRG_POS	Positive Topographic Openness based on DEMMRG5
MOR_MRG_SLP	Terrain slope based on DEMMRG5 derived in SAGA GIS and expressed in radians x 100.
MOR_MRG_TPI	Topographic Position Index is the difference to the mean calculation (residual analysis) proposed by Wilson & Gallant (2000).

MOR_MRG_TWI	SAGA Wetness Index based on DEMMRG5. SAGA TWI is based on a modified catchment area calculation, which does not think of the flow as very thin film. As result it predicts for cells situated in valley floors with a small vertical distance to a channel a more realistic, higher potential soil moisture compared to the standard TWI calcul
MOR_MRG_VBF	Multiresolution Index of Valley Bottom Flatness (MRVBF) based on DEMMRG5. Derived in SAGA GIS at 500 m, then downscaled to 250 m. Computationally very intensive operatio
MOR_MRG_VDP	Valley depth based on DEMMRG5 i.e. vertical distance to a channel network base level derived in SAGA GIS.
MOR_USG_F01	Landform class: Breaks/Foothills
MOR_USG_F02	Landform class: Flat Plains
MOR_USG_F03	Landform class: High Mountains/Deep Canyons
MOR_USG_F04	Landform class: Hills
MOR_USG_F05	Landform class: Low Hills
MOR_USG_F06	Landform class: Low Mountains
MOR_USG_F07	Landform class: Smooth Plains
SAT_L07_B3RED00	Landsat Band 3 (red) for year 2000
SAT_L07_B3RED14	Landsat Band 3 (red) for year 2014
SAT_L07_B4NIR00	Landsat Band 4 (NIR) for year 2000
SAT_L07_B4NIR14	Landsat Band 4 (NIR) for year 2014
SAT_L07_B5SWIR00	Landsat Band 5 (SWIR) for year 2000
SAT_L07_B5SWIR14	Landsat Band 5 (SWIR) for year 2014
SAT_L07_B7SWIR00	Landsat Band 7 (SWIR) for year 2000
SAT_L07_B7SWIR14	Landsat Band 7 (SWIR) for year 2014
SAT_MOD_MIR01AVG	Long-term averaged mean monthly surface reflectance (MIR) band 7 MODIS for January. Derived using a stack of MCD43A4 band 7 images.
SAT_MOD_MIR02AVG	Long-term averaged mean monthly surface reflectance (MIR) band 7 MODIS for February. Derived using a stack of MCD43A4 band 7 images.
SAT_MOD_MIR03AVG	Long-term averaged mean monthly surface reflectance (MIR) band 7 MODIS for March. Derived using a stack of MCD43A4 band 7 images.
SAT_MOD_MIR04AVG	Long-term averaged mean monthly surface reflectance (MIR) band 7 MODIS for April. Derived using a stack of MCD43A4 band 7 images.
SAT_MOD_MIR05AVG	Long-term averaged mean monthly surface reflectance (MIR) band 7 MODIS for May. Derived using a stack of MCD43A4 band 7 images.
SAT_MOD_MIR06AVG	Long-term averaged mean monthly surface reflectance (MIR) band 7 MODIS for June. Derived using a stack of MCD43A4 band 7 images.
SAT_MOD_MIR07AVG	Long-term averaged mean monthly surface reflectance (MIR) band 7 MODIS for July. Derived using a stack of MCD43A4 band 7 images.
SAT_MOD_MIR08AVG	Long-term averaged mean monthly surface reflectance (MIR) band 7 MODIS for August. Derived using a stack of MCD43A4 band 7 images.
SAT_MOD_MIR09AVG	Long-term averaged mean monthly surface reflectance (MIR) band 7 MODIS for September. Derived using a stack of MCD43A4 band 7 images.
SAT_MOD_MIR10AVG	Long-term averaged mean monthly surface reflectance (MIR) band 7 MODIS for October. Derived using a stack of MCD43A4 band 7 images.
SAT_MOD_MIR11AVG	Long-term averaged mean monthly surface reflectance (MIR) band 7 MODIS for November. Derived using a stack of MCD43A4 band 7 images.
SAT_MOD_MIR12AVG	Long-term averaged mean monthly surface reflectance (MIR) band 7 MODIS for December. Derived using a stack of MCD43A4 band 7 images.
SAT_MOD_MIRYRAVG	Mean yearly MODIS MIR band 4
SAT_MOD_NIR01AVG	Long-term averaged mean monthly surface reflectance (NIR) band 4 MODIS for January. Derived using a stack of MCD43A4 band 4 images.
SAT_MOD_NIR02AVG	Long-term averaged mean monthly surface reflectance (NIR) band 4 MODIS for February. Derived using a stack of MCD43A4 band 4 images.
SAT_MOD_NIR03AVG	Long-term averaged mean monthly surface reflectance (NIR) band 4 MODIS for March. Derived using a stack of MCD43A4 band 4 images.
SAT_MOD_NIR04AVG	Long-term averaged mean monthly surface reflectance (NIR) band 4 MODIS for April. Derived using a stack of MCD43A4 band 4 images.
SAT_MOD_NIR05AVG	Long-term averaged mean monthly surface reflectance (NIR) band 4 MODIS for May. Derived using a stack of MCD43A4 band 4 images.
SAT_MOD_NIR06AVG	Long-term averaged mean monthly surface reflectance (NIR) band 4 MODIS for June. Derived using a stack of MCD43A4 band 4 images.
SAT_MOD_NIR07AVG	Long-term averaged mean monthly surface reflectance (NIR) band 4 MODIS for July. Derived using a stack of MCD43A4 band 4 images.
SAT_MOD_NIR08AVG	Long-term averaged mean monthly surface reflectance (NIR) band 4 MODIS for August. Derived using a stack of MCD43A4 band 4 images.
SAT_MOD_NIR09AVG	Long-term averaged mean monthly surface reflectance (NIR) band 4 MODIS for September. Derived using a stack of MCD43A4 band 4 images.
SAT_MOD_NIR10AVG	Long-term averaged mean monthly surface reflectance (NIR) band 4 MODIS for October. Derived using a stack of MCD43A4 band 4 images.
SAT_MOD_NIR11AVG	Long-term averaged mean monthly surface reflectance (NIR) band 4 MODIS for November. Derived using a stack of MCD43A4 band 4 images.
SAT_MOD_NIR12AVG	Long-term averaged mean monthly surface reflectance (NIR) band 4 MODIS for December. Derived using a stack of MCD43A4 band 4 images.
SAT_MOD_NIRYRAVG	Mean yearly MODIS NIR band 4
VEG_L07_NDWIB5Y00	Normalized Difference Water Index in 2010 computed with NIRL00 and SW1L00
VEG_L07_NDWIB5Y14	Normalized Difference Water Index in 2014 computed with NIRL00 and SW1L14
VEG_L07_NDWIB7Y00	Normalized Difference Water Index in 2010 computed with NIRL00 and SW2L00
VEG_L07_NDWIB7Y14	Normalized Difference Water Index in 2014 computed with NIRL00 and SW2L14
VEG_MOD_EVI01AVG	Long-term averaged mean monthly MODIS Enhanced Vegetation Index (EVI) for months January and February. Derived using a stack of MOD13Q1 EVI images.
VEG_MOD_EVI01STD	Long-term s.d. of the monthly MODIS Enhanced Vegetation Index (EVI) for months January and February. Derived using a stack of MOD13Q1 EVI images.
VEG_MOD_EVI03AVG	Long-term averaged mean monthly MODIS Enhanced Vegetation Index (EVI) for months March and April. Derived using a stack of MOD13Q1 EVI images.
VEG_MOD_EVI03STD	Long-term s.d. of the monthly MODIS Enhanced Vegetation Index (EVI) for months March and April. Derived using a stack of MOD13Q1 EVI images.
VEG_MOD_EVI05AVG	Long-term averaged mean monthly MODIS Enhanced Vegetation Index (EVI) for months May and June. Derived using a stack of MOD13Q1 EVI images.
VEG_MOD_EVI05STD	Long-term s.d. of the monthly MODIS Enhanced Vegetation Index (EVI) for months May and June. Derived using a stack of MOD13Q1 EVI images.
VEG_MOD_EVI07AVG	Long-term averaged mean monthly MODIS Enhanced Vegetation Index (EVI) for months July and August. Derived using a stack of MOD13Q1 EVI images.
VEG_MOD_EVI07STD	Long-term s.d. of the monthly MODIS Enhanced Vegetation Index (EVI) for months July and August. Derived using a stack of MOD13Q1 EVI images.
VEG_MOD_EVI09AVG	Long-term averaged mean monthly MODIS Enhanced Vegetation Index (EVI) for months September and October. Derived using a stack of MOD13Q1 EVI images.
VEG_MOD_EVI09STD	Long-term s.d. of the monthly MODIS Enhanced Vegetation Index (EVI) for months September and October. Derived using a stack of MOD13Q1 EVI images.
VEG_MOD_EVI11AVG	Long-term averaged mean monthly MODIS Enhanced Vegetation Index (EVI) for months November and December. Derived using a stack of MOD13Q1 EVI images.
VEG_MOD_EVI11STD	Long-term s.d. of the monthly MODIS Enhanced Vegetation Index (EVI) for months November and December. Derived using a stack of MOD13Q1 EVI images.
VEG_MOD_EVIENT	Entropy Disorderliness of EVI
VEG_MOD_EVIEVN	Evenness of MODIS EVI
VEG_MOD_EVIMAX	Maximum Dominance of EVI combinations between adjacent pixels
VEG_MOD_EVIRNG	Range of EVI
VEG_MOD_EVIYRAVG	Mean yearly MODIS EVI
VEG_MOD_EVIYRSTD	SD yearly MODIS EVI
VEG_MOD_NPPAVG	Net Primary Productivity (2000-2015 average)
VEG_MOD_NPPY00	Net Primary Productivity in 2015
VEG_MOD_NPPY15	Net Primary Productivity in 2000
WTR_GIE_MSD	Global Inundation Extent from Multi-Satellites - Downscaled to 15 arc-seconds
WTR_GIE_C00	Global Inundation Extent from Multi-Satellites - Downscaled to 15 arc-seconds
WTR_GIE_C01	Global Inundation Extent from Multi-Satellites - Downscaled to 15 arc-seconds
WTR_GIE_C02	Global Inundation Extent from Multi-Satellites - Downscaled to 15 arc-seconds
WTR_GIE_C03	Global Inundation Extent from Multi-Satellites - Downscaled to 15 arc-seconds
WTR_GSW_CHA	Surface water change
WTR_GSW_EXT	Global surface water maximum extent
WTR_GSW_OCC	Occurrence probability
WTR_HYS_GTD	Global Water Table Depth in meters based on Fan and Miguez-Macho (2015).

III Homosoil results

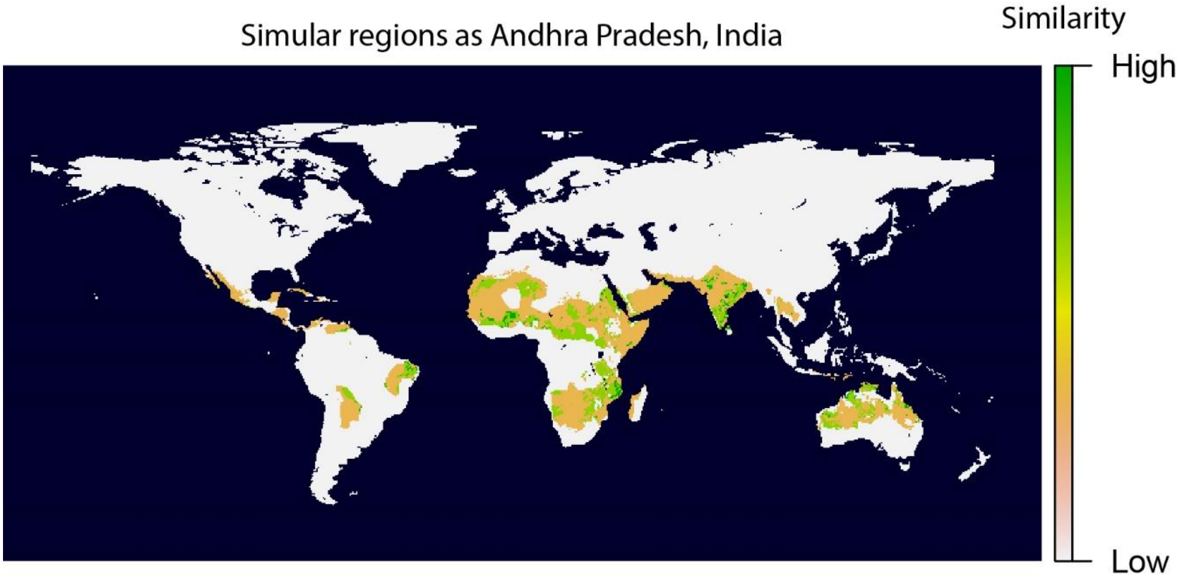
Simular regions as Andhra Pradesh, India
Similarity
High
Low